Republic of Iraq

Ministry of Higher Education & Scientific Research

University of Kerbala

College of Engineering

Mechanical Engineering Department

Optimal Design and Control of an Upper-Limb Exoskeleton

A Thesis Submitted to the Council of the Faculty of the College of Engineering/University Of Kerbala in Partial Fulfillment of the Requirements for the Master's Degree in /Applied Mechanical Engineering

Written By:

Zahraa Abd Al-Elah Khaleel

Supervised By:

Asist. Prof. Dr. Muslim Muhsin Ali

Asist. Prof. Dr. Fawaz F. Al Bakri

January 2026 **Rajab 1447**

بسم الله الرحمن الرحيم

﴿ وَتَرَى الْجِبَالَ تَحْسَبُهَا جَامِدَةً
وَهِيَ تَمُرُّ مَرَّ السَّحَابِ صُنْعَ اللَّهِ الَّذِي
أَتْقَنَ كُلَّ شَيْءٍ إِنَّهُ خَبِيرٌ بِمَا تَفْعَلُونَ﴾

صدق الله العلي العظيم

(سورة النمل 88)

Examination committee certification

We certify that we have read the thesis entitled " **Optimal Design and Control of an Upper-Limb Exoskeleton** " and as an examining committee, we examined the student " **Zahraa Abd Al-Elah Khaleel**" in its content and in what is connected with it and that, in our opinion, it is adequate as a thesis for the degree of Master of Science in Mechanical Engineering.

Supervisor
Signature:
Name : Asist prof. Dr.
Muslim Muhsin Ali
Date: 21/ 1/ 2026

Supervisor
Signature:
Name:Asist prof. Dr.
Fawaz F. Al Bakri
Date: 21/ 1/ 2026

Member
Signature:
Name :. Prof. Dr.
Salwan Obaid Waheed
Date: ٢١/ ١/ 2026

Member
Signature:
Name :. Asist prof. Dr.
Dhirgaam A.Kadhim
Date: 21/ 1/ 2026

Chairman
Signature:
Name :. Prof. Dr.
Emad Qasem Hussein
Date: 21/ 1/ 2026

Signature:
Name : Prof.Dr.
Salah N.Alnomani
Head of the Department of Mechanical Engineering
Date: 25/ 1/ 2026

Signature:
Name : Prof.Dr.
Haider Nadhom Azizz
Dean of the Engineering College
Date: / / 2026

Supervisor Certificate

We certify that the thesis entitled " **Optimal Design and Control of an Upper-Limb Exoskeleton** " was prepared by **Zahraa Abd Al-Elah Khaleel** under our supervision at the Department of Mechanical Engineering, Faculty of Engineering, University of Kerbala as a partial of fulfilment of the requirements for the Degree of Master of Science in Mechanical Engineering.

Signature:

Asist prof. Dr. Muslim Muhsin Ali

Date: ٢١ / ١ / **2026**

Signature:

Asist Prof. Dr. Fawaz F. Al-Bakri

Date: ٢١ / ١ / **2026**

Linguistic Certificate

I certify that the thesis entitled " **Optimal Design and Control of an Upper-Limb Exoskeleton** " which has been submitted by **Zahraa Abd Al-Elah Khaleel,** has been proofread, and its language has been amended to meet the English style.

Signature:
Dr. Hasan Qahtan Hussein
Date: / /

Undertaking

I certify that research work titled " **Optimal Design and Control of an Upper-Limb Exoskeleton**" is my own work. The work has not been presented elsewhere for assessment. Where material has been used from other sources, it has been properly referred.

Signature:

Zahraa Abd Al-Elah Khaleel

Date:20/ 1 / 2026

Dedication

-To my mother, who is like no other and who was my homeland when the world became narrow.

-To my father,whom I never met,but whose name and memory have been my slient strength.

-To my husband, who was my support and companion, who shared the road with me, with all its hardships and details.

-To my beloved children*Sarah and Zain*,You are the most beautiful meaning of this journey .

-To my brother and sister,who have always been my support and strength.

-To my dear professors, who were candles that lit my path.

-To those who asked for nothing,yet gave me everything.

-To those who stood quitly behind the scenes,lighting my path without being seen.

This effort is not mine alone, but rather it is a story woven from many hearts.

Acknowledgements

I extend my sincere thanks and appreciation to a group of distinguished professors who have had a significant impact on the completion of this research. Without their support and guidance, this work would not have been possible. I would especially like to mention:

- Dr. Fawaz F. Al-Bakri, who was the cornerstone of this research and deserves all the credit for guiding me from the beginning and supporting me academically and intellectually. His comments and guidance had the greatest impact in building this work on sound scientific foundations.
- Dr. Muslim Mohsen, who spared effort and time, and whose scholarly and critical contributions were an important support in the development of this research.
- Dr. Ali Abdul Rasool, the Graduate Studies Department coordinator, who played a significant role in overcoming obstacles. We extend our sincere thanks to him for all the cooperation and facilitation he provided.
- Dr. Hassan Qahtan, although not a member of the supervisory committee, his academic support and assistance throughout the various stages of the research were clear and influential. To him I extend my sincere gratitude and appreciation.

Abstract

Smart upper limbs prosthetics play a significant role in enhancing mobility and independence for disabilities people with disabilities. These mechanical devices are utilized to provide functional movements of the human arm in various applications such as rehabilitation, sports, and technological innovation, one of these devices is a robotic arm exoskeleton. Therefore, it becomes essential to assess the dynamic response of robotic arm prosthetics. This study focuses on studying the dynamic response of a five-degree-of-freedom (5-DOF) prosthetic robotic arm.

The robotic arm system was modeled by using Lagrange-Euler method, resulting in five-second-order ordinary differential equations. To facilitate the optimization process required and obtain locally optimal system parameters. The nonlinear model was linearized around a specific operating point. A comparative analysis between the linear and nonlinear system responses was conducted to ensure that the linearized model can adequately represent and compensate for the real nonlinear system dynamics.

The arm parameters, including masses, damping coefficients, and stiffness values, were determined using a Lagrange multipliers optimization method with the objective of achieving a short settling time and minimal overshoot. Furthermore, eight-term exponential functions were employed to generate the desired displacement profiles for the hand, forearm, horizontal elbow, vertical elbow, and elbow angular motions while satisfying initial, intermediate, and final boundary conditions as well as elbow torque limitations.

The reference elbow torque was analytically computed based on the predefined displacement trajectories. To validate the proposed approach, numerical simulations were preformed using Monte Carlo simulation technique under a wide range of initial conditions and system parameter variations of $\pm 6\%$ from the nominal values. The obtained results demonstrated rapid convergence of all arm segments, achieving steady-state responses within 0.25 seconds with zero overshoot in both system displacements and elbow torque. Moreover, the steady-state errors remained extremely small, with a maximum elbow angular error of (4×10^{-3}) degrees, a minimum vertical elbow displacement error of (-1×10^{-5}) m in the vertical, and an elbow torque error as low as (-0.4) N.m across 1000 simulation trials.

Table of Contents

List of Tables

List of Figures

List of Symbols

Symbol	Description	Units
A_n	Hand coefficients	
B_n	Forearm coefficients	
c_1	Damper coefficient between ground and mass m_1	$\frac{N.s}{m}$
c_2	Damper coefficient between m_1 and m_2	$\frac{N.s}{m}$
c_3	Damper coefficient between m_2 and m_3	$\frac{N.s}{m}$
c_4	Horizontal damper between trunk and point z_4	$\frac{N.s}{m}$
c_5	Vertical damper coefficient between trunk and point y_2	$\frac{N.s}{m}$
c_t	Torsional damper coefficient of the elbow	$\frac{N.m.s}{rad}$
C_n	Horizontal elbow coefficients	
D_{E_1}	First dissipated energy	J
D_{E_2}	Second dissipated energy	J
D_{E_3}	Third dissipated energy	J
D_{E_4}	Forth dissipated energy	J
D_{E_5}	Fifth dissipated energy	J
D_{E_6}	Sixth dissipated energy	J
D_E	Total dissipated energy	J
D_n	Vertical elbow coefficients	
E_n	Elbow angular coefficients	

g	Acceleration of gravity	$\frac{m}{s^2}$
J	Rotational inertia of the elbow joint system	0.0149kg.m^2
k_1	Spring stiffness between ground and mass m_1	$\frac{N}{m}$
k_2	Spring stiffness between m_1 and m_2	$\frac{N}{m}$
k_3	Spring stiffness between m_2 and m_3	$\frac{N}{m}$
k_4	Horizontal spring stiffness between trunk and point z_4	$\frac{N}{m}$
k_5	Vertical spring stiffness between trunk and point y_2	$\frac{N}{m}$
k_t	Torsional spring stiffness of the elbow	$\frac{N.m}{rad}$
K_{E_1}	Kinetic energy of the hand	J
K_{E_2}	Kinetic energy of the forearm	J
K_{E_3}	Kinetic energy of the elbow	J
K_E	Total kinetic energy	J
L	Upper arm length	0.29 m
L_g	Distance from the elbow to the upper arm	0.44 L m
m_1	Effective mass of the hand	k_g
m_2	Effective mass of the forearm segment	k_g
m_3	Mass of the upper arm	k_g
OS_i	Initial over shoot	

$OS_{i,desired}$	Initial desired over shoot	
P_{E_1}	First potential energy	J
P_{E_2}	Second potential energy	J
P_{E_3}	Third potential energy	J
P_{E_4}	Forth potential energy	J
P_{E_5}	Fifth potential energy	J
P_{E_6}	Sixth potential energy	J
P_{E_7}	Potential energy from the gravitational force	J
P_E	Total potential energy	J
r_g	Distance to the center of gravity of the upper arm	m
T_{ref}	Reference torque	$N.m$
t	Time	s
$t_{s,i}$	Initial settling time	s
$t_{s,i,desired}$	Initial desired settling time	s
v_g	Relative velocity of the upper arm center	$\frac{m}{s}$
y_1	Displacement of the vertical motions of the elbow	m
y_2	Displacement of the vertical motions of the shoulder	m
$y_{1_{ref}}$	Reference displacement of the vertical motions of the elbow	m
y_{10}	Initial vertical elbow displacement	m
y_{1f}	Final vertical elbow displacement	m
$\dot{y_1}$	Velocity of the vertical motions of the elbow	$\frac{m}{s}$

$\dot{y}_2$	Velocity of the vertical motions of the shoulder	$\frac{m}{s}$
$\dot{y}_{1_{ref}}$	Reference velocity of the vertical motions of the elbow	$\frac{m}{s}$
$\dot{y}_{10}$	Initial vertical elbow velocity	$\frac{m}{s}$
$\dot{y}_{1f}$	Final vertical elbow velocity	$\frac{m}{s}$
$\ddot{y}_1$	Acceleration of the vertical motions of the elbow	$\frac{m}{s^2}$
$\ddot{y}_{1ref}$	Reference acceleration of the vertical motions of the elbow	$\frac{m}{s^2}$
z_1	Displacement of the horizontal motions of the hand	m
z_2	Displacement of the horizontal motions of the forearm	m
z_3	Displacement of the horizontal motions of the elbow	m
z_4	Displacement of the horizontal motions of the shoulder	m
$z_{1_{ref}}$	Reference displacement of the horizontal motions of the hand	m
$z_{2_{ref}}$	Reference displacement of the horizontal motions of the forearm	m
$z_{3_{ref}}$	Reference displacement of the horizontal motions of the elbow	m
z_0	External displacement acting on the hand	m
z_{10}	Initial hand displacement	m

z_{1f}	Final hand displacement	m
z_{20}	Initial forearm displacement	m
z_{2f}	Final forearm displacement	m
z_{30}	Initial horizontal elbow displacement	m
z_{3f}	Final horizontal elbow displacement	m
$\dot{z_1}$	Velocity of the horizontal motions of the hand	$\frac{m}{s}$
$\dot{z_2}$	Velocity of the horizontal motions of the forearm	$\frac{m}{s}$
$\dot{z_3}$	Velocity of the horizontal motions of the elbow	$\frac{m}{s}$
$\dot{z_4}$	Velocity of the horizontal motions of the shoulder	$\frac{m}{s}$
$\dot{z}_{1_{ref}}$	Reference velocity of the horizontal motions of the hand	$\frac{m}{s}$
$\dot{z}_{2_{ref}}$	Reference velocity of the horizontal motions of the forearm	$\frac{m}{s}$
$\dot{z}_{3_{ref}}$	Reference velocity of the horizontal motions of the elbow	$\frac{m}{s}$
$\dot{z_0}$	External velocity acting on the hand	$\frac{m}{s}$
$\dot{z}_{10}$	Initial hand velocity	$\frac{m}{s}$
$\dot{z}_{1f}$	Final hand velocity	$\frac{m}{s}$
$\dot{z}_{20}$	Initial forearm velocity	$\frac{m}{s}$

$\dot{z}_{2f}$	Final forearm velocity	$\frac{m}{s}$
$\dot{z}_{30}$	Initial horizontal elbow velocity	$\frac{m}{s}$
$\dot{z}_{3f}$	Final horizontal elbow velocity	$\frac{m}{s}$
$\ddot{z}_1$	Acceleration of the horizontal motions of the hand	$\frac{m}{s^2}$
$\ddot{z}_2$	Acceleration of the horizontal motions of the forearm	$\frac{m}{s^2}$
$\ddot{z}_3$	Acceleration of the horizontal motions of the elbow	$\frac{m}{s^2}$
$\ddot{z}_{1ref}$	Reference acceleration of the horizontal motions of the hand	$\frac{m}{s^2}$
$\ddot{z}_{2ref}$	Reference acceleration of the horizontal motions of the forearm	$\frac{m}{s^2}$
$\ddot{z}_{3ref}$	Reference acceleration of the horizontal motions of the elbow	$\frac{m}{s^2}$
θ	Displacement of the elbow angular	rad
$\tilde{\theta}$	Nominal position of the upper arm	10 deg
θ_{ref}	Reference displacement of the elbow angular	rad
θ_0	Initial elbow angular displacement	rad
θ_f	Final elbow angular displacement	rad
$\dot{\theta}$	Angular velocity of the elbow angular	$\frac{rad}{s}$

$\dot{\theta}_{ref}$	Reference velocity of the rotational elbow angular	$\frac{rad}{s}$
$\dot{\theta}_0$	Initial elbow angular velocity	$\frac{rad}{s}$
$\dot{\theta}_f$	Final elbow angular velocity	$\frac{rad}{s}$
$\ddot{\theta}$	Acceleration of the elbow angular	$\frac{rad}{s^2}$
$\ddot{\theta}_{ref}$	Reference acceleration of the elbow angular	$\frac{rad}{s^2}$

Chapter One: Introduction

1.1 Introduction

The development of artificial human arms has the potential to significantly improve the mobility and independence of individuals who have lost their arms, enabling them to perform daily activities with greater ease. In recent years, the world has witnessed remarkable developments in the field of mechanical systems and robotics. Robots have become an essential part of many industrial and medical applications. Among these applications, exoskeletons and mechanical arms have emerged, capturing the attention of researchers and engineers. These systems are characterized by their ability to simulate the movement of human limbs in a very realistic manner and are considered among the most important innovations in medical applications for the motor rehabilitation of patients with injuries to the nervous system[1].

1.2 Exoskeletons

Exoskeletons are not merely mechanical structures; rather, they represent integrated systems that combine mechanical components, electronic hardware, and control software working synergistically to enable natural and balanced human movement. Consequently, extensive research has been conducted on the design of upper-limb exoskeletons and their significance in various applications.

(Smith et al., 2021)[2] reviewed recent advancements in upper-limb exoskeletal robots and their rehabilitation applications, with particular emphasis on design requirements and the classification of mechanical models employed in upper-limb exoskeletons. In addition, the authors discussed the

key challenges associated with the design processes and highlighted the differences among existing approaches.

As illustrated below, upper-limb exoskeleton robot can be classified as follows:

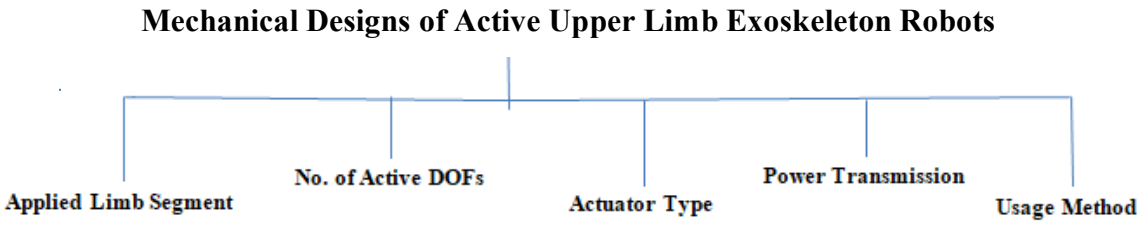

Actuators are a fundamental component of exoskeleton systems, as they are responsible for generating the forces and torques required to assist or enhance human motion. The overall performance of an exoskeleton strongly depends on the type of actuator used, particularly in terms of dynamic response, efficiency, weight, safety, and controllability. Due to the wide range of exoskeleton applications, including medical rehabilitation, industrial assistance, and human performance augmentation, several types of actuators have been developed and employed [3]

The upper-limb exoskeleton robot actuators are classified as follow:

1.2.1 Exoskeleton actuated by electric motors

This type of exoskeleton uses precise electric motors to generate the torque required to move the joints according to the required movements, with control of speed and accuracy as shown as Figure (1.1). It is useful in rehabilitation after injuries or after exposure to a stroke. It helps patients perform repetitive movements to strengthen muscles, making it an effective tool for movement training and daily assistance for people with muscle weakness.

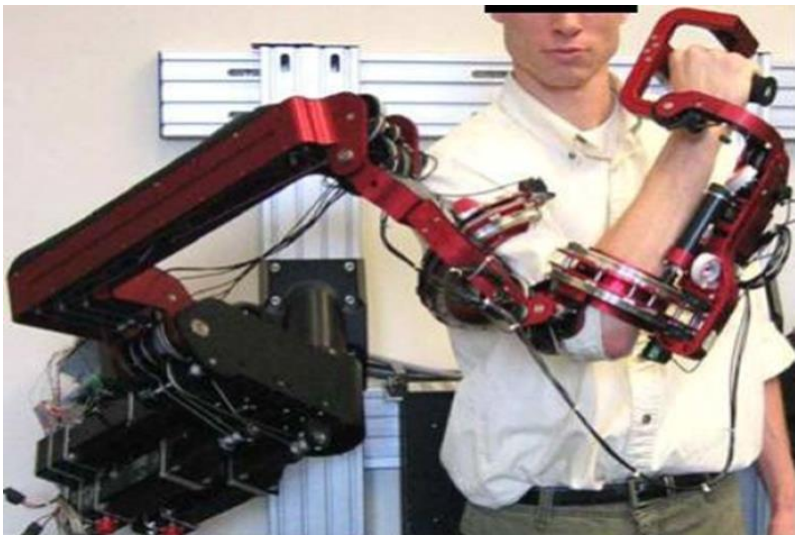

Figure (1.1): Exoskeleton actuated by electric motors [2]

1.2.2. Exoskeleton actuated by pneumatic actuator

This type relies on the use of pneumatic actuators that mimic the work of natural muscles in generating force and movement. When air is pumped or emptied into these artificial muscles, they expand or contract, leading to smooth movement of the arm joints as shown in Figure 1.2. These systems are characterized by their light weight and flexibility compared to electric motors and are used in motor rehabilitation. In addition to the possibility of programming its movement to repeat specific exercises to enhance muscle strength and improve motor coordination.

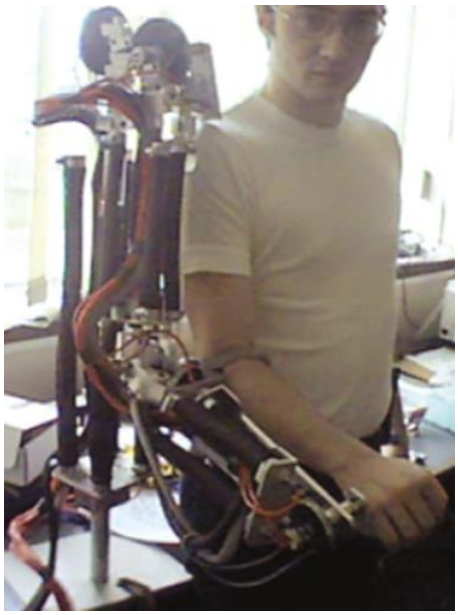

Figure (1.2): Exoskeleton actuated by pneumatic muscles [2]

1.2.3. Exoskeleton actuated by hydraulic power

A hydraulically powered exoskeleton uses pressurized fluid to generate the force needed to move the arm joints. When this fluid is pumped under pressure into hydraulic cylinders, it generates linear or rotational motion, which powers the arm, as shown in Figure 1.3. These systems are characterized by their ability to generate great torque when compared to electric motors or pneumatic muscles, making them suitable for moving heavy loads or patients who need significant assistance in rehabilitation. The speed and force of movement can be controlled by hydraulic valves and pumps, providing smooth and guaranteed performance.[4]

Figure (1.3): Exoskeleton actuated by hydraulic power [2]

1.3 Parts of a human arm

1.3.1 Hand

It is one of the most complex and functional parts of the arm, as it consists of the palm of the hand and the fingers and contains fine muscles and tendons that allow movements such as writing, holding objects, and other tasks.[5]

1.3.2 Wrist

It is the part of the arm that connects the hand to the forearm and consists of eight small bones arranged in a complex manner that enables flexion and extension movements, giving the hand its high flexibility, as shown in Figure 1.4.

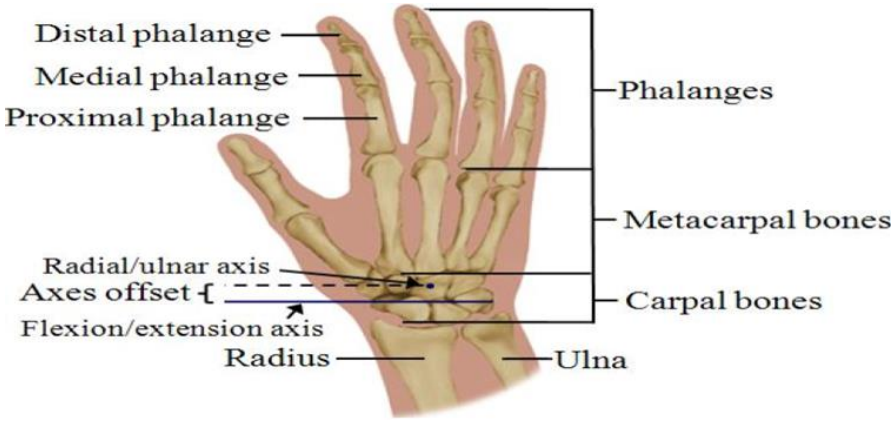

Figure (1.4): Wrist joint[2]

1.3.3 Forearm

The forearm extends from the elbow to the wrist and consists of the ulna and radius bones. It contains a large group of muscles responsible for the movements of the wrist and fingers, as well as the possibility of rotation.

1.3.4 Elbow

It is a complex joint that connects the humerus and the forearm, assists in flexion, extension, and rotational movements, and acts as a mechanical link that coordinates between the shoulder and wrist to achieve high flexibility of movement as shown in Figure 1.5.

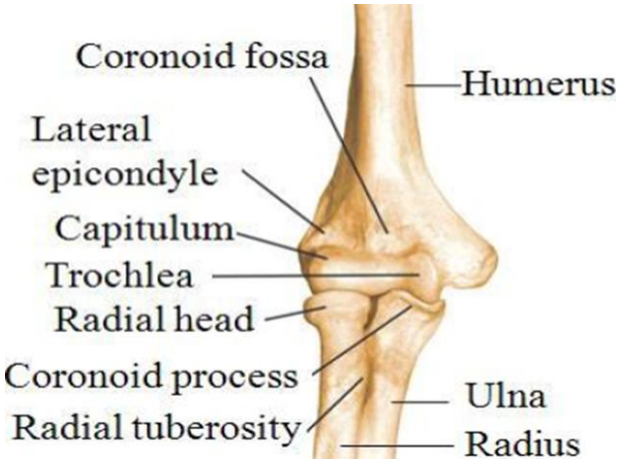

Figure (1.5): Elbow joint[2]

1.3.5 Upper Arm

It extends from the shoulder to the elbow. It contains the humerus bone and is surrounded by major muscles such as the biceps, which are responsible for flexing the elbow, and the triceps, which are responsible for extending the elbow.

1.3.6 Shoulder

It is the point of connection of the arm to the trunk. It is a ball-and-socket joint that allows movements in all directions, such as lifting, rotating, and twisting. It plays an important role in determining the general range of motion of the arm, as shown in Figure 1.6.

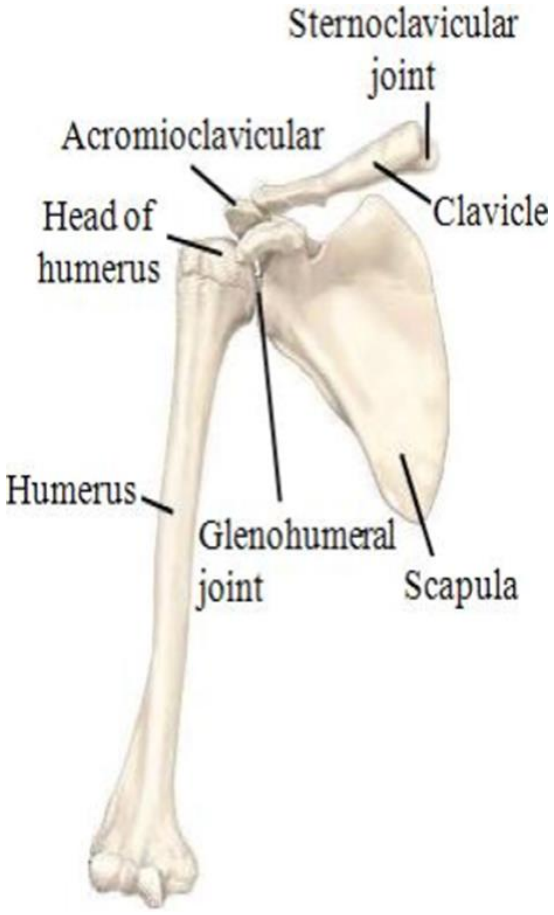

Figure (1.6): Shoulder joint[2]

Figure (1-7) shows the main parts of the human arm

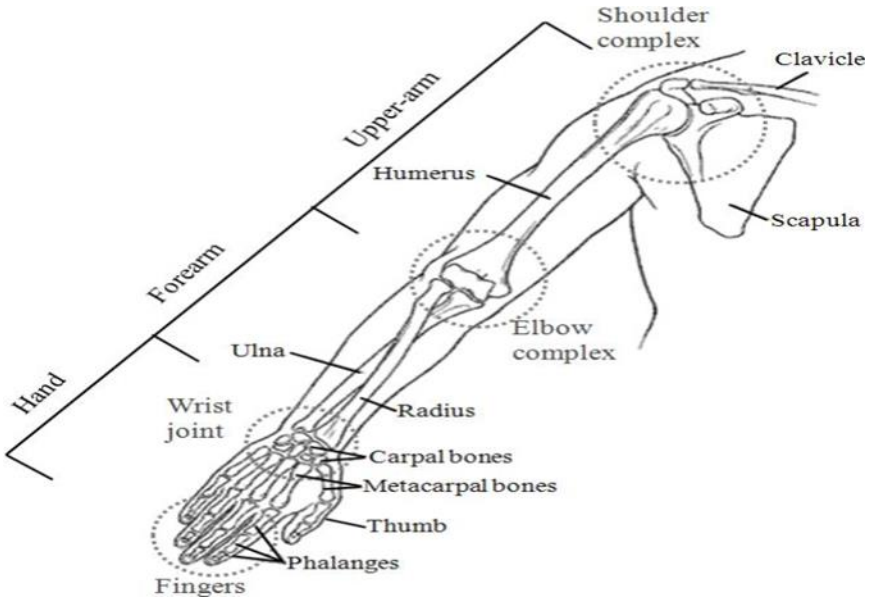

Figure (1.7): Segments of upper limb [2]

1.4 The Objectives of this Work

The primary aim of this thesis is to develop and validate an optimized and analytically controlled dynamic model of a five-degree-of-freedom (5-DOF) human arm–exoskeleton system that achieves fast, stable, and accurate motion with minimal overshoot under a wide range of operating conditions. The system is modeled using the Lagrange-Euler method to develop a set of second-order equations, which are then linearized to optimize the system parameters using Lagrangian multipliers optimization method.

To achieve this aim, the following objectives are addressed:

1.To model the nonlinear dynamics of a 5-DOF human arm using the Lagrange–Euler method and obtain a linearized model for control and optimization.

2. To optimize the system parameters (masses, damping, and stiffness) using the Lagrangian multipliers method to achieve short settling time and

minimum overshoot.
3. To design an analytical exoskeleton controller based on eight-term exponential reference functions while satisfying torque constraints.
4. To evaluate the system performance under a wide range of initial conditions and parameter variations.
5. To validate the proposed approach using numerical simulations and Monte Carlo analysis.

The main contributions of this thesis is development of an analytical eight-term exponential reference trajectory that satisfies initial, intermediate, and final boundary conditions with explicitly enforcing elbow torque constraints.

1.5 Summary

This chapter serves as a general introduction to the research, presenting the scientific background of the topic of mechanical arms and exoskeletons, clarifying the importance and objectives of the research, and providing an overview of the research structure. In the next chapter, previous studies related to the topic of artificial arms will be reviewed to identify this research within the current scientific efforts.

Chapter Two: Literature Review

2.1 Introduction

In this chapter, a brief overview of innovative approaches and methodologies developed to enhance the control of human arm movements, particularly focusing on trajectory control, optimization of control strategies, and the use of artificial muscles in robotic systems. In recent years, researchers have increasingly turned to advanced computational techniques to tackle the challenges associated with controlling the nonlinear dynamics of human arm movements. The structure of the human upper limb is presented. Then, the types of human arm and control approaches are presented. Control approaches are highlighted, and recent advances in human arm movements are described. In recent years, researchers have increasingly turned to advanced computational techniques to tackle the challenges associated with controlling the nonlinear dynamics of human arm movements.

2.2 Mathematical Model

The mathematical model describes the dynamic response behavior of a system and is usually represented by a set of linear and nonlinear ordinary differential equations. For the actuator valve example, the mathematical model consists of a differential equation describing the armature valve mass combined with linear viscous friction.

The research presented in this thesis addresses this modeling approach.

(Artemiadis et al., 2010)[6] estimated the mechanical impedance of the human upper limb in three-dimensional space using a 7-DOF robotic arm. Small Cartesian displacements were applied to the hand, and the end-point dynamics were modeled as a linear second-order system to identify stiffness, viscosity, and inertia. The results confirmed that mechanical impedance

effectively describes human arm dynamics and is useful for human–robot interaction and exoskeleton design.

(Ao, 2009)[7] focused on the movements of the human upper arm(shoulder, wrist, elbow and finger).These analyzes have been extended to design a humanoid robot manipulator. They designed a simulator direct kinematic and inverse kinematic of the upper arm. MATLAB software was used using Virtual Reality Modeling Language (VRML). The Denavit-Hartenberg (D-H) method was used to solve the equations, the Lagrange method to determine the equations of motion, and the Newton-Euler method to formulate the model. The results provide a basis for designing robotic manipulators that can follow prescribed human-like motion trajectories.

(Mailah et al., 2009)[8] studied a two-link planar mechanical manipulator that mimics a human arm. They focuses on a simple and computationally efficient control algorithm. The arm is subjected to vibrations while performing 2D trajectory tracking, considering mathematical models of "muscle" elements. A closed-loop active force control system is used to handle disturbances under predefined conditions. Results show that the method effectively compensates for vibrations, achieving robust and accurate tracking, which can help in designing precise mechatronic devices like robotic arms or smart gloves.

(Hao et al., 2011)[9] presented the design and development of a 6-DOF PC-based robotic arm (PC-ROBOARM). The arm is modeled as a three-link system with servomotors at each joint and is controlled using custom software called SMART ARM. The software provides a user-friendly GUI for virtual design, trajectory simulation, and control of the actual robotic arm, helping to optimize design, reduce building costs, and simplify control implementation.

The arm, based on the PUMA jointed-arm model, is tested for both point-to-point and continuous path motions, demonstrating accurate simulation and real-world performance.

(Jolly Shah, S.S.Rattan & Abstract—Automatic, 2011)[10] used artificial neural networks to analyze the robot's kinematics with two degrees of freedom. Forward and inverse kinematics were solved using artificial neural networks, as using them the solution is faster, acceptable, and has no error. It is also considered an effective way to deal with nonlinear systems and to model complex systems. The Denavit-Hartenberg (D-H) method was used to model the robot's joints.

(Al-zu et al., 2012)[11] develops a 2D three-segment coupled pendulum system to model the human arm using the Lagrangian energy-based approach. The equations of motion are solved iteratively as both an initial value problem and a two-point boundary value problem. Results show the system is sensitive to small changes in forces and initial/boundary conditions, and a new approach is proposed to reduce this sensitivity.

(Fadhil Abbas, 2013)[12] presented a mathematical model for direct forward kinematic analysis of a 5-degree-of-freedom articulated robot arm. The modelling method adopted the coordinates of each joint of the robot as it moved from one location to another. The Lab-volt R5150 educational robot was used to test the proposed models. The D-H method was used to calculate the site coordinates, and the MATLAB program was used for simulation and evaluation.The results of several experiments demonstrated the accuracy of the proposed model for representation and simulation, as it was found that the maximum error does not exceed (0.001).

(Serbest et al., 2016)[13] presented a 16-DOF kinematic model of the human hand developed in MATLAB using SimMechanics and Simulink. Joint torques of the index finger and wrist are calculated via inverse dynamics from video recordings of a healthy subject. The model allows analysis of various finger and wrist movements and provides an easy way to estimate joint torques without complex equations or external devices.

(Sheng et al., 2016)[14] proposed a model of a universal robot (6 degrees of freedom) used in the rehabilitation system. The Denavit-Hartenberg (D-H) method was used for dynamic analysis. The Newton-Euler equation was used, which is inspired by the Lagrange equation and is suitable for a multi-degree of freedom system. Each joint was actuated by a single motor separately to achieve relative motion of adjacent links. The simulation results showed that the proposed mathematical model can provide an effective environment for designing a rehabilitation robot and planning clinical trials. The actual mathematical model was implemented based on MATLAB SimMechanics.

(Barakat et al., 2017)[15] studied the kinematics of a robotic arm, designing its parameters and analyzing forward and inverse kinematics using the Denavit–Hartenberg (DH) method. A MATLAB 3D simulation is created to visualize joint movements and trajectory planning, successfully enabling the arm to draw a sine wave on a writing board.

(Agarana & Akinlabi, 2018a)[16] studied models the human arm as a three-segment dynamical pendulum system using the Euler-Lagrange method. The resulting differential equations are solved analytically, and simulations in Maple show that angular displacements are proportional to angular accelerations. Longer arm segments lead to slower swings and fewer oscillations per second.

(Agarana & Akinlabi, 2018b)[17] modeled the human arm as a dynamic triangular pendulum system. The arm motion equation was obtained using the Lagrange-Euler equation. The second-order differential equation is solved analytically. The results were simulated using the Maple program in MATLAB.

(Li et al., 2020)[18] created a serial-parallel hybrid arm (6 DOF).The electric cylinder was used to convert the rotating mechanical force generated by the electric motor into linear motion .The influence of the external force, the force of gravity and the force of inertia is taken into account, and the forces of friction are neglected. The dynamic model was created by the D-H method. The inertia force was calculated by the Lagrange method. It was concluded that the energy decreases to 23.77% after optimization.

(Khan et al., 2020)[19] proposed a dual particle swarm optimization (DPSO) approach for solving the inverse kinematics of a 6-DOF SCARA robot. By separating position and orientation optimization, DPSO achieves faster convergence with fewer iterations. Implemented in MATLAB/Simulink and tested with dual joysticks, the method effectively controls the robot in real-time within joint constraints.

(Mohanto et al., 2020)[20] presents the mathematical modeling of a three-degree-of-freedom (3-DOF) robotic arm using forward and inverse kinematics to determine the position and orientation of the end effector. Based on the developed model, a physical prototype was implemented using an Arduino Mega, along with a MATLAB GUI for simulation and visualization. The system is capable of RGB-based color sorting, allowing objects of different colors to be placed in specified locations. Experimental results

confirm the effectiveness of the proposed approach, which offers high efficiency at low cost.

(Dawood Salman et al., 2021)[21] presented a kinematic model of a three-degree-of-freedom articulated robot arm. The forward kinematics was calculated using the D.-H method. An algebraic solution based on trigonometric formulas combined with the geometric method was adopted to calculate the inverse kinematics. MATLAB GUI was used to simulate the results. The robot is designed based on SolidWorks. Microstepping drivers are used to realise more precise control and smooth movement. The results showed that the theoretical analysis supports the actual implementation with some minor differences.

(Moses et al., 2022)[22] focused on a robotic arm controlled using accelerometers to capture natural human arm movements and replicate them in the robotic system. Such a control approach offers greater flexibility compared to conventional methods that control each actuator independently. A processing unit interprets accelerometer inputs to generate appropriate control signals for each actuator. Robotic arms resemble human arms in structure, with joints and customizable end effectors that enable them to perform a wide variety of tasks depending on their intended application.

(Rohit Kumar et al, 2021)[23] analyzed the effect of vibrations on a standing human body to reduce discomfort and potential injuries. A 3D CAD model of a 76-kg human subject was created and analyzed using FEM harmonic response in the frequency range of 2–20 Hz. The results showed resonance at 6 Hz in the vertical direction and significant vibration in the fore-and-aft direction at 4 Hz. These findings help in designing more comfortable supports

and reducing vibration-related discomfort, and they agree well with existing studies.

(Dong et al., 2021)[24] conducted studies on hand-transmitted vibration exposure, biodynamic responses, and biological effects over the past 20 years, systematically reviewing the literature and identifying areas requiring further research. These studies collectively demonstrate the ongoing efforts in modeling and optimizing both robotic and prosthetic arms, employing a variety of advanced mathematical methods, computational tools, and design techniques to enhance their performance and functionality. The continued evolution of these models played a critical role in improving the capabilities of prosthetic devices, making them more effective and versatile for users.

2.3 Control system

Control systems are one of the most important fields of modern engineering, as they regulate the behavior of mechanical systems and make them operate according to the required objectives. The control principle works by comparing actual outputs with reference values and adjusting inputs to achieve optimal system performance. Through control science, system stability is improved, errors are reduced, response speed is increased, and vibrations are reduced. Therefore, control systems are not limited to the theoretical aspect, but rather extend to practical applications that increase the efficiency of engineering systems. The work presented in this thesis investigates the above.

(Liu et al., 2008) [25] described the study as a musculoskeletal model with two degrees of freedom. The study aims to control the movement of the human arm on the sagittal plane, i.e. the vertical plane, where a controller was implemented by integrating DRNN (a neural network that is more suitable for

dynamic representations) with the genetic algorithm (GA) and the evolutionary program. (EP) The results were compared and it was noted that DRNN is the best way to control the movement of the human arm in the sagittal plane.

(Mohammed Z. Al-Faiz et al, 2012)[26] used soft computing methodologies to control the human arm with seven degrees of freedom. presented a PID tuning method by Particle Swarm Optimization (PSO) to improve the time response of the system such as settling and overshoot time. MATLAB is used with virtual reality tools as it is easy to manipulate 3D objects defined using VRML. The human arm was implemented by virtual reality technology and the joints were realized by MATLAB.

(Rashidifar et al., 2013)[27] designed a control technology aimed at using the high-precision performance of robotic manipulators in complex and dangerous environments. Both forward and inverse kinematics were derived based on the D-H method. The PID controller was used as a reference to compare the results with the (FLC) fuzzy logic controller and (FSC) fuzzy supervisory control. FSC is a hybrid between a PID controller and an FLC designed to overcome the problem of PID tuning in nonlinear systems by using the FLC as an adaptive controller. All simulations were presented using Matlab Simulink. Simulation results prove that FLC gives better results than the classical PID controller in terms of time response and reducing error and overshoot, and that FSC is better than classical methods such as (ZN) Ziegler-Nichols.

(Mourya et al., 2015)[28] designed and manufactured a robotic manipulator with 4 degrees of freedom. His project is self-run. DC motors were used instead of hydraulic and pneumatic motors because of the lower power

required and their light weight. The controller used is AT Mega 16, and a continuous path controller (PIC) is used. AutoCAD model (cero program) was used to design the arm as it provides a three-dimensional image. The kinematic equations were solved by the D-H method. The ANSYS program was used to formulate the finite method used to calculate the displacement of components.

(Mohit Dhaka et al., 2016)[29] used Solid Works Motion, a 3D CAD program, to design articulated robotic arms and mechanisms. Simulated using LabVIEW. The control system is designed using Arduino, where a virtual prototyping system was developed using Arduino instead of making a physical prototype**.**

(Nasr et al., n.d.)[30] designed and controlled a robot arm with six degrees of freedom. MATLAB SimMechanics was used to model and simulate the arm and development between MATLAB SimMechanics and Autodesk was used to move the robot arm. Laser pins were used to sense the position of the clutch. The D.G. method was used to solve the kinematic equation. Stresses and deflections were checked using Autodesk. Due to the high nonlinearity in the robotic inverse, the inverse kinematics was used to manufacture the PID controller and obtain the required angular displacement.

(Okubanjo et al., 2017)[31] modelled the dynamics of a 2-degree-of-freedom arm using a set of second-order nonlinear elements. The dynamics were carefully simulated using the Lagrange-Euler method. The PID controller is designed and tuned based on the trial and error method. Different articulation angles were established and responses were observed before implementing the actual model. The robot arm was controlled to reach and remain within

the desired joint angle position by implementing and simulating the PID controller using MATLAB Simulink.

(Ghaleb & Aly, 2018)[32] modelled, simulated, and controlled a 2-degree of freedom robot arm. Kinematics were analyzed by the D-H method. The Euler-Lagrange equation was used. The design was made by PID controller. MATLAB Simulink program was used. A permanent magnet DC motor is used to operate the system, which contains an electrical part and a mechanical part. Through experience, it has been shown that the slightest change in the control unit parameter leads to overshoot and more oscillations, and this requires adjusting the gains of the PID controllers and rotating them at every moment to prevent overshoot.

(Bi, 2020)[33] focuses on the design of a two-degree-of-freedom PID control algorithm. The traditional PID control method has been improved to 2DOF PID control by introducing a fuzzy trapezoid MATLAB was used for simulation because the robot arm cannot be modeled, studied and controlled through fuzzy control theory.It has been observed through experiments that the system response speed is faster, the error is smaller, and the control effect is better.

(Nguyen et al., 2020)[34] studied the construction of a mechanical model of a robotic arm featuring a pneumatic artificial muscle motor to rehabilitate the elbow joint. An adaptive fast tip-slip mode controller was developed and experimentally evaluated to obtain the desired response .The stability of the control unit was analyzed according to Lyapunov's theory and the laws of the fuzzy model were obtained. Experimental results have proven that the proposed controller works successfully with nonlinear dynamic information.

(Salman et al., 2021)[35] The Lagrange-Euler method was used to dynamically model the robot with five degrees of freedom. The PID controller is implemented with a PIDN pass filter, which improves the control performance .The Ziegler-Nichols method was used to tune the PID controller. The model simulation was performed in MATLAB.

(Majeed et al., 2022)[36] designed a device to control the finger of the human hand. The string is modelled and controlled instead of the actuators with 3 degrees of freedom. The Lagrange equation was used. Classic sliding mode control (CSMC) techniques were used to control finger movement, and to overcome the disadvantages of CSMC, an adaptive sliding mode controller was used. MATLAB simulation was used for the simulation. The results showed the superiority of ASMC over CSMC in reducing the phenomenon of chatter and responding quickly.

2.4 Exoskeleton

An exoskeleton is defined as an external wearable mechanism that is worn and moves parallel to the human body. In general, exoskeletons could be categorized into upper-extremity, lower-extremity, and whole-body types. The functions of the exoskeleton are varied. An exoskeleton may be used for augmentation or supplementation, for rehabilitation or assistance. Issues of significant importance that need to be considered in the research and development of an exoskeleton, such as design and control challenges.

(Grimm et al., 2021) [37] A gravity-compensating multi-joint exoskeleton (Armeo spring) was used for the arm. This sensor-based assessment was compared to the clinical outcome scale (COS) of the Vogel-Meyer assessment of the upper extremity,where the range of motion in the joint space of four

individual joints was assessed, and an exoskeleton-based subjective assessment of single-joint movements was applied. A valid clinical assessment of the upper extremity range of motion can be performed in stroke patients with severe impairment. The shoulder concussion rate significantly contributed to the prediction of clinical status. Real-time sensor data from the exoskeleton was used to display a 3D multi-joint visualisation of the user's arm using virtual reality technology. A virtual representation of the patient's arm was displayed on a computer screen. The programming was done in the Microsoft XNA framework. MATLAB and SPSS were used to conduct statistical analysis.

(Kansal et al., 2022)[38] An upper limb exoskeleton is designed and developed for remote control of an industrial robot using an immersive environment (i.e. avoiding the operator being in dangerous, dirty and boring environments) as a visual response to the operator. This work can be applied in nuclear power plants. In this research, a new interactive technique based on hand gestures for 3D navigation in virtual environments is presented, the proposed technology also allows users to efficiently control speed during navigation. A low-cost exoskeleton for the attachment was presented, and a control scheme was used to control the upper limb exoskeleton with seven degrees of freedom. Two systems were used, one to measure the kinematics produced by the exoskeleton and the other for the KUKA control unit.

(de Vries et al., 2023)[39]A field study was conducted in which 39 plasterers were fitted with an exoskeleton for 6 weeks to study the use of the exoskeleton, including workload, fatigue, behavior, productivity, quality, advantages, disadvantages, and acceptance. The study showed that 65% of plasterers would like to use the exoskeleton and are enthusiastic about its load-

reducing effect. This is the first study to introduce exoskeletons to a target group and monitor the use of the exoskeleton.

(Chen et al., 2023)[40] Presented a machine learning computing approach for processing 12 channels of myoelectric signals from the shoulder and upper limb to recognize shoulder movement patterns and control the upper arm exoskeleton in real time. The accuracy of the three machine learning algorithms was evaluated and compared to determine the optimal machine learning algorithm. The results showed that the SVM algorithm achieved better accuracy than the LR and ANN algorithms. The study also demonstrated that machine learning computing provides a reliable approach for recognizing shoulder motion patterns and that the offline pattern recognition system outperforms the current exoskeleton motion control accuracy.

(Ramella et al., 2024)[41] An experiment was designed to test different levels of anti-gravity support using a passive upper limb exoskeleton and its effects on electromyographic signals were determined. Average muscle activation was calculated over complete cycles and sub-cycles, particularly during the arm raising and lowering phases. The results showed that the use of the exoskeleton led to a decrease in electromyographic activation for all muscles compared to the case without the exoskeleton.

(Grazi et al., 2024)[42] The first systematic analysis of muscle activation in the context of electrical stimulation is presented, demonstrating its potential to enhance understanding of the biomechanical effects of this technique. Dynamic and repetitive upper extremity movements were targeted. The results showed that peak and mean levels of co-activation decreased linearly with increasing anti-gravity support provided by the upper extremity exoskeleton.

This study represents the first case in which passive upper extremity movements have been shown to reduce co-activation of the shoulder muscles, paving the way for a new methodology for its assessment.

2.5 Summary

The reviewed studies show that most previous research focused on the modeling and control of human arm and upper-limb exoskeleton systems using conventional control techniques and numerical trajectory generation methods. While acceptable tracking performance was achieved, limited attention was given to analytical trajectory design and analytical torque computation with guaranteed fast response and low overshoot.

In this work, a novel analytical approach is proposed for a five-degree-of-freedom human arm model, where the system parameters are optimally selected using a Lagrangian multipliers method. An eight-term exponential function is used to generate the reference trajectory, and the corresponding joint torques are analytically derived. The proposed approach is validated through Monte Carlo simulations, demonstrating improved performance and robustness compared to existing methods.

Chapter Three

Theoretical Analysis (Linear and Nonlinear Models)

3.1 Introduction

The objective of the present chapter will be divided into three main sections. The first section focuses on mathematical modelling, in which critical main equations related to kinetic, potential, and dissipation energies are used to model the proposed arm system using the Lagrangian method . To simlify the system model, the second section includes converting a nonlinear set of equations to a linear set of equations. Evantually, the third section involves optimizing (15) system's parameters to obtain a short settling time and low overshoot. Figure 3.1 represents the flowchart of the research methodology.

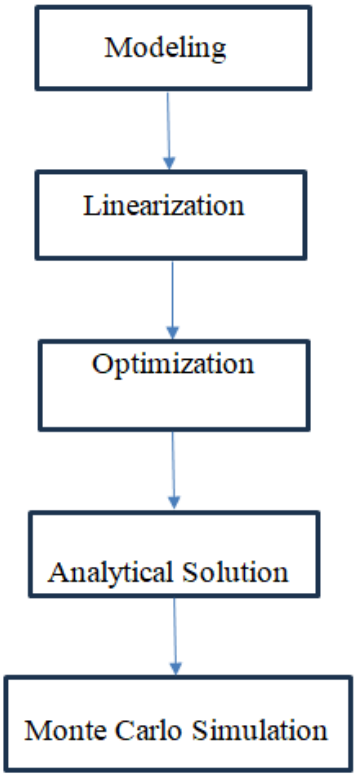

Figure (3.1): Flowchart of the research methodology.

3.2 Robotic Arm System Model

A mathematical model provides a formal description of the dynamic behavior of a system, typically illustrated by a set of nonlinear ordinary differential equations. For the artificial human arm, the model consists of differential equations that represent its mechanical motion, taking into account inertia, joint torques, external forces, and energy dissipation. Figure (3-2) shows a model of an artificial human arm, which may be used by mechanical devices to provide functional movements of a human arm in diverse applications such as rehabilitation, sports, and innovation.

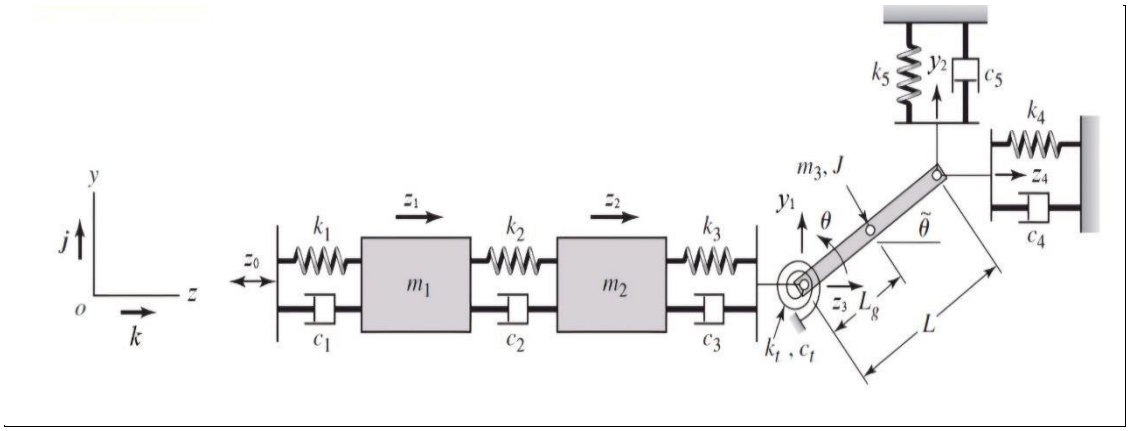

Figure (3.2): Modelling of an Artificial human arm[43]

A mathematical model of the human arm system can indeed be exhibited using a Mass-Damper-Spring model. The system has five degrees of freedom, which are represented by the coordinates: $z_1, z_2, z_3, y_1, \theta$. The angle $\tilde{\theta}$ shows the nominal position of the upper arm where we will analyze the vibrations. The coordinates z_1, z_2, z_3 represent the longitudinal motions of the hand, the forearm, and the elbow, respectively, while the coordinates y_1, θ introduces the vertical and rotational motions of the elbow joint, respectively. The value z_0 describes the external displacement acting on the hand.

3.2.1 Kinetic energy

In our system, energy can be obtained from different forms: kinetic energy, potential energy, and dissipated energy. The human arm system generates kinetic energy due to the motion of the hand, forearm and the elbow. In this model, the kinetic energy of the hand and forearm components comes from the horizontal motion only.

$$K_{E_1} = \frac{1}{2} m_1 \dot{z}_1{}^2 \tag{3.1}$$

$$K_{E_2} = \frac{1}{2} m_2 \dot{z}_2{}^2 \tag{3.2}$$

Where m_1 & m_2 represented the masses of the hand and forearm, respectively. The kinetic energy at the elbow results from both horizontal and vertical motion. Therefore, the distance to the center of gravity of the upper arm is represented as a vector, indicating the displacement of the third mass.

$$\overrightarrow{r_g} = \left[z_3 + L_g \cos\left(\theta + \tilde{\theta}\right)\right] i + \left[y_1 + L_g sin\left(\theta + \tilde{\theta}\right)\right] k \tag{3.3}$$

L_g: The half − length of the upper arm

Deriving equation (3.3) to get the velocity.

$$\overrightarrow{v_g} = \left[\dot{z}_3 - L_g \dot{\theta} \sin\left(\theta + \tilde{\theta}\right)\right] i + \left[\dot{y}_1 + L_g \dot{\theta} \cos\left(\theta + \tilde{\theta}\right)\right] k \tag{3.4}$$

The product of the two velocity vectors for equation (3.4) is calculated using the dot product:

$$\overrightarrow{v_g}.\overrightarrow{v_g} = \left\{\left[\dot{z}_3 - L_g \dot{\theta} \sin\left(\theta + \tilde{\theta}\right)\right] i + \left[\dot{y}_1 + L_g \dot{\theta} \cos\left(\theta + \tilde{\theta}\right)\right] k\right\}.\left\{\left[\dot{z}_3 - L_g \dot{\theta} \sin\left(\theta + \tilde{\theta}\right)\right] i + \left[\dot{y}_1 + L_g \dot{\theta} \cos\left(\theta + \tilde{\theta}\right)\right] k\right\}$$

$$\overrightarrow{v_g}.\overrightarrow{v_g} = \left[\dot{z}_3 - L_g \dot{\theta} \sin\left(\theta + \tilde{\theta}\right)\right]^2 + \left[\dot{y}_1 + L_g \dot{\theta} \cos\left(\theta + \tilde{\theta}\right)\right]^2 \tag{3.5}$$

Kinetic energy of mass m moving with velocity v_g and moment of inertia J rotating with angular velocity $\dot{\theta}$.

$$K_{E_3} = \frac{1}{2} m_3 \overrightarrow{v_g}.\overrightarrow{v_g} + \frac{1}{2} J \dot{\theta}^2 \tag{3.6}$$

Where m_3 is called the mass of the upper arm, J is the rotational inertia.

By substitute eq.(3.5) into eq.(3.6)

$$K_{E_3} = \frac{1}{2} m_3 \left\{ \left[\dot{z}_3 - L_g \dot{\theta} \sin(\theta + \tilde{\theta}) \right]^2 + \left[\dot{y}_1 + L_g \dot{\theta} \cos(\theta + \tilde{\theta}) \right]^2 \right\} + \frac{1}{2} J \dot{\theta}^2 \quad (3.7)$$

Therefore, the total kinetic energy can be obtained by summing all the kinetic energy equations:

$$K_E = \frac{1}{2} m_1 \dot{z}_1{}^2 + \frac{1}{2} m_2 \dot{z}_2{}^2 + \frac{1}{2} m_3 \begin{Bmatrix} \left[\dot{z}_3 - L_g \dot{\theta} \sin(\theta + \tilde{\theta}) \right]^2 \\ + \left[\dot{y}_1 + L_g \dot{\theta} \cos(\theta + \tilde{\theta}) \right]^2 \end{Bmatrix} + \frac{1}{2} J \dot{\theta}^2 \quad (3.8)$$

3.2.2 Potential energy

The second source of energy in this system is potential energy, which primarily depends on elastic and gravitational forces. In a mechanical system, potential energy can be stored exclusively by mass and spring components. Therefore, the muscles in the arms exhibit elastic properties, allowing them to absorb and release energy similarly to a spring. This system contains five possible forms of potential energy:

$$P_{E_1} = \frac{1}{2} k_1 (z_1 - z_0)^2 \quad (3.9)$$

$$P_{E_2} = \frac{1}{2} k_2 (z_2 - z_1)^2 \quad (3.10)$$

$$P_{E_3} = \frac{1}{2} k_3 (z_3 - z_2)^2 \quad (3.11)$$

$$P_{E_4} = \frac{1}{2} k_t (\theta + \tilde{\theta})^2 \quad (3.12)$$

$$P_{E_5} = \frac{1}{2} k_4 z_4{}^2 \quad (3.13)$$

The springs and dampers at $z_4$and y_2 have displacements that are related by (z_3, y_1, θ) in order to find the potential energy of all the springs and dampers, respectively.

$$z_4 = z_3 + Lcos(\theta + \tilde{\theta}) \tag{3.14}$$

Substitute eq.(3.14) in eq.(3.13)

$$P_{E_5} = \frac{1}{2} k_4 [z_3 + Lcos(\theta + \tilde{\theta})]^2 \tag{3.15}$$

$$P_{E_6} = \frac{1}{2} k_5 {y_2}^2 \tag{3.16}$$

$$y_2 = y_1 + Lsin(\theta + \tilde{\theta}) \tag{3.17}$$

Substitute eq.(3.17) in eq.(3.16)

$$P_{E_6} = \frac{1}{2} k_5 [y_1 + Lsin(\theta + \tilde{\theta})]^2 \tag{3.18}$$

Furthermore, the elbow exhibits gravitational force due to its position relative to the reference point

$$P_{E_7} = m_3 g [y_1 + L_g sin(\theta + \tilde{\theta}] \tag{3.19}$$

The total potential energy can be extracted as the sum of the potential energy equations :

$$\begin{aligned} P_E = \frac{1}{2} \{ & k_1 (z_1 - z_0)^2 + k_2 (z_2 - z_1)^2 + k_3 (z_3 - z_2)^2 + k_t (\theta + \tilde{\theta})^2 \\ & + k_4 [z_3 + Lcos(\theta + \tilde{\theta})]^2 + k_5 [y_1 + Lsin(\theta + \tilde{\theta})]^2 \} \\ & + m_3 g [y_1 \, L_g sin(\theta + \tilde{\theta}] \end{aligned} \tag{3.20}$$

3.2.3 Dissipated energy

It is energy that has been converted into forms that are unhelpful or unusable for work. It is essentially energy that gets "lost" from a system, frequently manifesting as heat or sound, rendering it unavailable for its original function. The arm muscles can resist movement, allowing them to

absorb energy and reduce fluctuations, as with a damper. This system has five forms of dissipated energy:

$$D_{E_1} = \frac{1}{2} c_1 (\dot{z_1} - \dot{z_0})^2 \quad (3.21)$$

$$D_{E_2} = \frac{1}{2} c_2 (\dot{z_2} - \dot{z_1})^2 \quad (3.22)$$

$$D_{E_3} = \frac{1}{2} c_3 (\dot{z_3} - \dot{z_2})^2 \quad (3.23)$$

$$D_{E_4} = \frac{1}{2} c_t \dot{\theta}^2 \quad (3.24)$$

$$D_{E_5} = \frac{1}{2} c_4 \dot{z_4}^2 \quad (3.25)$$

By deriving equation (3.14)

$$\dot{z_4} = \dot{z_3} - L\dot{\theta} \sin(\theta + \tilde{\theta}) \quad (3.26)$$

Substitute eq.(3.26) in eq.(3.25)

$$D_{E_5} = \frac{1}{2} c_4 \left[\dot{z_3} - L\dot{\theta} \sin(\theta + \tilde{\theta})\right]^2 \quad (3.27)$$

In addition, energy can be lost due to friction at the elbow joint

$$D_{E_6} = \frac{1}{2} c_5 \dot{y_2}^2 \quad (3.28)$$

By deriving equation (3.17)

$$\dot{y_2} = \dot{y_1} + L\dot{\theta} \cos(\theta + \tilde{\theta}) \quad (3.29)$$

Substitute eq.(3.29) in eq.(3.28)

$$D_{E_6} = \frac{1}{2} c_5 \left[\dot{y_1} + L\dot{\theta} \cos(\theta + \tilde{\theta})\right]^2 \quad (3.30)$$

The total wasted energy can be presented as shown below:

$$D_E = \frac{1}{2}\Big\{c_1(\dot{z}_1 - \dot{z}_0)^2 + c_2(\dot{z}_2 - \dot{z}_1)^2 + c_3(\dot{z}_3 - \dot{z}_2)^2 + c_t\dot{\theta}^2 + c_4\big[\dot{z}_3 - L\dot{\theta}\sin(\theta + \tilde{\theta})\big]^2 + c_5\big[\dot{y}_1 + L\dot{\theta}\cos(\theta + \tilde{\theta})\big]^2\Big\} \quad (3.31)$$

The proposed human arm model, like any mechanical engineering system, follows the principle of energy conservation. The Euler-Lagrange method will be used to describe the arm's motion by including the effects of kinetic, potential, and dissipated energies[43].

$$\frac{d}{dt}\left[\frac{\partial K_E}{\partial \dot{q}_i}\right] - \frac{\partial K_E}{\partial q_i} + \frac{\partial P_E}{\partial q_i} + \frac{\partial D_E}{\partial \dot{q}_i} = Q_i \quad (3.32)$$

where q represents the state variable and the index i refers to the number of degrees of freedom. To find the governing equations of motion, the human arm system is assumed to have five degrees of freedom, with no external forces (Q) acting on it. The first nonlinear governing equation of motion can be derived as follows

$$\frac{d}{dt}\left[\frac{\partial K_E}{\partial \dot{z}_1}\right] - \frac{\partial K_E}{\partial z_1} + \frac{\partial D_E}{\partial \dot{z}_1} + \frac{\partial P_E}{\partial z_1} = Z_1 \quad (3.33)$$

$$\frac{d}{dt}\left[\frac{\partial K_E}{\partial \dot{z}_1}\right] = \frac{d}{dt}(m_1\dot{z}_1) = m_1\ddot{z}_1$$

$$\frac{\partial K_E}{\partial z_1} = 0$$

$$\frac{\partial D_E}{\partial \dot{z}_1} = \frac{1}{2} * 2c_1(\dot{z}_1 - \dot{z}_0) + \frac{1}{2} * 2c_2(\dot{z}_2 - \dot{z}_1) * -1$$

$$\frac{\partial D_E}{\partial \dot{z}_1} = c_1(\dot{z}_1 - \dot{z}_0) - c_2(\dot{z}_2 - \dot{z}_1)$$

$$\frac{\partial P_E}{\partial z_1} = \frac{1}{2} * 2k_1(z_1 - z_0) + \frac{1}{2} * 2k_2(z_2 - z_1) * -1$$

$$\frac{\partial P_E}{\partial z_1} = k_1(z_1 - z_0) - k_2(z_2 - z_1)$$

Then equation (3.33) can be eventually expressed by:

$$m_1\ddot{z}_1 + c_1(\dot{z}_1 - \dot{z}_0) - c_2(\dot{z}_2 - \dot{z}_1) + k_1(z_1 - z_0) - k_2(z_2 - z_1) = 0$$

$$m_1\ddot{z}_1 + (c_1 + c_2)\dot{z}_1 - c_2\dot{z}_2 + (k_1 + k_2)z_1 - k_2z_2 = c_1\dot{z}_0 + k_1z_0 \quad (3.34)$$

The second nonlinear governing equation of motion can be derived as follows

$$\frac{d}{dt}\left[\frac{\partial K_E}{\partial \dot{z}_2}\right] - \frac{\partial K_E}{\partial z_2} + \frac{\partial D_E}{\partial \dot{z}_2} + \frac{\partial P_E}{\partial z_2} = Z_2 \quad (3.35)$$

$$\frac{d}{dt}\left[\frac{\partial K_E}{\partial \dot{z}_2}\right] = \frac{d}{dt}(m_2\dot{z}_2) = m_2\ddot{z}_2$$

$$\frac{\partial K_E}{\partial z_2} = 0$$

$$\frac{\partial D_E}{\partial \dot{z}_2} = \frac{1}{2} * 2c_2(\dot{z}_2 - \dot{z}_1) + \frac{1}{2} * 2c_3(\dot{z}_3 - \dot{z}_2) * -1$$

$$\frac{\partial D_E}{\partial \dot{z}_2} = c_2(\dot{z}_2 - \dot{z}_1) - c_3(\dot{z}_3 - \dot{z}_2)$$

$$\frac{\partial P_E}{\partial z_2} = \frac{1}{2} * 2k_2(z_2 - z_1) + \frac{1}{2} * 2k_3(z_3 - z_2) * -1$$

$$\frac{\partial P_E}{\partial z_2} = k_2(z_2 - z_1) - k_3(z_3 - z_2)$$

$$m_2\ddot{z}_2 + c_2(\dot{z}_2 - \dot{z}_1) - c_3(\dot{z}_3 - \dot{z}_2) + k_2(z_2 - z_1) - k_3(z_3 - z_2) = 0$$

$$m_2\ddot{z}_2 + (c_2 + c_3)\dot{z}_2 - c_2\dot{z}_1 - c_3\dot{z}_3 + (k_2 + k_3)z_2 - k_2z_1 - k_3z_3 = 0 \quad (3.36)$$

The third nonlinear governing equation of motion can be derived as follows

$$\frac{d}{dt}\left[\frac{\partial K_E}{\partial \dot{z}_3}\right] - \frac{\partial K_E}{\partial z_3} + \frac{\partial D_E}{\partial \dot{z}_3} + \frac{\partial P_E}{\partial z_3} = Z_3 \quad (3.37)$$

$$\frac{d}{dt}\left[\frac{\partial K_E}{\partial \dot{z}_3}\right] = \frac{d}{dt}\left[\frac{1}{2} * 2m_3\dot{z}_3 - \frac{1}{2}m_3 * 2L_g\dot{\theta}\sin\left(\theta + \tilde{\theta}\right)\right]$$

$$= \frac{d}{dt}\left[m_3(\dot{z}_3 - L_g\dot{\theta}\sin\left(\theta + \tilde{\theta}\right))\right]$$

$$\frac{d}{dt}\left[\frac{\partial K_E}{\partial \dot{z}_3}\right] = m_3\left\{\ddot{z}_3 - L_g\left[\dot{\theta}cos\left(\theta + \tilde{\theta}\right)\dot{\theta} + sin\left(\theta + \tilde{\theta}\right)\ddot{\theta}\right]\right\}$$

$$= m_3[\ddot{z}_3 - L_g\cos\left(\theta + \tilde{\theta}\right)\dot{\theta}^2 - L_g\sin\left(\theta + \tilde{\theta}\right)\ddot{\theta}]$$

$$\frac{\partial K_E}{\partial z_3} = 0$$

$$\frac{\partial D_E}{\partial \dot{z}_3} = \frac{1}{2} * 2c_3(\dot{z}_3 - \dot{z}_2) + \frac{1}{2} * 2c_4[\dot{z}_3 - L\dot{\theta}si\,n\left(\theta + \tilde{\theta}\right)]$$

$$\frac{\partial D_E}{\partial \dot{z}_3} = c_3(\dot{z}_3 - \dot{z}_2) + c_4\left[\dot{z}_3 - L\dot{\theta}si\,n\left(\theta + \tilde{\theta}\right)\right]$$

$$\frac{\partial P_E}{\partial z_3} = \frac{1}{2} * 2k_3(z_3 - z_2) + \frac{1}{2} * 2k_4[z_3 + Lcos\left(\theta + \tilde{\theta}\right)]$$

$$\frac{\partial P_E}{\partial z_3} = k_3(z_3 - z_2) + k_4\left[z_3 + Lcos\left(\theta + \tilde{\theta}\right)\right]$$

$$m_3[\ddot{z}_3 - L_g\cos\left(\theta + \tilde{\theta}\right)\dot{\theta}^2 - L_g\sin\left(\theta + \tilde{\theta}\right)\ddot{\theta}] + c_3(\dot{z}_3 - \dot{z}_2)$$
$$+ c_4\left[\dot{z}_3 - L\dot{\theta}si\,n\left(\theta + \tilde{\theta}\right)\right] + k_3(z_3 - z_2)$$
$$+ k_4\left[z_3 + Lcos\left(\theta + \tilde{\theta}\right)\right] = 0$$

$$m_3[\ddot{z}_3 - L_g\cos\left(\theta + \tilde{\theta}\right)\dot{\theta}^2 - L_g\sin\left(\theta + \tilde{\theta}\right)\ddot{\theta}] + (c_3 + c_4)\dot{z}_3 - c_3\dot{z}_2$$
$$- c_4Lsin\left(\theta + \tilde{\theta}\right)\dot{\theta} + (k_3 + k_4)z_3 - k_3z_2 + k_4Lcos\left(\theta + \tilde{\theta}\right)$$
$$= 0 \qquad (3.38)$$

The forth nonlinear governing equation of motion can be derived as follows

$$\frac{d}{dt}\left[\frac{\partial K_E}{\partial \dot{y}_1}\right] - \frac{\partial K_E}{\partial y_1} + \frac{\partial D_E}{\partial \dot{y}_1} + \frac{\partial P_E}{\partial y_1} = Y_1 \qquad (3.39)$$

$$\frac{d}{dt}\left[\frac{\partial K_E}{\partial \dot{y}_1}\right] = \frac{d}{dt}\left[\frac{1}{2} * 2m_3[\dot{y_1} + L_g\dot{\theta}\cos(\theta + \tilde{\theta})\right]$$

$$= \frac{d}{dt}[m_3(\dot{y_1} + L_g\dot{\theta}\cos(\theta + \tilde{\theta})]$$

$$\frac{d}{dt}\left[\frac{\partial K_E}{\partial \dot{y}_1}\right] = m_3\{\ddot{y}_1 + L_g[\dot{\theta}(-sin(\theta + \tilde{\theta}))\dot{\theta} + cos(\theta + \tilde{\theta})\ddot{\theta}]\}$$

$$= m_3[\ddot{y}_1 - L_g\sin(\theta + \tilde{\theta})\dot{\theta}^2 + L_g\cos(\theta + \tilde{\theta})\ddot{\theta}]$$

$$\frac{\partial K_E}{\partial z_3} = 0$$

$$\frac{\partial D_E}{\partial \dot{y}_1} = \frac{1}{2} * 2c_5[\dot{y}_1 + L\dot{\theta}\cos(\theta + \tilde{\theta})]$$

$$\frac{\partial D_E}{\partial \dot{y}_1} = c_5[\dot{y}_1 + L\dot{\theta}\cos(\theta + \tilde{\theta})]$$

$$\frac{\partial P_E}{\partial y_1} = \frac{1}{2} * 2k_5[y_1 + Lsin(\theta + \tilde{\theta})] + m_3g$$

$$\frac{\partial P_E}{\partial y_1} = k_5[y_1 + Lsin(\theta + \tilde{\theta})] + m_3g$$

$$m_3[\ddot{y}_1 - L_g\sin(\theta + \tilde{\theta})\dot{\theta}^2 + L_g\cos(\theta + \tilde{\theta})\ddot{\theta}] + c_5[\dot{y}_1 + L\dot{\theta}\cos(\theta + \tilde{\theta})]$$
$$+ k_5[y_1 + Lsin(\theta + \tilde{\theta})] + m_3g$$

$$m_3[\ddot{y}_1 - L_g\sin(\theta + \tilde{\theta})\dot{\theta}^2 + L_g\cos(\theta + \tilde{\theta})\ddot{\theta} + g]$$
$$+ c_5[\dot{y}_1 + L\dot{\theta}\cos(\theta + \tilde{\theta})] + k_5[y_1 + Lsin(\theta + \tilde{\theta})]$$
$$= 0 \qquad (3.40)$$

The fifth nonlinear governing equation of motion can be derived as follows

$$\frac{d}{dt}\left[\frac{\partial K_E}{\partial \dot{\theta}}\right] - \frac{\partial K_E}{\partial \theta} + \frac{\partial D_E}{\partial \dot{\theta}} + \frac{\partial P_E}{\partial \theta} = \theta \qquad (3.41)$$

$$\frac{\partial K_E}{\partial \dot{\theta}} = \frac{1}{2} * 2m_3\left[\dot{z_3} - L_g\dot{\theta}\sin(\theta+\tilde{\theta})\right] * \left(-L_g\sin(\theta+\tilde{\theta})\right) + \frac{1}{2}$$

$$* 2m_3\left[\dot{y_1} + L_g\dot{\theta}\cos(\theta+\tilde{\theta})\right] * \left(L_g cos(\theta+\tilde{\theta})\right) + \frac{1}{2} * 2J\dot{\theta}$$

$$= m_3L_g\{-\sin(\theta+\tilde{\theta})\left[\dot{z_3} - L_g\dot{\theta}\sin(\theta+\tilde{\theta})\right]$$

$$+ cos(\theta+\tilde{\theta})\left[\dot{y_1} + L_g\dot{\theta}\cos(\theta+\tilde{\theta})\right]\} + J\dot{\theta}$$

$$\frac{d}{dt}\left[\frac{\partial K_E}{\partial \dot{\theta}}\right] = m_3L_g\{-\sin(\theta+\tilde{\theta})\left[\ddot{z_3} - L_g\ddot{\theta}sin(\theta+\tilde{\theta})\right] + \cos(\theta+\tilde{\theta})\left[\ddot{y_1}\right.$$

$$\left. + L_g\ddot{\theta}cos(\theta+\tilde{\theta})\right]\} + J\ddot{\theta}$$

$$\frac{d}{dt}\left[\frac{\partial K_E}{\partial \dot{\theta}}\right] = m_3L_g\{\left[-\ddot{z_3}\,sin(\theta+\tilde{\theta}) + \ddot{y_1}cos(\theta+\tilde{\theta})\right.$$

$$\left. + L_g\ddot{\theta}\left[sin^2(\theta+\tilde{\theta}) + cos^2(\theta+\tilde{\theta})\right]\right\} + J\ddot{\theta}$$

$$\frac{d}{dt}\left[\frac{\partial K_E}{\partial \dot{\theta}}\right] = \left(J + m_3{L_g}^2\right)\ddot{\theta} + m_3L_g[-\ddot{z_3}\,sin(\theta+\tilde{\theta}) + \ddot{y_1}cos(\theta+\tilde{\theta})]$$

$$\frac{\partial K_E}{\partial \theta} = 0$$

$$\frac{\partial D_E}{\partial \dot{\theta}} = \frac{1}{2} * 2c_t\dot{\theta} + \frac{1}{2} * 2c_4\left[\dot{z_3} - L\dot{\theta}\sin(\theta+\tilde{\theta})\right] * \left(-L\sin(\theta+\tilde{\theta})\right) + \frac{1}{2}$$

$$* 2c_5\left[\dot{y_1} + L\dot{\theta}\cos(\theta+\tilde{\theta})\right] * \left(L\cos(\theta+\tilde{\theta})\right)$$

$$\frac{\partial D_E}{\partial \dot{\theta}} = c_t\dot{\theta} - c_4L\sin(\theta+\tilde{\theta})\left[\dot{z_3} - L\dot{\theta}\sin(\theta+\tilde{\theta})\right]$$

$$+ c_5\,L\cos(\theta+\tilde{\theta})\left[\dot{y_1} + L\dot{\theta}\cos(\theta+\tilde{\theta})\right]$$

$$\frac{\partial P_E}{\partial \theta} = \frac{1}{2} * 2k_t(\theta+\tilde{\theta}) + \frac{1}{2} * 2k_4\left[z_3 + Lcos(\theta+\tilde{\theta})\right] * \left(-Lsin(\theta+\tilde{\theta})\right)$$

$$+ \frac{1}{2} * 2k_5\left[y_1 + Lsin(\theta+\tilde{\theta})\right] * \left(Lcos(\theta+\tilde{\theta})\right)$$

$$+ m_3gL_g\cos(\theta+\tilde{\theta})$$

$$\frac{\partial P_E}{\partial \theta} = k_t(\theta+\tilde{\theta}) - k_4\, Lsin(\theta+\tilde{\theta})\left[z_3 + Lcos(\theta+\tilde{\theta})\right] + k_5\, Lcos(\theta+\tilde{\theta})\left[y_1 + Lsin(\theta+\tilde{\theta})\right] + m_3 g L_g \cos(\theta+\tilde{\theta})$$

$$(J + m_3 {L_g}^2)\ddot{\theta} + m_3 L_g[-\ddot{z_3}\, sin(\theta+\tilde{\theta}) + \ddot{y_1} cos(\theta+\tilde{\theta})] + c_t\dot{\theta} - c_4 L \sin(\theta+\tilde{\theta})\left[\dot{z_3} - L\dot{\theta}\sin(\theta+\tilde{\theta})\right] + c_5\, L\cos(\theta+\tilde{\theta})\left[\dot{y_1} + L\dot{\theta}\cos(\theta+\tilde{\theta})\right] + k_t(\theta+\tilde{\theta}) - k_4\, Lsin(\theta+\tilde{\theta})\left[z_3 + Lcos(\theta+\tilde{\theta})\right] + k_5\, Lcos(\theta+\tilde{\theta})\left[y_1 + Lsin(\theta+\tilde{\theta})\right] + m_3 g L_g \cos(\theta+\tilde{\theta}) = 0 \quad (3.42)$$

The five nonlinear governing equations of motion can be derived as follows

$$\begin{cases} m_1\ddot{z_1} + (c_1+c_2)\dot{z_1} - c_2\dot{z_2} + (k_1+k_2)z_1 - k_2 z_2 = c_1\dot{z_0} + k_1 z_0 & (1) \\ m_2\ddot{z_2} + (c_2+c_3)\dot{z_2} - c_2\dot{z_1} - c_3\dot{z_3} + (k_2+k_3)z_2 - k_2 z_1 - k_3 z_3 = 0 & (2) \\ m_3[\ddot{z_3} - L_g\cos(\theta+\tilde{\theta})\,\dot{\theta}^2 - L_g\sin(\theta+\tilde{\theta})\,\ddot{\theta}] + (c_3+c_4)\dot{z_3} & \\ -c_3\dot{z_2} - c_4 Lsin(\theta+\tilde{\theta})\dot{\theta} + (k_3+k_4)z_3 - k_3 z_2 + k_4 Lcos(\theta+\tilde{\theta}) = 0 & (3) \\ m_3\left[\ddot{y_1} - L_g\sin(\theta+\tilde{\theta})\,\dot{\theta}^2 + L_g\cos(\theta+\tilde{\theta})\ddot{\theta} + g\right] & \\ +c_5\left[\dot{y_1} + L\dot{\theta}\cos(\theta+\tilde{\theta})\right] + k_5\left[y_1 + Lsin(\theta+\tilde{\theta})\right] = 0 & (4) \\ (J + m_3 {L_g}^2)\ddot{\theta} + m_3 L_g[-\ddot{z_3}\, sin(\theta+\tilde{\theta}) + \ddot{y_1} cos(\theta+\tilde{\theta})] + c_t\dot{\theta} & \\ -c_4 L \sin(\theta+\tilde{\theta})\left[\dot{z_3} - L\dot{\theta}\sin(\theta+\tilde{\theta})\right] + c_5\, Lcos(\theta+\tilde{\theta})[\dot{y_1} + & \\ L\dot{\theta}\cos(\theta+\tilde{\theta})] + k_t(\theta+\tilde{\theta}) - k_4\, Lsin(\theta+\tilde{\theta})\left[z_3 + Lcos(\theta+\tilde{\theta})\right] & \\ +k_5\, Lcos(\theta+\tilde{\theta})\left[y_1 + Lsin(\theta+\tilde{\theta})\right] + m_3 g L_g\cos(\theta+\tilde{\theta}) = 0 & (5) \end{cases} \quad (3.43)$$

3.3 Linearization

Most dynamic systems in the real world are nonlinear and are described by nonlinear differential equations. However, many control system design and analysis techniques are applicable only to linear system models. Linearization is therefore used to approximate a nonlinear system by a linear model around an operating point, which simplifies analysis and controller design. In this work, the nonlinear dynamic equations were linearized and implemented in MATLAB using the state-space approach. The original five

second-order differential equations of the system were converted into ten first-order state equations, enabling efficient numerical simulation and control design. This transformation provides a convenient framework for system analysis, stability evaluation, and controller implementation. The general equation of the linearization:

$$\Delta Y = \frac{\partial Y}{\partial X_1}\Big|_i \Delta X_1 + \frac{\partial Y}{\partial X_2}\Big|_i \Delta X_2 + \cdots + \frac{\partial Y}{\partial X_n}\Big|_i \Delta X_n \quad (3.44)$$

In our proposed model, the human arm is characterized as a mechanical system, enabling it to oscillate naturally due to its mechanical properties while being controlled by actuator systems. During the oscillation, the system undergoes a nonlinear behavior, which makes it difficult to find the transmissibility of the arm. Therefore, a linearization technique is used to assess the system's response while oscillating near an operating point to estimate linear motion. To achieve this, the system is linearized around an equilibrium elbow angle ($\tilde{\theta}$), predicting small perturbations. Applying the identities of sine and cosine addition formulas:

$$sin(\theta + \tilde{\theta}) = sin\theta cos\tilde{\theta} + sin\tilde{\theta} cos\theta \quad (3.45)$$

$$cos(\theta + \tilde{\theta}) = cos\theta cos\tilde{\theta} - sin\theta sin\tilde{\theta} \quad (3.46)$$

Assuming that the arm oscillates with a small motion ($sin\theta = \theta, cos\theta = 1$)

$$sin(\theta + \tilde{\theta}) = \theta cos\tilde{\theta} + sin\tilde{\theta} \quad (3.47)$$

$$cos(\theta + \tilde{\theta}) = cos\tilde{\theta} - \theta sin\tilde{\theta} \quad (3.48)$$

Substituting eq.(3.47) and eq.(3.48)in eq.(3.43) , yields to:

$$\left\{\begin{array}{l} m_1\ddot{z}_1 + (c_1+c_2)\dot{z}_1 - c_2\dot{z}_2 + (k_1+k_2)z_1 - k_2z_2 = c_1\dot{z}_0 + k_1z_0 \quad (1) \\ m_2\ddot{z}_2 + (c_2+c_3)\dot{z}_2 - c_2\dot{z}_1 - c_3\dot{z}_3 + (k_2+k_3)z_2 - k_2z_1 - k_3z_3 = 0 \quad (2) \\ m_3[\ddot{z}_3 - L_g sin\tilde{\theta}\ddot{\theta}] + (c_3+c_4)\dot{z}_3 - c_3\dot{z}_2 - c_4Lsin\tilde{\theta}\dot{\theta} \\ +(k_3+k_4)z_3 - k_3z_2 + k_4L\big(cos\tilde{\theta} - sin\tilde{\theta}\theta\big)0 = 0 \quad (3) \\ m_3\big[\ddot{y}_1 + L_g cos\tilde{\theta}\ddot{\theta} + g\big] + c_5\big[\dot{y}_1 + Lcos\tilde{\theta}\dot{\theta}\big] + \\ k_5\big[y_1 + L(\theta cos\tilde{\theta} + sin\tilde{\theta})\big] = 0 \quad (4) \\ \big(J + m_3{L_g}^2\big)\ddot{\theta} + m_3L_g\big[-sin\tilde{\theta}\ddot{z}_3 + cos\tilde{\theta}\ddot{y}_1\big] \\ + c_t\dot{\theta} - c_4Lsin\tilde{\theta}\big[\dot{z}_3 - Lsin\tilde{\theta}\dot{\theta}\big] \\ +c_5\, L\, cos\tilde{\theta}\ \big[\dot{y}_1 + Lcos\tilde{\theta}\dot{\theta}\big] + k_t\big(\theta + \tilde{\theta}\big) \\ -k_4\, L\big(\theta cos\tilde{\theta} + sin\tilde{\theta}\big)\big[z_3 + L(cos\tilde{\theta} - \theta sin\tilde{\theta})\big] \\ +k_5\, L(cos\tilde{\theta} - \theta sin\tilde{\theta})\big[y_1 + L(\theta cos\tilde{\theta} + sin\tilde{\theta})\big] + m_3gL_g(cos\tilde{\theta} - \theta sin\tilde{\theta}) \\ = 0 \quad (5) \end{array}\right\} \quad (3.49)$$

The equations of motion for the human arm system in matrix form, involving mass, damping, and stiffness, can be obtained in Eq. (3.50)

$$M\ddot{\tilde{z}} + C\dot{\tilde{z}} + K\tilde{z} = [F] \quad (3.50)$$

where:

$$[M] = \begin{bmatrix} m_1 & 0 & 0 & 0 & 0 \\ 0 & m_2 & 0 & 0 & 0 \\ 0 & 0 & m_3 & 0 & -L_g m_3 sin\tilde{\theta} \\ 0 & 0 & 0 & m_3 & L_g m_3 cos\tilde{\theta} \\ 0 & 0 & -L_g m_3 sin\tilde{\theta} & L_g m_3 cos\tilde{\theta} & J + {L_g}^2 m_3 \end{bmatrix}$$

$$[C] = \begin{bmatrix} c_1+c_2 & -c_2 & 0 & 0 & 0 \\ -c_2 & c_2+c_3 & -c_3 & 0 & 0 \\ 0 & -c_3 & c_3+c_4 & 0 & -c_4Lsin\tilde{\theta} \\ 0 & 0 & 0 & c_5 & c_5Lcos\tilde{\theta} \\ 0 & 0 & -c_4Lsin\tilde{\theta} & c_5Lcos\tilde{\theta} & \begin{pmatrix} c_t + c_4L^2sin\tilde{\theta}^2 \\ +c_5L^2cos\tilde{\theta}^2 \end{pmatrix} \end{bmatrix}$$

$$[K] = \begin{bmatrix} k_1 + k_2 & -k_2 & 0 & 0 & 0 \\ -k_2 & k_2 + k_3 & -k_3 & 0 & 0 \\ 0 & -k_3 & k_3 + k_4 & 0 & -k_4 L sin\tilde{\theta} \\ 0 & 0 & 0 & k_5 & k_5 L cos\tilde{\theta} \\ 0 & 0 & -k_4 L sin\tilde{\theta} & k_5 L cos\tilde{\theta} & \begin{pmatrix} k_t - k_4 L^2 (cos\tilde{\theta}^2 \\ -sin\tilde{\theta}^2 + k_5 L^2 \\ (cos\tilde{\theta}^2 - sin\tilde{\theta}^2) \\ -m_3 g L_g sin\tilde{\theta} \end{pmatrix} \end{bmatrix}$$

$$[F] = \begin{bmatrix} c_1 \dot{z_0} + k_1 z_0 \\ 0 \\ -k_4 L cos\tilde{\theta} \\ -m_3 g - k_5 L sin\tilde{\theta} \\ -k_t \tilde{\theta} + k_4 L^2 sin\tilde{\theta} cos\tilde{\theta} - k_5 L^2 sin\tilde{\theta} cos\tilde{\theta} - m_3 g L_g cos\tilde{\theta} \end{bmatrix}$$

The initial and final states occur under static conditions where the arm is at a stable state. The initial displacements of the system can be determined by solving Equation (3.50), considering that both the velocity and acceleration are zero, and that no torque is applied at the elbow joint while applying a certain external displacement. The initial displacements can be computed using Eq. (3.51)

$$\begin{bmatrix} z_1 \\ z_2 \\ z_3 \\ y_1 \\ \theta \end{bmatrix}_0 = \begin{bmatrix} k_1+k_2 & -k_2 & 0 & 0 & 0 \\ -k_2 & k_2+k_3 & -k_3 & 0 & 0 \\ 0 & -k_3 & k_3+k_4 & 0 & -k_4 L sin\tilde{\theta} \\ 0 & 0 & 0 & k_5 & k_5 L cos\tilde{\theta} \\ 0 & 0 & -k_4 L sin\tilde{\theta} & k_5 L cos\tilde{\theta} & \begin{pmatrix} k_t - k_4 L^2 (cos\tilde{\theta}^2 \\ -sin\tilde{\theta}^2 + k_5 L^2 \\ (cos\tilde{\theta}^2 - sin\tilde{\theta}^2) \\ -m_3 g L_g sin\tilde{\theta} \end{pmatrix} \end{bmatrix}^{-1} \begin{bmatrix} c_1 \dot{z}_0 + k_1 z_0 \\ 0 \\ -k_4 L sin\tilde{\theta} \\ -m_3 g - k_5 L sin\tilde{\theta} \\ -k_t\tilde{\theta} + k_4 L^2 sin\tilde{\theta} cos\tilde{\theta} - k_5 L^2 sin\tilde{\theta} cos\tilde{\theta} - m_3 g L_g cos\tilde{\theta} \end{bmatrix} \quad (3.51)$$

In the same manner, the final displacements of the human arm can be determined under the same assumptions as the initial displacements, without considering the effect of external displacement. The final displacements can be computed using Eq. (3.52)

$$\begin{bmatrix} z_1 \\ z_2 \\ z_3 \\ y_1 \\ \theta \end{bmatrix}_f$$

$$= \begin{bmatrix} k_1 + k_2 & -k_2 & 0 & 0 & 0 \\ -k_2 & k_2 + k_3 & -k_3 & 0 & 0 \\ 0 & -k_3 & k_3 + k_4 & 0 & -k_4 L sin\tilde{\theta} \\ 0 & 0 & 0 & k_5 & k_5 L cos\tilde{\theta} \\ 0 & 0 & -k_4 L sin\tilde{\theta} & k_5 L cos\tilde{\theta} & \begin{pmatrix} k_t - k_4 L^2 (cos\tilde{\theta}^2 \\ -sin\tilde{\theta}^2 + k_5 L^2 \\ (cos\tilde{\theta}^2 - sin\tilde{\theta}^2) \\ -m_3 g L_g sin\tilde{\theta} \end{pmatrix} \end{bmatrix}^{-1}$$

$$\begin{bmatrix} 0 \\ 0 \\ -k_4 L sin\tilde{\theta} \\ -m_3 g - k_5 L sin\tilde{\theta} \\ -k_t\tilde{\theta} + k_4 L^2 sin\tilde{\theta} cos\tilde{\theta} - k_5 L^2 sin\tilde{\theta} cos\tilde{\theta} - m_3 g L_g cos\tilde{\theta} \end{bmatrix} \quad (3.52)$$

3.4 Optimization

Optimization is a fundamental concept in many branches of science and engineering. It aims to find the best possible solution to a given problem within a set of constraints or conditions. Optimization techniques rely on mathematical models that describe the relationship between variables and use various algorithms to find the optimal solution. Given its critical significance, optimization has become a vital component of decision-making in complex systems, playing a key role in enhancing performance, minimizing waste, and boosting efficiency. The Lagrange multiplier technique is utilized to reduce the objective function while accommodating constraints related to system parameters. To achieve this, the linear model of the human arm (Eq. (3.50)) is propagated numerically from the equilibrium position using estimated

system parameters. The overshooting and settling time characteristics are evaluated after integrating the system using MATLAB program. In this study, we plan to optimize the system's parameters (masses, spring stiffness, and damper coefficients) while achieving the desired overshooting and settling time as illustrated in Table (3.1). In order to solve this optimization problem using the method of Lagrange multipliers, the objective function is defined as follows[44]

$$f(x) = \sum_{i=1}^{5} \left(OS_i - OS_{i,desired}\right)^2 + \left(t_{s,i} - t_{s,i,desired}\right)^2 \quad (3.53)$$

The human arm operates as a complex biomechanical structure, including multiple degrees of freedom (DOF) due to its diverse joints (shoulder, elbow, wrist) and muscles. In the arm, the damping ratio for each part is based on various factors such as mechanical and material properties of the joints and tissues. Therefore, knowing the human arm damping ratios is not simple and needs experimental information. However, it simply possible to perform the human arm system by improving the overshooting and reducing the settling time. Table (3.1) presents the desired overshooting and settling time parameterizes.

Table 3.1: The desired overshooting and settling time values

Response parameter	Constraints
Settling Time, t_s (s)	< 0.1 sec
Overshooting (100%), os	< 15 %

To apply the proposed optimization method, the Lagrangian function can be expressed as

$$\text{ב}(x, \lambda_1, \lambda_2, \lambda_3, \lambda_4, \lambda_5, \lambda_6, \lambda_7, \lambda_8, \lambda_9, \lambda_{10}, \lambda_{11}, \lambda_{12}, \lambda_{13}, \lambda_{14}, \lambda_{15})$$

$$= f(x) - \sum_{j=1}^{15} \lambda_j \, g_j(x) \qquad (3.54)$$

Where x is the vector of the optimal parameters $(m_1, m_2, m_3, k_1, k_2, k_3, k_4, k_5, k_t, c_1, c_2, c_3, c_4, c_5, c_t)$, $f(x)$and $g_j(x)$ are the objective and constraints functions, respectively, and λ_j are Lagrangian multipliers required to satisfy the optimization .

Figure (3.3) represents the flow chart of the optimization.

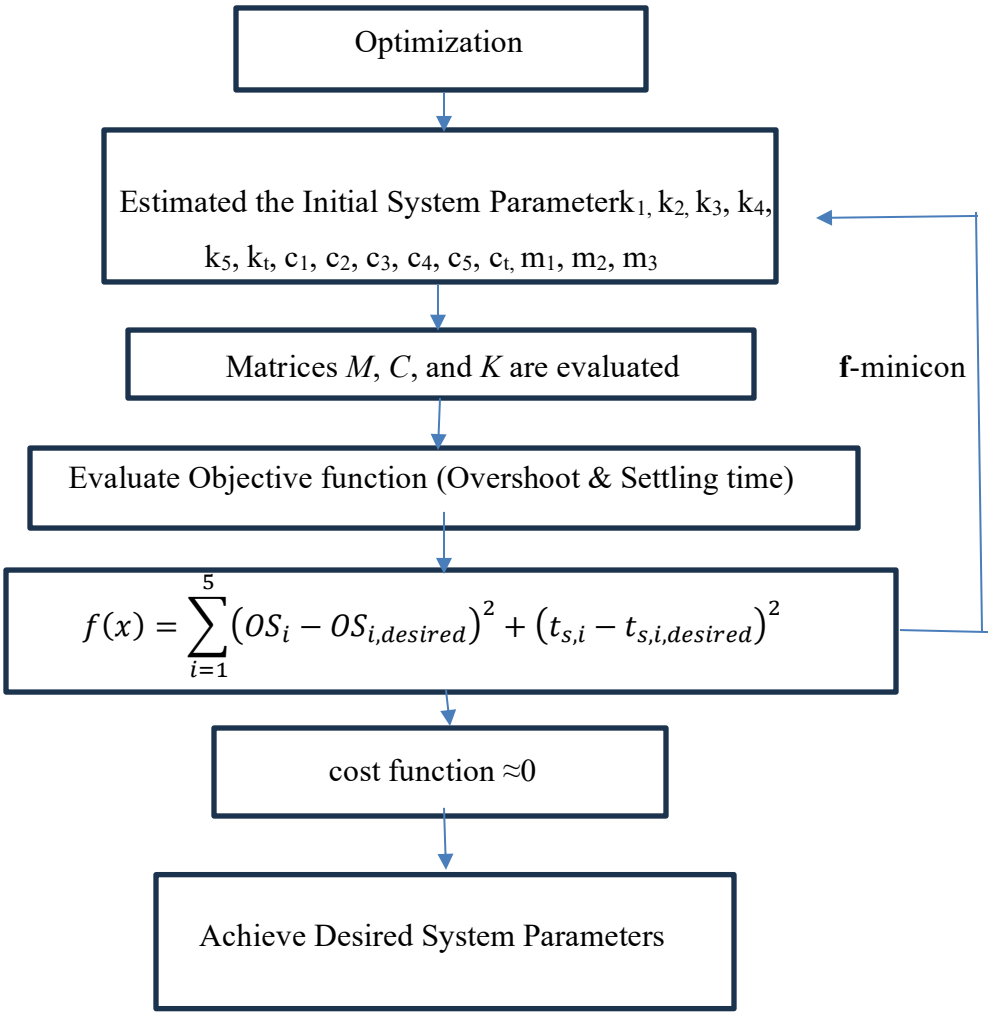

Figure (3.3):Flow chart of the optimization

Thus, the optimization algorithm relying on the Lagrangian multipliers method can effectively stabilize the human arm model while ensuring a faster settling time and low overshoot under nominal conditions. However, it is unlikely that the human model will only encounter nominal conditions without experiencing severe off-nominal conditions. Hence, the optimal system parameters that were computed under the nominal conditions will be used to evaluate the system performance while exhibiting the off-nominal conditions ($\dot{z_0} = 0, z_0 = 5\ cm$ and $\dot{z_0} = 0\ , z_0 = 25\ cm$).

3.5 Summary

This chapter outlined the mathematical representation of the human arm model and demonstrated how this model specifies the parameters for real-world applications. As mentioned, the human arm model is considered a mathematical model that consists of a differential equation of mechanical motion. This modelling will facilitate the straightforward design and examination of the human arm model.

Chapter Four: Control System

4.1 Introduction

In this chapter, an investigation through simulation of the control of a human arm exoskeleton is presented. Control systems are one of the most important fields of modern engineering, as they regulate the behavior of mechanical systems and make them operate according to the required objectives. The control principle works by comparing actual outputs with reference values and adjusting inputs to achieve optimal system performance. Through control science, system stability is improved, errors are reduced, response speed is increased, and vibrations are reduced. This chapter includes two main aspects. The first aspect presents the analytical methodology used to compute the reference elbow torque, while the second aspect focuses on numerical simulations with different initial conditions and system parameters using then Monte Carlo simulation technique to validate the proposed algorithm[45].

4.2 Analytical Methodology

After deriving the model of the human arm, linearizing the nonlinear equations of motion at a specific operating point, and representing the model in matrix form [M, C, K, F], it becomes possible to design the elbow torque required to guide the human arm exoskeleton toward the desired steady state in a smooth manner as shown in equation (4.1)

$$\begin{cases} m_1\ddot{z}_1 + (c_1 + c_2)\dot{z}_1 - c_2\dot{z}_2 + (k_1 + k_2)z_1 - k_2z_2 = c_1\dot{z}_0 + k_1z_0 & (1) \\ m_2\ddot{z}_2 + (c_2 + c_3)\dot{z}_2 - c_2\dot{z}_1 - c_3\dot{z}_3 + (k_2 + k_3)z_2 - k_2z_1 - k_3z_3 = 0 & (2) \\ m_3[\ddot{z}_3 - L_g sin\tilde{\theta}\ddot{\theta}] + (c_3 + c_4)\dot{z}_3 - c_3\dot{z}_2 - c_4Lsin\tilde{\theta}\dot{\theta} & \\ +(k_3 + k_4)z_3 - k_3z_2 + k_4L(cos\tilde{\theta} - sin\tilde{\theta}\theta)0 = 0 & (3) \\ m_3[\ddot{y}_1 + L_g cos\tilde{\theta}\ddot{\theta} + g] + c_5[\dot{y}_1 + Lcos\tilde{\theta}\dot{\theta}] + & \\ k_5[y_1 + L(\theta cos\tilde{\theta} + sin\tilde{\theta})] = 0 & (4) \\ (J + m_3{L_g}^2)\ddot{\theta} + m_3L_g[-sin\tilde{\theta}\ddot{z}_3 + cos\tilde{\theta}\ddot{y}_1] & \\ + c_t\dot{\theta} - c_4Lsin\tilde{\theta}[\dot{z}_3 - Lsin\tilde{\theta}\dot{\theta}] & \\ +c_5\, L\, cos\tilde{\theta}\ [\dot{y}_1 + Lcos\tilde{\theta}\dot{\theta}] + k_t(\theta + \tilde{\theta}) & \\ -k_4\, L(\theta cos\tilde{\theta} + sin\tilde{\theta})[z_3 + L(cos\tilde{\theta} - \theta sin\tilde{\theta})] & \\ +k_5\, L(cos\tilde{\theta} - \theta sin\tilde{\theta})[y_1 + L(\theta cos\tilde{\theta} + sin\tilde{\theta})] + m_3gL_g(cos\tilde{\theta} - \theta sin\tilde{\theta}) & \\ = T_{ref} & (5) \end{cases} \quad (4.1)$$

The arm equations can be formulated as a matrix representation where the mass, damping, and stiffness matrices are included as shown in Equation (4.2).

$$\begin{bmatrix} m_1 & 0 & 0 & 0 & 0 \\ 0 & m_2 & 0 & 0 & 0 \\ 0 & 0 & m_3 & 0 & -L_g m_3 sin\tilde{\theta} \\ 0 & 0 & 0 & m_3 & L_g m_3 cos\tilde{\theta} \\ 0 & 0 & -L_g m_3 sin\tilde{\theta} & L_g m_3 cos\tilde{\theta} & J + {L_g}^2 m_3 \end{bmatrix} \begin{bmatrix} \ddot{z}_1 \\ \ddot{z}_2 \\ \ddot{z}_3 \\ \ddot{y}_1 \\ \ddot{\theta} \end{bmatrix}$$

$$+ \begin{bmatrix} c_1 + c_2 & -c_2 & 0 & 0 & 0 \\ -c_2 & c_2 + c_3 & -c_3 & 0 & 0 \\ 0 & -c_3 & c_3 + c_4 & 0 & -c_4 L sin\tilde{\theta} \\ 0 & 0 & 0 & c_5 & c_5 L cos\tilde{\theta} \\ 0 & 0 & -c_4 L sin\tilde{\theta} & c_5 L cos\tilde{\theta} & \begin{pmatrix} c_t + c_4 L^2 sin\tilde{\theta}^2 \\ + c_5 L^2 cos\tilde{\theta}^2 \end{pmatrix} \end{bmatrix} \begin{bmatrix} \dot{z}_1 \\ \dot{z}_2 \\ \dot{z}_3 \\ \dot{y}_1 \\ \dot{\theta} \end{bmatrix}$$

$$+ \begin{bmatrix} k_1 + k_2 & -k_2 & 0 & 0 & 0 \\ -k_2 & k_2 + k_3 & -k_3 & 0 & 0 \\ 0 & -k_3 & k_3 + k_4 & 0 & -k_4 L sin\tilde{\theta} \\ 0 & 0 & 0 & k_5 & k_5 L cos\tilde{\theta} \\ 0 & 0 & -k_4 L sin\tilde{\theta} & k_5 L cos\tilde{\theta} & \begin{pmatrix} k_t - k_4 L^2 (cos\tilde{\theta}^2 \\ -sin\tilde{\theta}^2 + k_5 L^2 \\ (cos\tilde{\theta}^2 - sin\tilde{\theta}^2) \\ -m_3 g L_g sin\tilde{\theta} \end{pmatrix} \end{bmatrix} \begin{bmatrix} z_1 \\ z_2 \\ z_3 \\ y_1 \\ \theta \end{bmatrix}$$

$$= \begin{bmatrix} c_1 \dot{z}_0 + k_1 z_0 \\ 0 \\ -k_4 L sin\tilde{\theta} \\ -m_3 g - k_5 L sin\tilde{\theta} \\ \left(-k_t \tilde{\theta} + k_4 L^2 sin\tilde{\theta} cos\tilde{\theta} - k_5 L^2 sin\tilde{\theta} cos\tilde{\theta} - m_3 g L_g cos\tilde{\theta}\right) + T_{ref} \end{bmatrix} \quad (4.2)$$

An analytical controller has been utilized to direct the exoskeleton following the desired reference trajectories. The reference trajectories of the system's displacements are shaped using five eight-term exponential functions, with one function designated for each displacement. Hence, the reference hand, forearm, horizontal elbow, vertical elbow, and elbow angular displacements, can be expressed in Eqs. (4.3), (4.4), (4.5), (4.6) and (4.7), respectively. Where each of Equation consists of eight coefficients, eight boundary conditions

must be imposed to solve for these coefficients. To perform this task, the initial, final, and intermediate displacements and velocities are used to generate the system's references while ensuring a fast response with no overshoot.

$$z_{1ref} = \sum_{n=1}^{8} A_n \exp(-1.5nt) \tag{4.3}$$

For the hand segment, four pairs of displacement: (0, z_{10}), (1,z_{1f}), (0.35,z_{1f}), and (0.65, z_{1f}), and four pairs of velocities: $(0, \dot{z}_{10})$, $(1, \dot{z}_{1f})$, $(0.35, \dot{z}_{1f})$, and $(0.65, \dot{z}_{1f})$ are significantly required at the initial, final, and intermediate states to compute the eight hand coefficients (A_1, A_2, A_3, A_4, A_5, A_6, A_7, and A_8).

$$z_{2\text{ref}} = \sum_{n=1}^{8} B_n \exp(-1.5nt) \tag{4.4}$$

For the forearm segment, four pairs of displacement: (0, z_{20}), (1,z_{2f}), (0.35,z_{2f}), and (0.65, z_{2f}), and four pairs of velocities: $(0, \dot{z}_{20})$, $(1, \dot{z}_{2f})$, $(0.35, \dot{z}_{2f})$, and $(0.65, \dot{z}_{2f})$ are significantly required at the initial, final, and intermediate states to compute the eight forearm coefficients (B_1, B_2, B_3, B_4, B_5, B_6, B_7, and B_8).

$$z_{3ref} = \sum_{n=1}^{8} C_n \exp(-1.5nt) \tag{4.5}$$

For the horizontal elbow segment, four pairs of displacement: (0, z_{30}), (1,z_{3f}), (0.35,z_{3f}), and (0.65, z_{3f}), and four pairs of velocities: $(0, \dot{z}_{30})$, $(1, \dot{z}_{3f})$, $(0.35, \dot{z}_{3f})$, and $(0.65, \dot{z}_{3f})$ are significantly required at the initial, final, and

intermediate states to compute the eight horizontal elbow coefficients (C_1, C_2, C_3, C_4, C_5, C_6, C_7, and C_8).

$$y_{1ref} = \sum_{n=1}^{8} D_n \exp(-1.5nt) \tag{4.6}$$

For the vertical elbow segment, four pairs of displacement: (0, y_{10}), (1,y_{1f}), (0.35,y_{1f}), and (0.65, y_{1f}), and four pairs of velocities: $(0, \dot{y}_{10})$, $(1, \dot{y}_{1f})$, $(0.35, \dot{y}_{1f})$, and $(0.65, \dot{y}_{1f})$ are significantly required at the initial, final, and intermediate states to compute the eight vertical elbow coefficients (D_1, D_2, D_3, D_4, D_5, D_6, D_7, and D_8).

$$\theta_{ref} = \sum_{n=1}^{8} E_n \exp(-0.5nt) \tag{4.7}$$

For the elbow angular segment, four pairs of displacement: (0, θ_0), (1, θ_f), (0.35, θ_f), and (0.65, θ_f), and four pairs of velocities: $(0, \dot{\theta}_0)$, $(1, \dot{\theta}_f)$, $(0.35, \dot{\theta}_f)$, and $(0.65, \dot{\theta}_f)$ are significantly required at the initial, final, and intermediate states to compute the eight elbow angular coefficients (E_1, E_2, E_3, E_4, E_5, E_6, E_7, and E_8).

Once computing the system's coefficients that define Eqs. (4.3), (4.4), (4.5), (4.6) and (4.7), the first time derivative of Eqs. (4.3), (4.4), (4.5), (4.6) and (4.7), and the second time derivative of Eqs. (4.3), (4.4), (4.5), (4.6) and (4.7), it becomes straightforward to find the system's reference states and reference input.

$$\dot{z}_{1ref} = -1.5 \sum_{n=1}^{8} nA_n \exp(-1.5nt) \tag{4.8}$$

$$\ddot{z}_{1ref} = +2.25 \sum_{n=1}^{8} n^2 A_n \exp(-1.5nt) \tag{4.9}$$

$$\dot{z}_{2ref} = -1.5 \sum_{n=1}^{8} nB_n \exp(-1.5nt) \tag{4.10}$$

$$\ddot{z}_{2ref} = +2.25 \sum_{n=1}^{8} n^2 B_n \exp(-1.5nt) \tag{4.11}$$

$$\dot{z}_{3ref} = -1.5 \sum_{n=1}^{8} nC_n \exp(-1.5nt) \tag{4.12}$$

$$\ddot{z}_{3ref} = +2.25 \sum_{n=1}^{8} n^2 C_n \exp(-1.5nt) \tag{4.13}$$

$$\dot{y}_{1ref} = -1.5 \sum_{n=1}^{8} nD_n \exp(-1.5nt) \tag{4.14}$$

$$\ddot{y}_{1ref} = +2.25 \sum_{n=1}^{8} n^2 D_n \exp(-1.5nt) \tag{4.15}$$

$$\dot{\theta}_{ref} = -0.5 \sum_{n=1}^{8} nE_n \exp(-1.5nt) \tag{4.16}$$

$$\ddot{\theta}_{ref} = +0.25 \sum_{n=1}^{8} n^2 E_n \exp(-1.5nt) \tag{4.17}$$

It is important to solve Eq. (4.2) in terms of the elbow torque to obtain

$$T_{ref} = -\ddot{z}_3 L_g m_3 sin\tilde{\theta} + \ddot{y}_1 L_g m_3 cos\tilde{\theta} + \left(J + {L_g}^2 m_3\right)\ddot{\theta} - c_4 L sin\tilde{\theta}\dot{z}_3 + c_5 L cos\tilde{\theta}\dot{y}_1 + \left(c_t + c_4 L^2 sin\tilde{\theta}^2 + c_5 L^2 cos\tilde{\theta}^2\right)\dot{\theta} - k_4 L sin\tilde{\theta} z_3 + k_5 L cos\tilde{\theta} y_1 + \left(k_t - k_4 L^2\left(cos\tilde{\theta}^2 - sin\tilde{\theta}^2\right) + k_5 L^2\left(cos\tilde{\theta}^2 - sin\tilde{\theta}^2\right) - m_3 g L_g sin\tilde{\theta}\right)\theta + k_t\tilde{\theta} - k_4 L^2 sin\tilde{\theta} cos\tilde{\theta} + k_5 L^2 sin\tilde{\theta} cos\tilde{\theta} + m_3 g L_g cos\tilde{\theta} \quad (4.18)$$

Thus, substitute Eqs. (4.3), (4.4), (4.5), (4.6) and (4.7), and the first and second time derivatives of Eqs. (4.3), (4.4), (4.5), (4.6) and (4.7) into Eq. (4.18) to determine the reference elbow torque required by the patient to achieve the desired movement.

$$
\begin{aligned}
T_{ref} = & -2.25\sum_{n=1}^{8} n^2 C_n \exp(-1.5nt)\, L_g m_3 sin\tilde{\theta} \\
& + 2.25\sum_{n=1}^{8} n^2 D_n \exp(-1.5nt)\, L_g m_3 cos\tilde{\theta} \\
& + 0.25\left(J + {L_g}^2 m_3\right)\sum_{n=1}^{8} n^2 E_n \exp(-0.5nt) \\
& + 1.5c_4 L sin\tilde{\theta}\sum_{n=1}^{8} nC_n \exp(-1.5nt) \\
& - 1.5c_5 L cos\tilde{\theta}\sum_{n=1}^{8} nD_n \exp(-1.5nt) \\
& - 0.5\left(c_t + c_4 L^2 sin\tilde{\theta}^2\right. \\
& \left. + c_5 L^2 cos\tilde{\theta}^2\right)\sum_{n=1}^{8} nE_n \exp(-0.5nt) \qquad (4.19) \\
& - k_4 L sin\tilde{\theta}\sum_{n=1}^{8} C_n \exp(-1.5nt) \\
& + k_5 L cos\tilde{\theta}\sum_{n=1}^{8} D_n \exp(-1.5nt) \\
& + \left(k_t - k_4 L^2\left(cos\tilde{\theta}^2 - sin\tilde{\theta}^2\right)\right. \\
& + k_5 L^2\left(cos\tilde{\theta}^2 - sin\tilde{\theta}^2\right) \\
& \left. - m_3 g L_g sin\tilde{\theta}\right)\sum_{n=1}^{8} E_n \exp(-0.5nt) + k_t\tilde{\theta} \\
& - k_4 L^2 sin\tilde{\theta} cos\tilde{\theta} + k_5 L^2 sin\tilde{\theta} cos\tilde{\theta} + m_3 g L_g cos\tilde{\theta}
\end{aligned}
$$

4.3 Monte Carlo Simulation

Monte Carlo simulation is one of the most important numerical methods used to analyze complex systems that contain random elements. It generates a large number of random values within a specific range of variables affecting the system and re-executes the model multiple times to study the behavior of the outputs and predict their probability distribution. The idea of Monte Carlo is based on the fact that random repetition of numerical experiments allows for estimating the expected values of variables and calculating performance indicators such as the probability distribution of error. The greater the number of repetitions in the simulation, the more accurate the results become and the closer they become to the actual behavior of the system. Thus, Monte Carlo provides an effective method for analyzing dynamic systems. Monte Carlo simulation can be represented as the equation (4.20)[46].

$$\bar{x} = \frac{1}{n}\sum_{i=1}^{n} f(x_i) \tag{4.20}$$

Where $\bar{x}$: Statistical estimation of output

n: Number of repetitions

$f(x_i)$: model output function

x_i: random input variables

In the introduced approach and in order to encompass a wide range of patient parameters, the Monte Carlo simulation method is conducted considering 1000 patients with variations in hand, forearm, and upper-arm masses, segment lengths, arm stiffness, and damping coefficients. These dispersions

are modelled as random variations, with ($\pm$6%) added relative to the nominal conditions of each parameter to consider whether the rehabilitated arm belongs to a man, a woman, or a child. Figure (4.1) shows the complete Simulink model of the human arm.

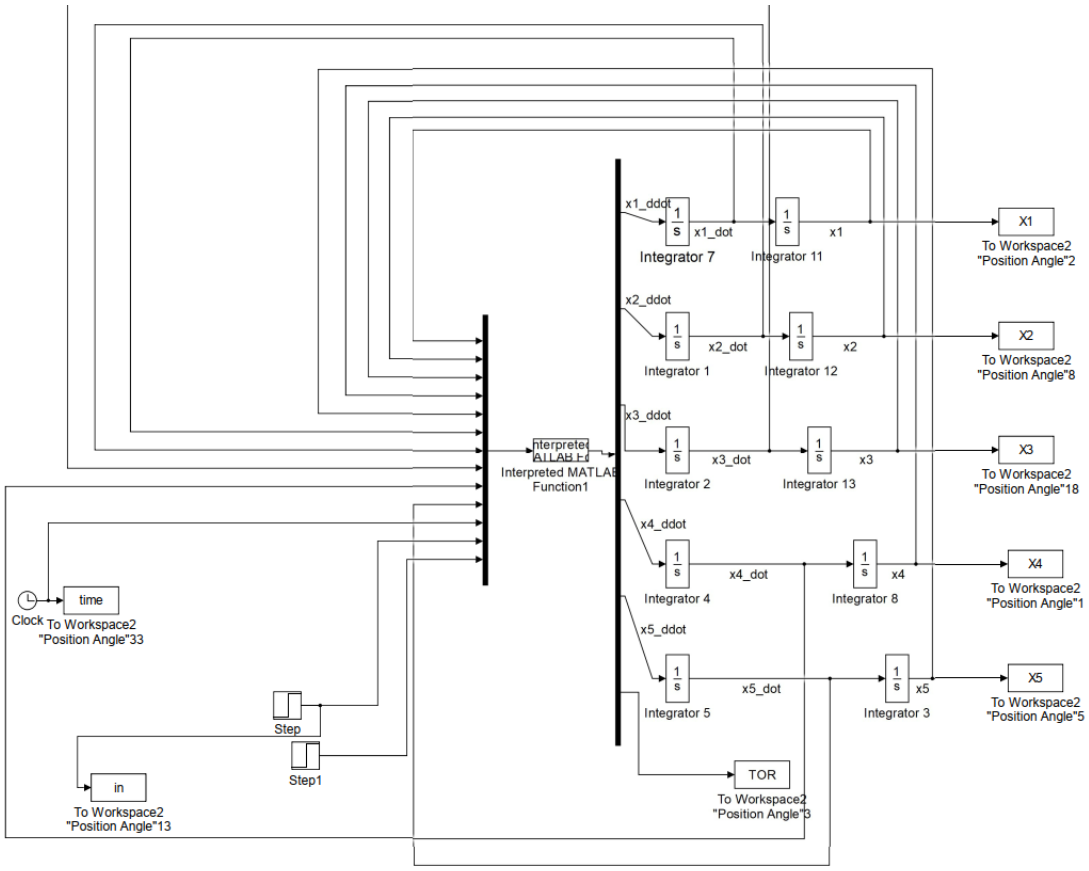

Figure (4.1): Simulink model of the human arm

4.4 Summary

In this chapter, eight-term exponential functions were used to describe the reference paths of the system displacements based on the initial, final, and intermediate conditions. The displacement, velocity, and acceleration were calculated, and thus the required elbow torque was calculated. Monte Carlo simulations were also performed under variable and random conditions.

Chapter Five: Results and Discussion

5.1 Introduction

In this chapter, the results will be presented and discussed for both the theoretical and numerical solutions presented in chapters three and four. This chapter includes four sections: The first section compares the linear and nonlinear simulations for small oscillations using MATLAB, the second section is obtaining the optimization and extracting the 15 optimal parameters of the system, human arm responses vs. time for three input values, the third section is obtaining the reference elbow torque computed analytically using the predefined reference displacement profiles and finally, numerical simulations with different initial conditions and system parameters using Monte Carlo simulation technique are adopted to confirm the presented algorithm.

5.2 Linear &nonlinear responses

Figures (5.1-5.5) illustrate the displacement responses of various segments of a human arm (hand, forearm, and elbow), considering both linear and nonlinear simulations. The system with both seniors oscillates to ensure similar underdamped patterns before stabilizing at steady states. Figs. (5.1-5.3) shows that the nonlinear hand, forearm, and elbow displacements exhibit a slightly larger initial amplitude due to the nonlinear behavior in the transient phase. Then, the simulations are satisfactorily matched, indicating successful linearization. On the other hand, as shown in Figs. (5.4-5.5), the nonlinear angular and vertical displacements of the elbow don't track the linear simulations as they should due to a significant role of the nonlinearity in the elbow joint. However, these differences in simulations might not be detrimental to creating an appropriate linear model, which can then be used to

compute the system response using the Lagrangian Optimization Method. The overshooting and settling time characteristics are evaluated after integrating the system using the MATLAB program. In this study, we plan to optimize the system's parameters (masses, spring stiffness, and damper coefficients) while achieving the desired overshooting and settling time as illustrated in Table 5-1. The objective function is defined as follows.

Table (5-1) The desired overshooting and settling time values

	Response Parameters	Constraints
1	Settling time t_s (s)	< 0.1 sec
2	Overshooting (100%), os	< 15 %

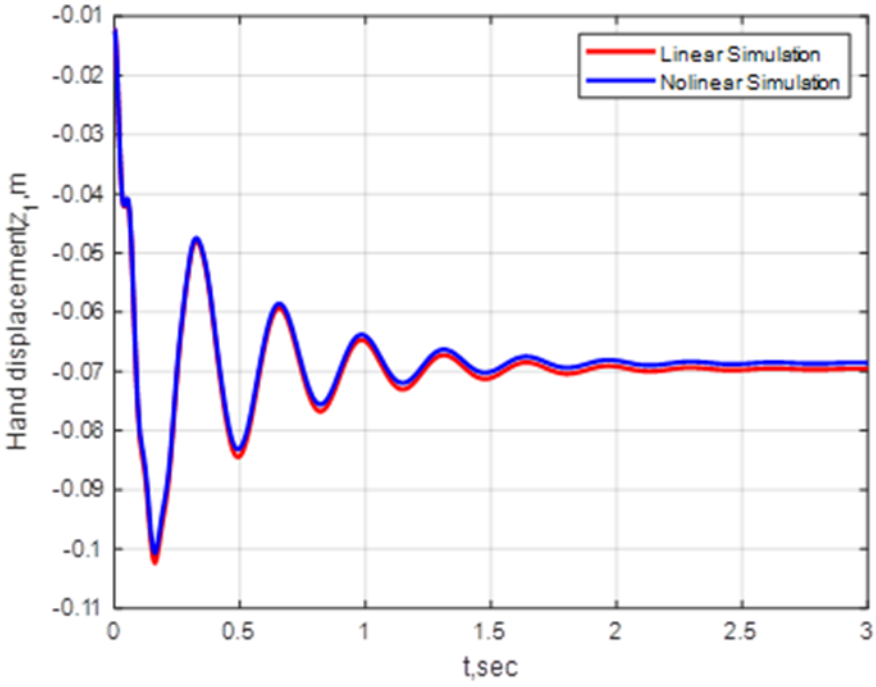

Figure 5.1: Time response of human hand displacement

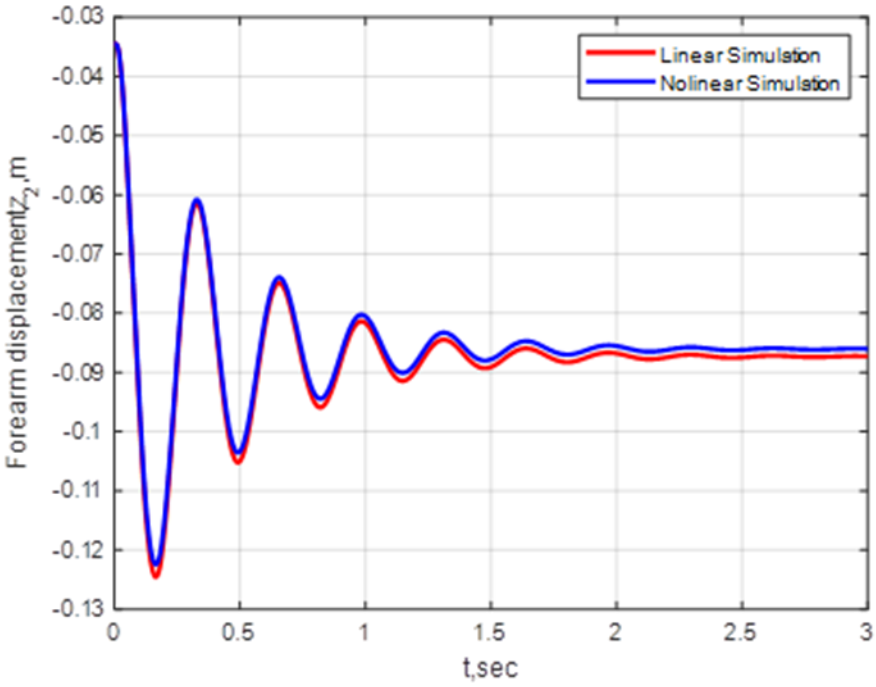

Figure 5.2: Time response of human forearm displacement

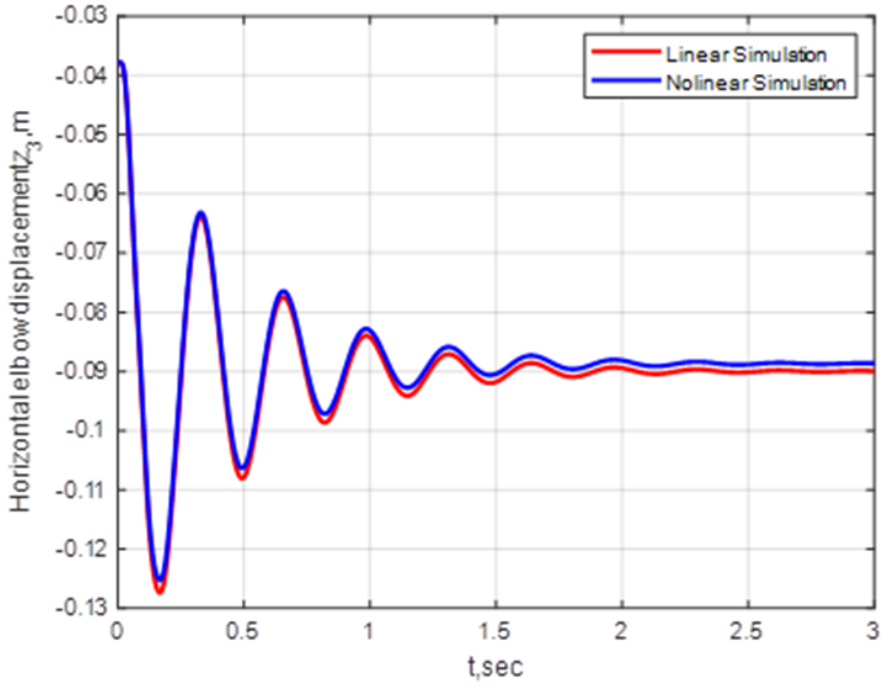

Figure 5.3: Time response of human elbow displacement

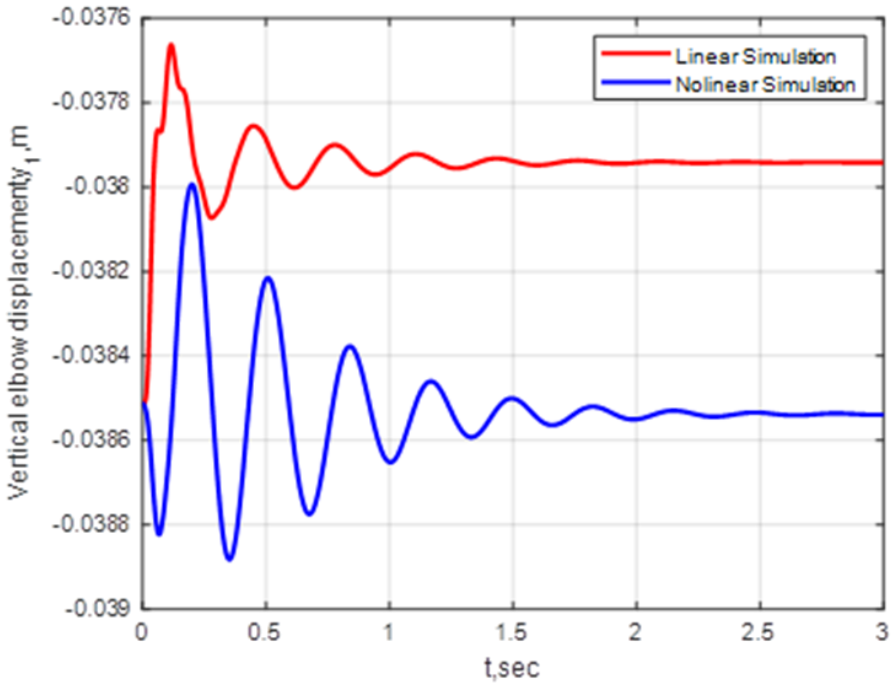

Figure 5.4: Time response of vertical elbow displacement

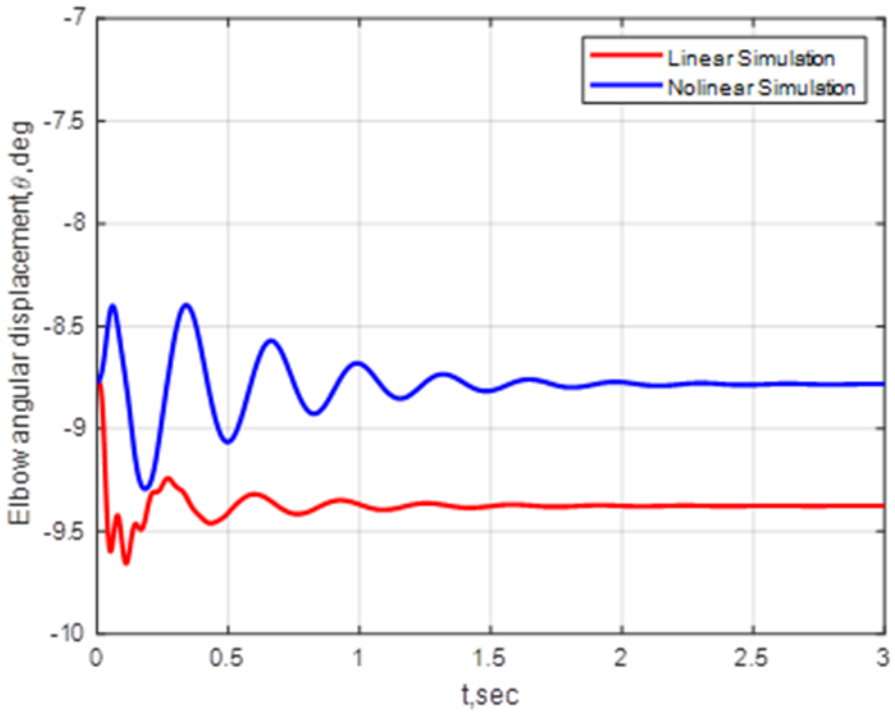

Figure 5.5: Time response of elbow angular displacement

5.3 Optimization

Figures (5.6a -5.6e) show a 3D representation of iterations, stiffness vector, and objective function during the optimization of human arm stiffness (k_1-k_t), respectively, under the nominal conditions ($\dot{z}_0$= 0, z_0 =15 cm). The objective function surface evolves rapidly from a cost function value of 500 (dark red) to a small value (light blue), then gradually captures nearly zero (dark blue). As we can see from Fig. (5.6) that quadratic objective function convergences as the iterations increase fulfilling the optimal stiffness values. Likewise, Figs. (5.7a-5.7e) and Figs. (5.8a-5.8c) present a 3D plot of iterations vs. damper vector vs. objective function and a 3D plot of iterations vs. mass vector vs. objective function in the optimization of human arm dampers (c_1-c_t) and masses (m_1-m_3), respectively. Following the same way as Fig. (5.6),

the Lagrangian multipliers method is used in Figs. (5.7) and (5.8) can successfully minimize the proposed objective function to approach the target values while involving the system parameters constraints. Thus, the optimization algorithm relying on the Lagrangian multipliers method can effectively stabilize the human arm model while ensuring a faster settling time and low overshoot under nominal conditions. However, it is unlikely that the human model will only encounter nominal conditions without experiencing severe off-nominal conditions. Hence, the optimal system parameters that were computed under the nominal conditions will be used to evaluate the system performance while exhibiting the off-nominal conditions($\dot{z}_0$ = 0, z_0 = 5 cm and $\dot{z}_0$ = 0, z_0 = 25 cm).

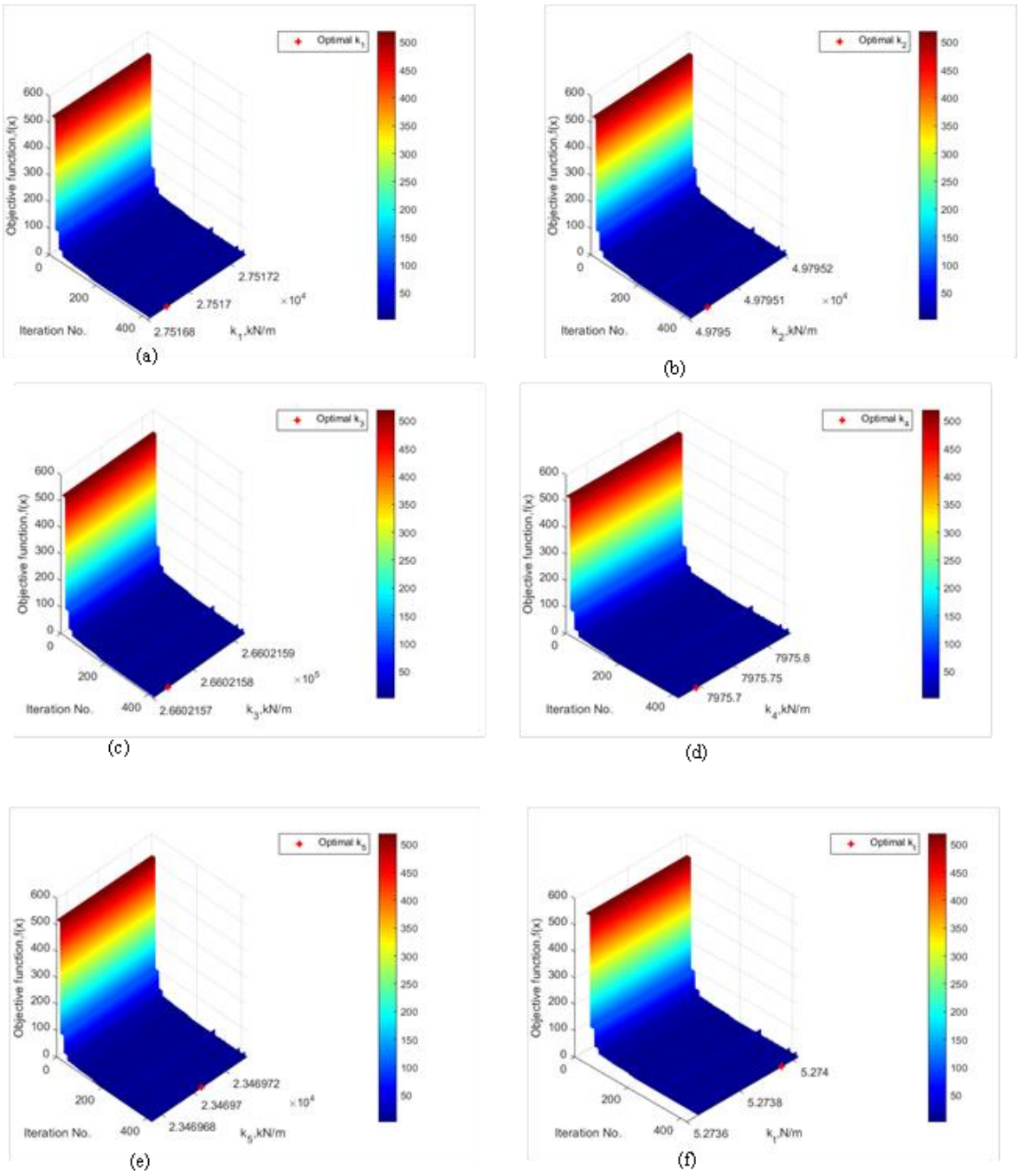

Fig 5.6: 3D objective function surface used to optimize the human arm stiffness; (a) stiffness (k_1); (b) stiffness (k_2); (c) stiffness (k_3); (d) stiffness (k_4); (e) stiffness (k_5); (f) stiffness (k_t).

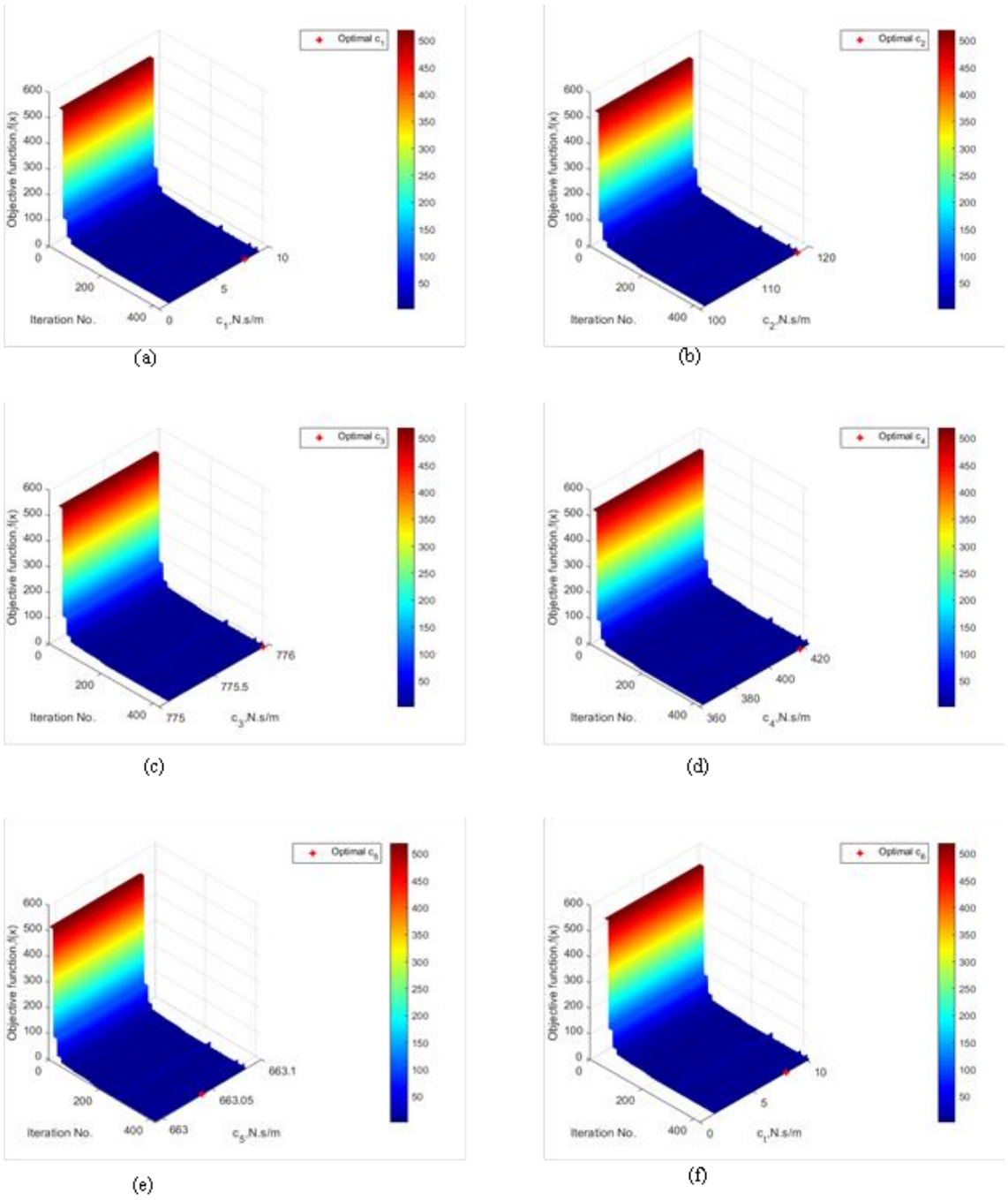

Fig 5.7: 3D objective function surface using to optimize the human arm dampers; (a) damper (c_1); (b) damper (c_2); (c) damper (c_3); (d) damper (c_4); (e) damper (c_5); (f) damper (c_t)

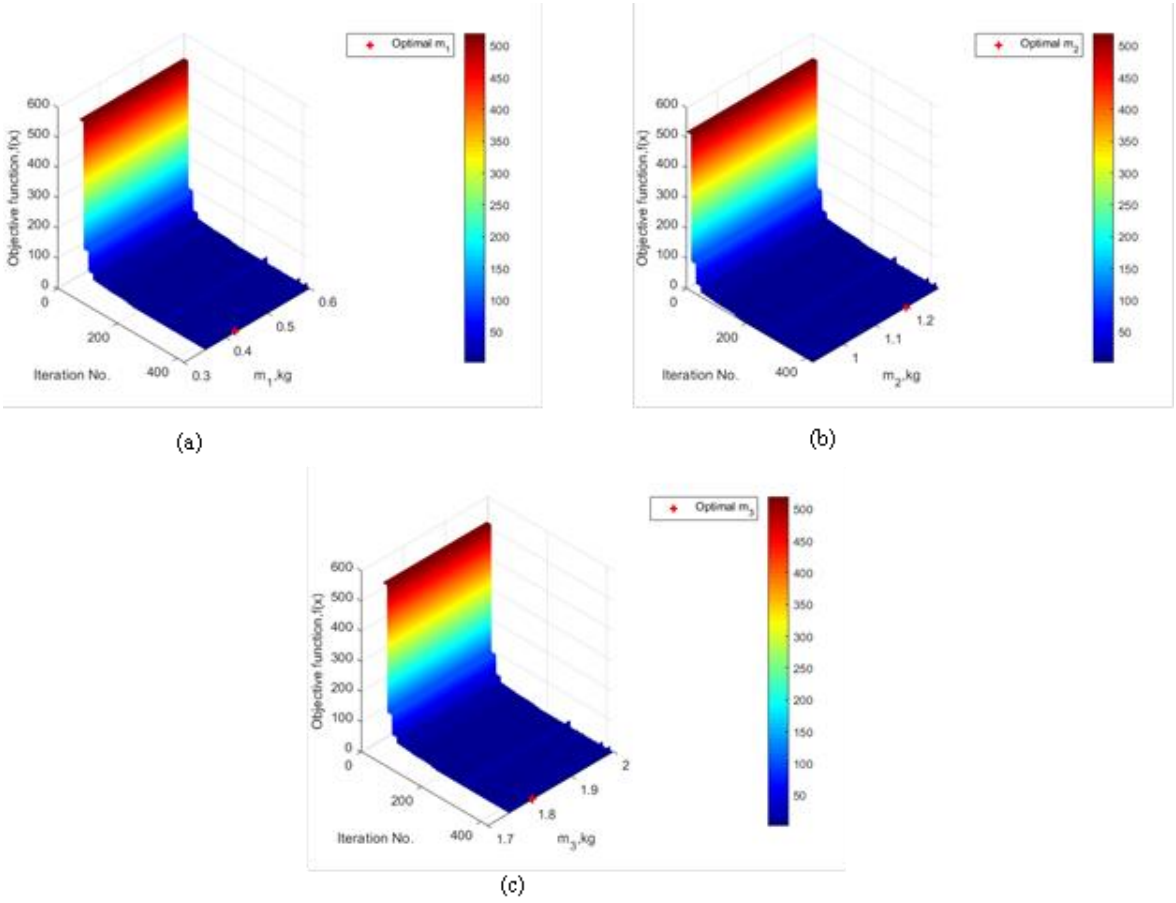

Fig 5.8: 3D objective function surface used to optimize the human arm masses;(a) hand mass (m_1); (b) forearm mass (m_2); (c) elbow mass (m_3)

Table (5-2) lists the system response characteristics for various system inputs. Table (5-2) shows that all the results are acceptable and do not exceed the system's constraints, resulting in good system performance.

Table(5.2): Optimal value of parameter

No.	Parameter	Value	Unit
1	k_1	27516.8906775296	N/m
2	k_2	49795.0379601206	N/m

3	k_3	266021.573689695	N/m
4	k_4	7975.69428129992	N/m
5	k_5	23469.7046188023	N/m
6	k_t	5273.95576943902	$N.m/rad$
7	c_1	7.83758878839669	$N.s/m$
8	c_2	117.817750777104	$N.s/m$
9	c_3	775.950122973788	$N.s/m$
10	c_4	418.050550772001	$N.s/m$
11	c_5	663.039914042647	$N.s/m$
12	c_t	80.4027185256979	$N.m.s/rad$
13	m_1	0.422425504229020	kg
14	m_2	1.19591727632143	kg
15	m_3	1.80742406776379	kg

Thus, the optimization algorithm relying on the Lagrangian multipliers method can effectively stabilize the human arm model while ensuring a faster settling time and low overshoot under nominal conditions. However, it is

unlikely that the human model will only encounter nominal conditions without experiencing severe off-nominal conditions. Hence, the optimal system parameters that were computed under the nominal conditions will be used to evaluate the system performance while exhibiting the off-nominal conditions ($\dot{z}_0 = 0$, $z_0 = 5$ cm and $\dot{z}_0 = 0$, $z_0 = 25$ cm).

Figures (5.9-5.13) present the human hand, forearm, horizontal elbow, vertical elbow, and elbow angular displacements vs. time, respectively, for three different input values. Figures (5.9-5.11) show decaying behavior of displacements; they start at higher initial values and decrease rapidly towards the desired values maintaining rapid settling time with a maximum value of (0.0352 s) and minimal overshoot with a maximum amount of(3.345%). On the other hand, as shown in Fig. (5.12), the vertical elbow displacement increases smoothly in the direction of the steady state vertical elbow without exceeding the proposed constraints of settling time (<0.1 s) and overshoot (<15%) Eventually, Fig. (5.13) illustrates that the elbow angle decreases gradually from the higher initial condition to the target value with 0.0904 s and 5.4% as the maximum settling time and the maximum overshot, respectively.

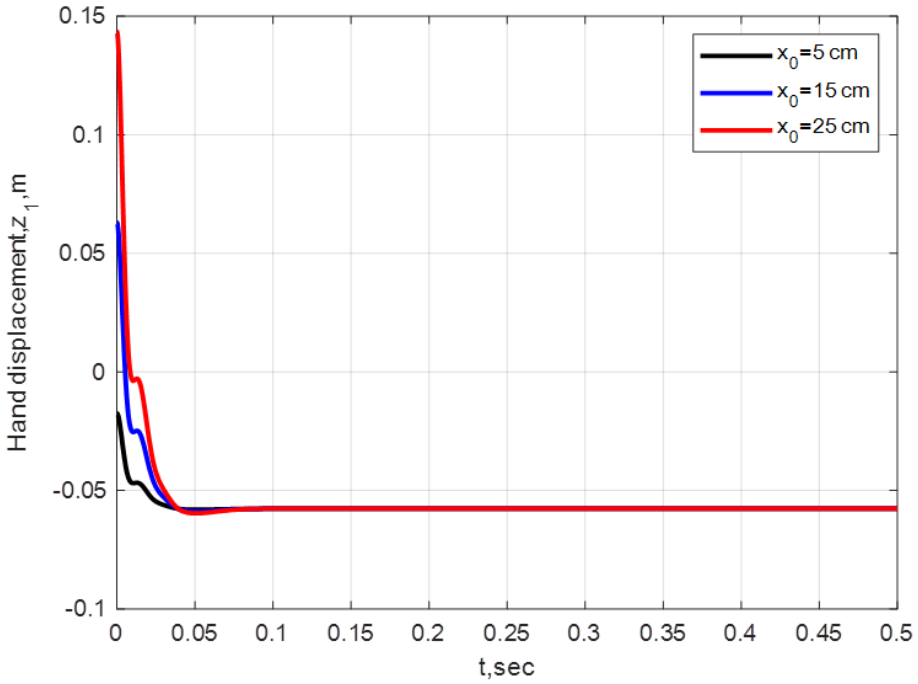

Figure 5.9: Hand displacement vs. time for three input values

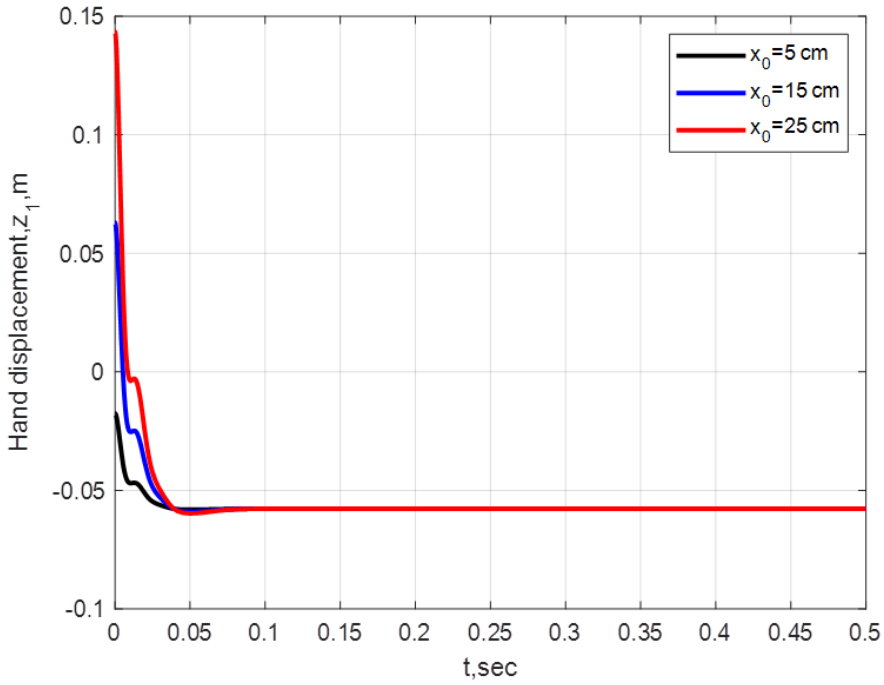

Figure 5.10: Forearm displacement vs. time for three input values

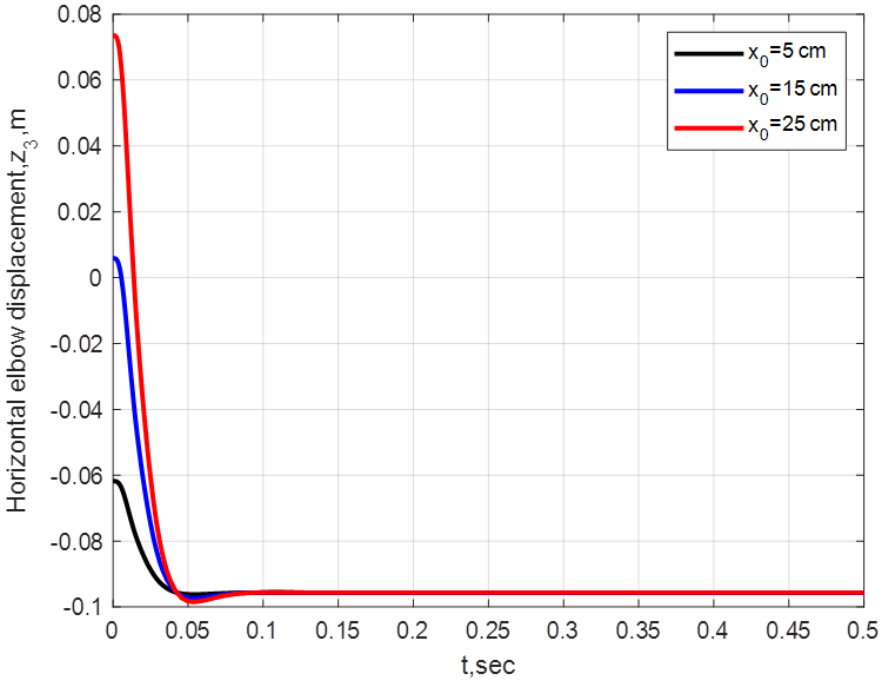

Figure 5.11: Horizontal elbow displacement vs. time for three input values

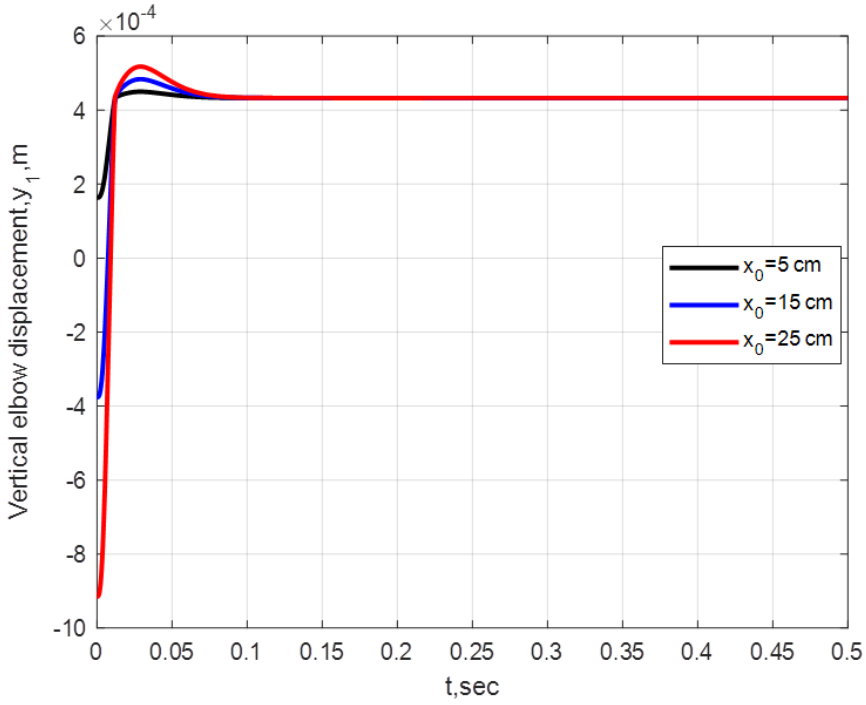

Figure 5.12: Vertical elbow displacement vs. time for three input values

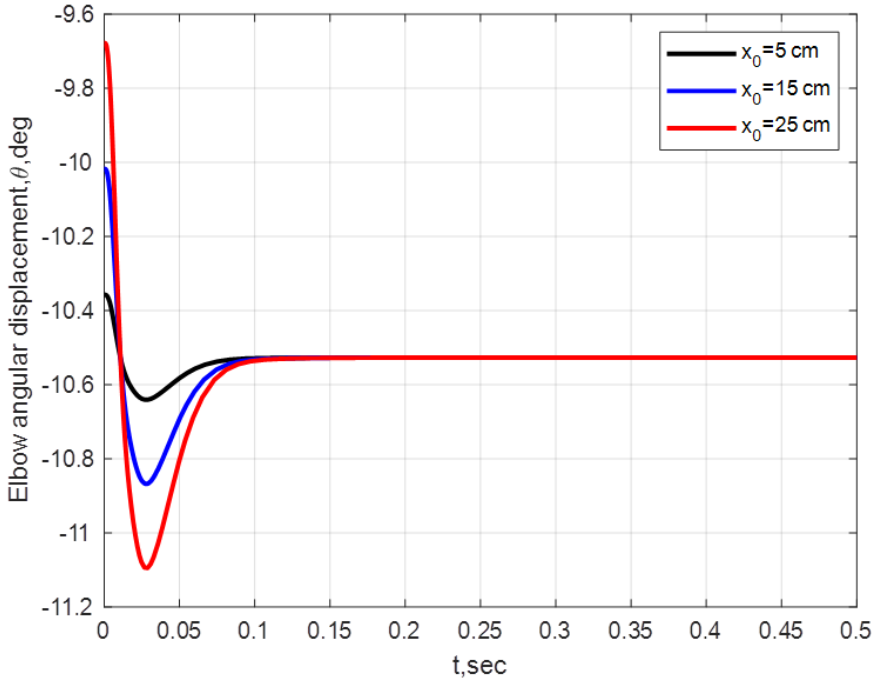

Figure 5.13: Elbow angular displacement vs. time for three input values

Table 5.3 shows that all the results are acceptable and do not exceed the system's constraints, resulting in good system performance.

Table (5.3) System response characteristics

No.	State	z_0=5 cm		z_0=15 cm		z_0=25 cm	
		Settling time (s)	Overshoot 100%	Settling time (s)	Overshoot 100%	Settling time (s)	Overshoot 100%
1	Hand displacement	0.0335	0.6721	0.0342	2.0143	0.0352	3.3450
2	Forearm displacement	0.0373	0.6224	0.0372	1.8666	0.0375	3.1428
3	Elbow displacement	0.0382	0.5885	0.0383	1.7713	0.0385	2.9628
4	Vertical elbow displacement	0.0563	3.4939	0.0581	9.4824	0.0563	14.4696
5	elbow angle	0.0904	1.0778	0.0899	3.2331	0.0897	5.3905

5.4 Analytical Methodology

Figures (5.14-5.19) display the reference hand displacement, forearm displacement, horizontal elbow displacement, vertical elbow displacement, elbow angular displacement, and elbow torque vs. time, respectively, under the nominal conditions for three excited displacements of (z_0 = 5 cm, z_0 = 15 cm and z_0 = 25 cm). The findings demonstrate that an increase in the excited displacement causes higher initial magnitudes of all the states due to a higher stored energy. Furthermore, the reference profiles indicate that the analytical controller is reliable and the reference displacement profiles can be easily followed to capture the desired steady states even under varying initial displacements and system parameters, as will be discussed in the section that follows.

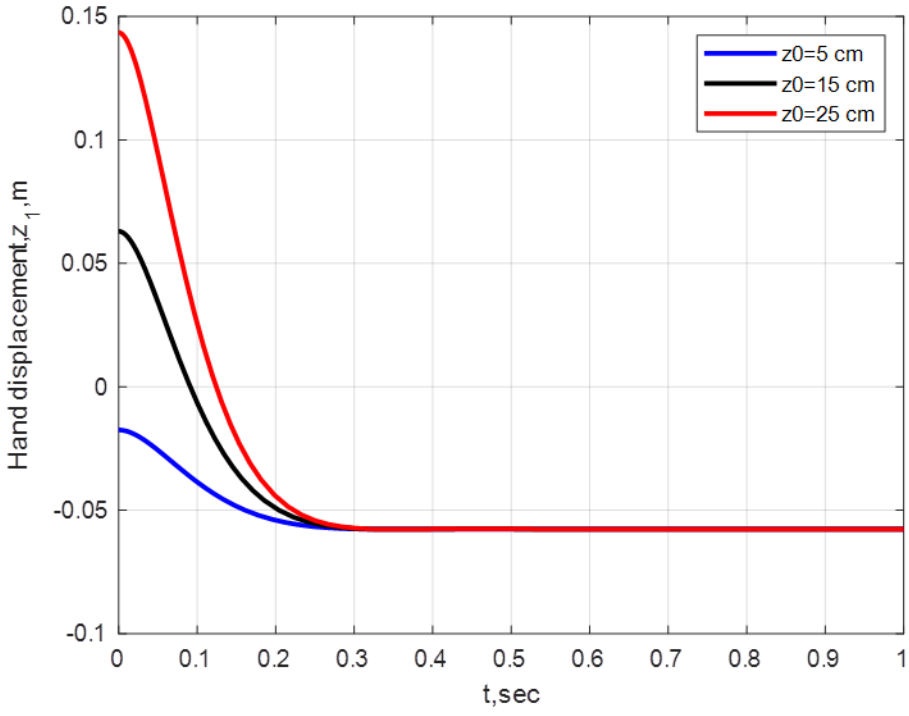

Figure 5.14: Reference hand displacement vs. time under nominal conditions for three excited displacements

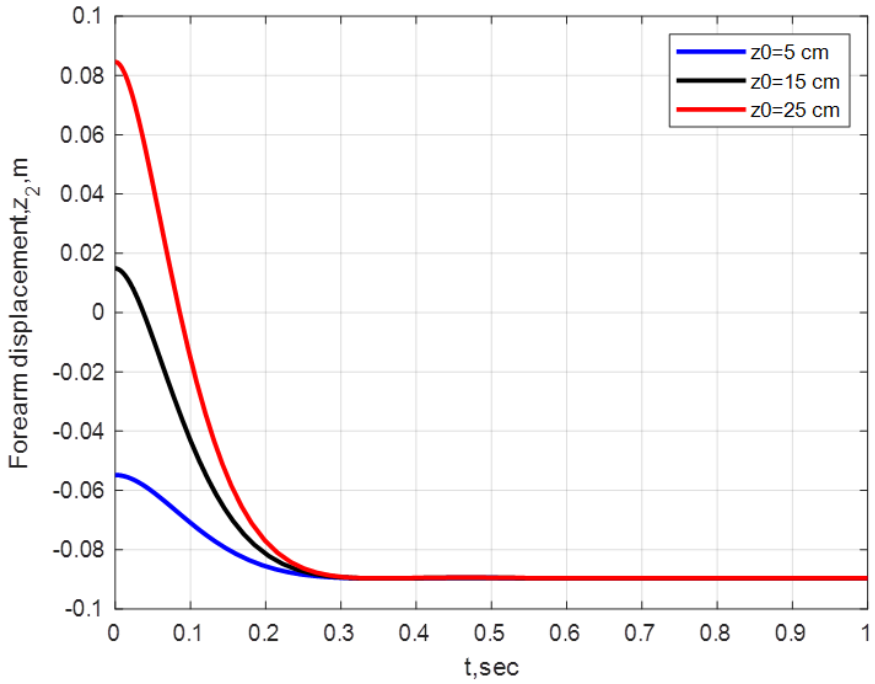

Figure 5.15: Reference forearm displacement vs. time under nominal conditions for three excited displacements

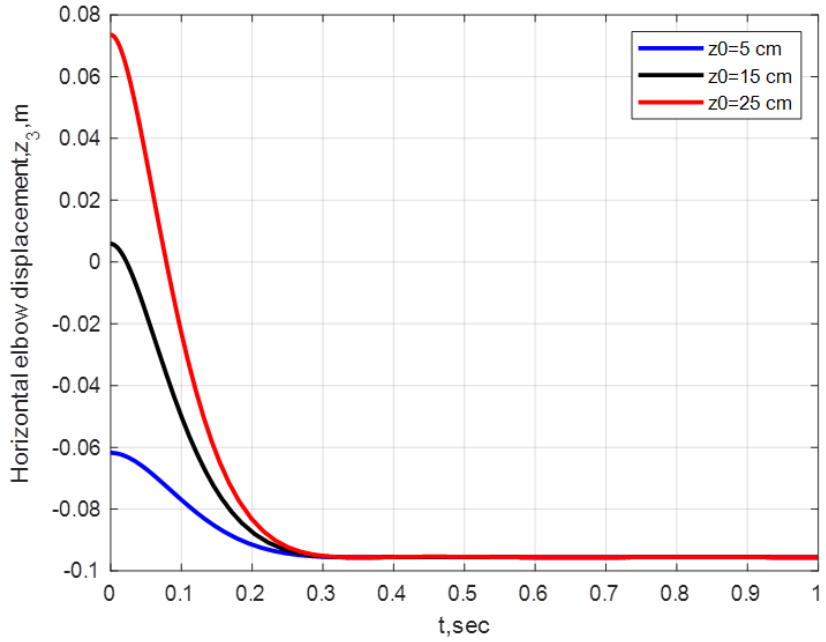

Figure 5.16: Reference horizontal elbow displacement vs. time under nominal conditions for three excited displacements

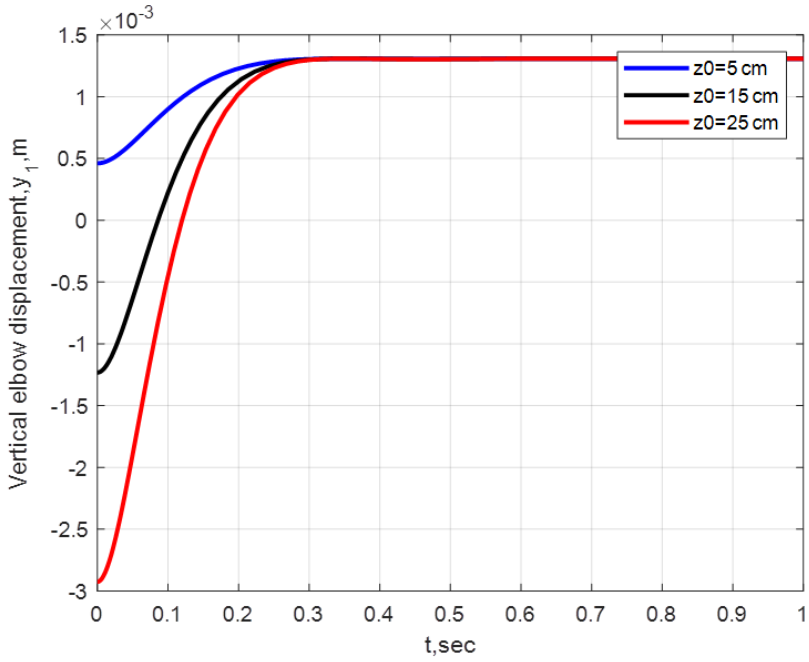

Figure 5.17: Reference vertical elbow displacement vs. time under nominal conditions for three excited displacements

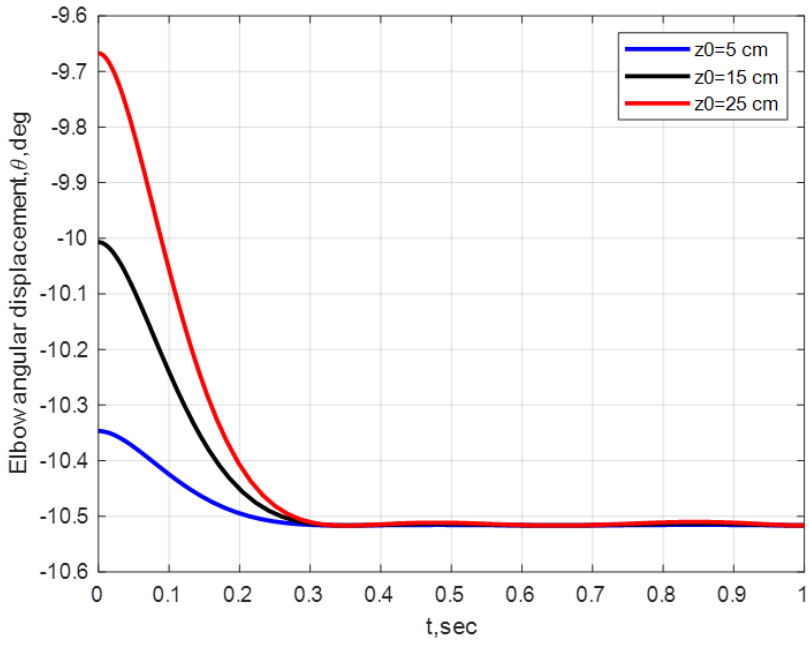

Figure 5.18: Reference elbow angular displacement vs. time under nominal conditions for three excited displacements

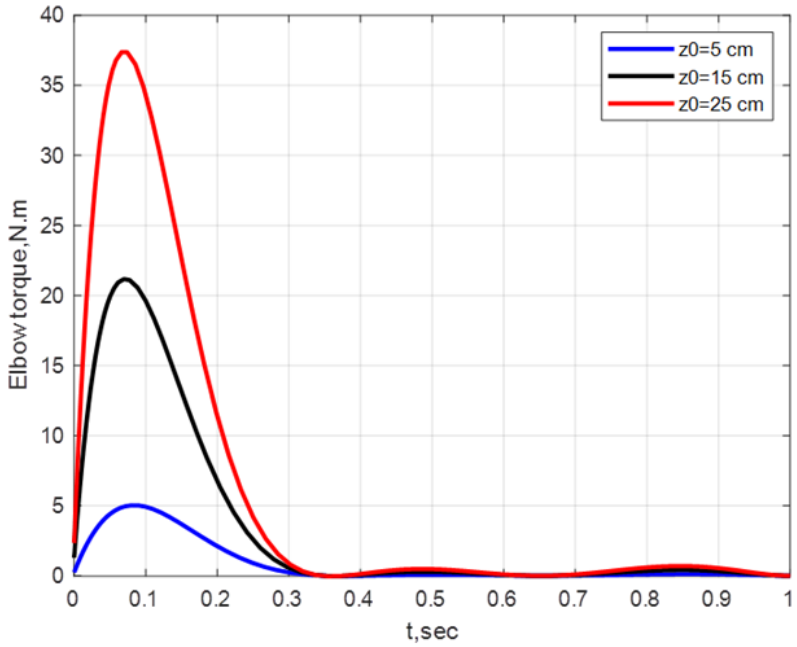

Figure 5.19: Elbow torque vs. time under nominal conditions for three excited displacements

Figures (5.20-5.24) show the reference hand, forearm, horizontal elbow, vertical elbow, and elbow angular profiles vs. time, respectively, under three different initial displacements of 5cm, 15 cm, and 25 cm, with the application of the proposed analytical controller. (5.21) and (5.22) indicate that the exoskeleton system is highly capable of tracking the reference displacements. While Figs. (5.20), (5.23) and (5.24) observe a well-suited agreement at the steady state phase with minor discrepancies at the start due to the stronger nonlinearity of the elbow angle. On the whole, the presented results denote the capability of the analytical control to guide the exoskeleton arm swiftly within 0.35 sec without necessitating any additional feedback elbow torque. The analytical solution showed accuracy in describing the dynamic behavior, and its results are consistent with the numerical simulation, confirming the validity of the mathematical model and its potential use in designing control systems.

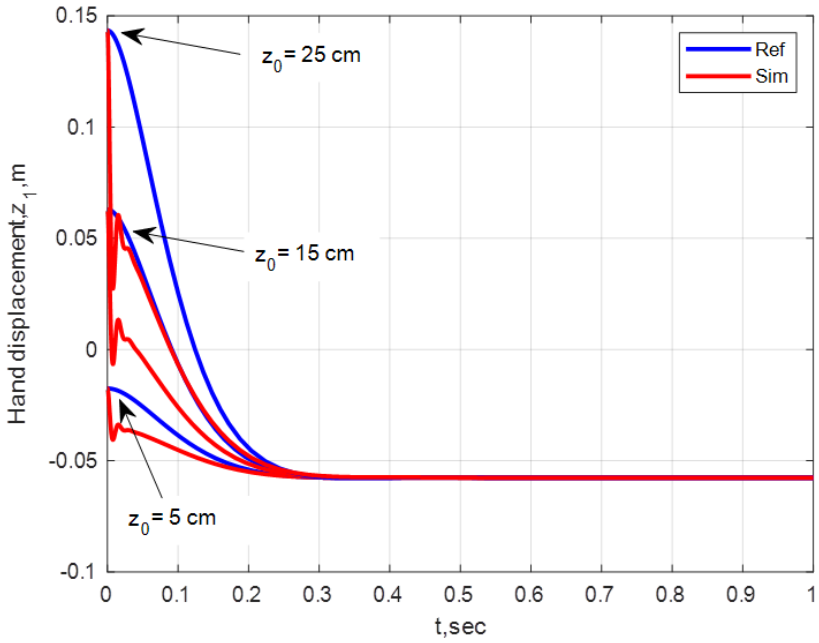

Figure (5.20): Reference and simulated hand displacement versus time under nominal conditions for three excited displacements

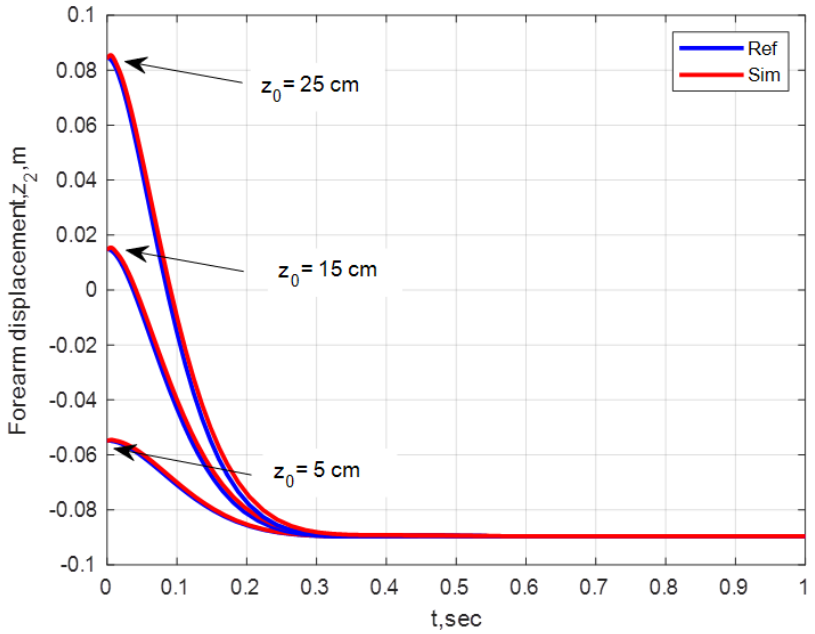

Figure (5.21): Reference and simulated forearm displacement versus time under nominal conditions for three excited displacements

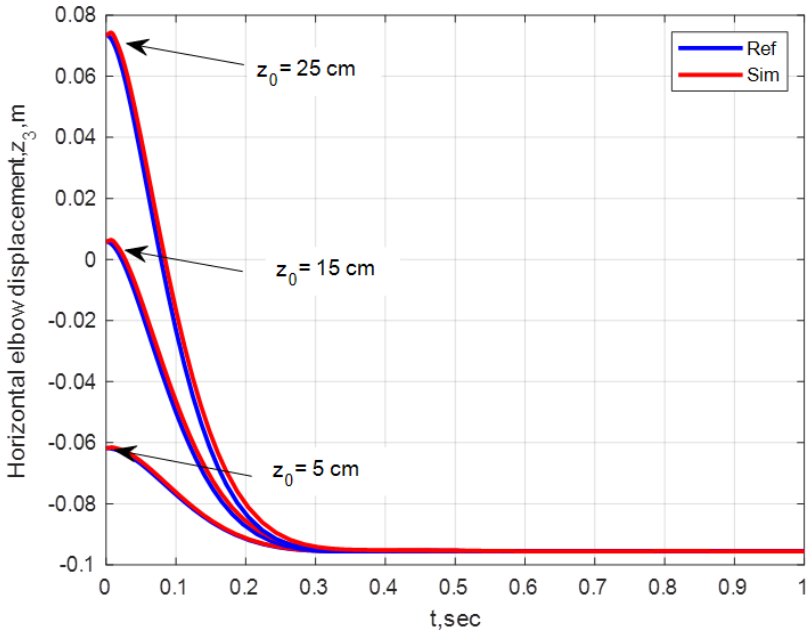

Figure (5.22): Reference and simulated horizontal elbow displacement versus time under nominal conditions for three excited displacements

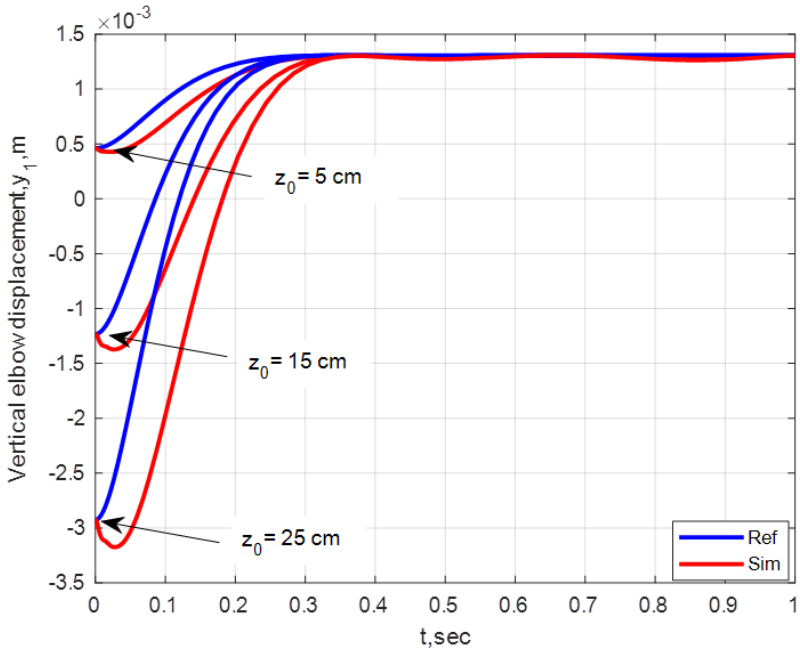

Figure (5.23): Reference and simulated vertical elbow displacement versus time under nominal conditions for three excited displacements

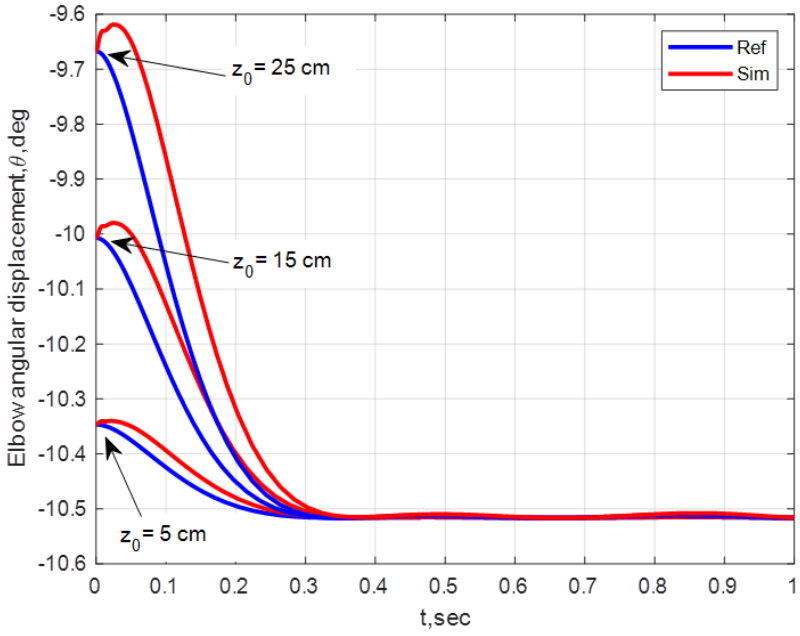

Figure (5.24): Reference and simulated elbow angular displacement versus time under nominal conditions for three excited displacements

5.5 Monte Carlo Simulation

Figures (5.25-5.30) show histories of hand, forearm, horizontal elbow, vertical elbow, and elbow angular displacements errors and histories of the required elbow torque vs. time, respectively, for 1000 patients. Figures (5.25-5.29) show that all the simulated displacement errors exhibit a fast decay during the first 0.25 sec and then the errors converge seamlessly to zero with no overshoot throughout the rest of the simulation. Finally, Figure (5.30) shows that the elbow torque profiles remain below the maximum permissible value (< 60 N.m), which reveals that the arm exoskeleton may reach the desired steady state with no chance of system damage.

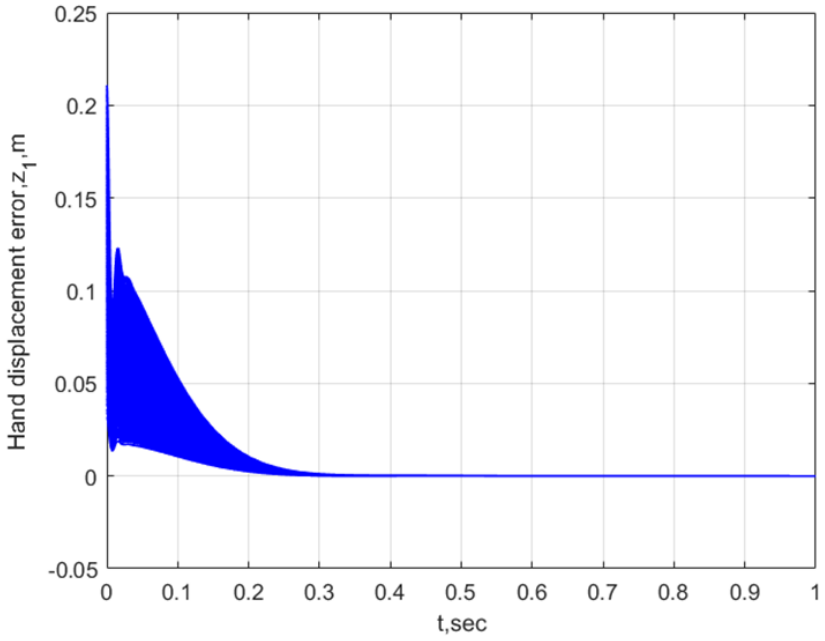

Figure (5.25): 1000 Human arm exoskeleton's histories versus time using analytical controller for hand displacement error versus time

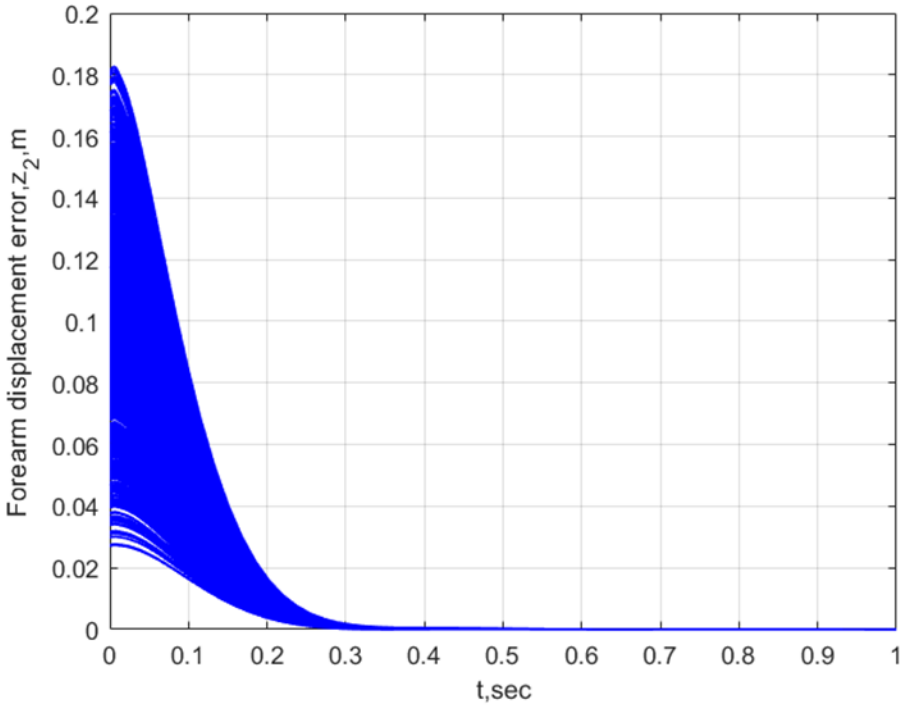

Figure (5.26): 1000 Human arm exoskeleton's histories versus time using analytical controller for forearm displacement error versus time

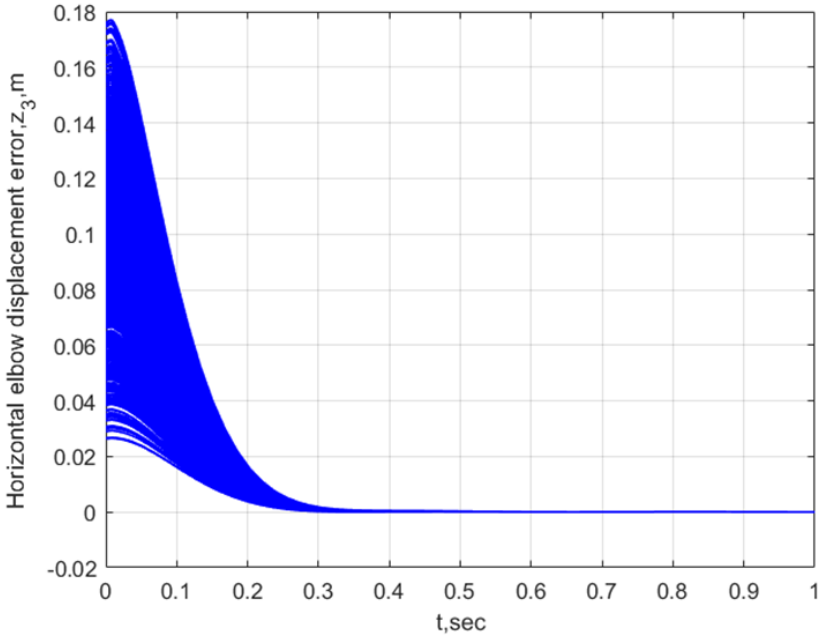

Figure (5.27): 1000 Human arm exoskeleton's histories versus time using analytical controller for horizontal elbow displacement error versus time

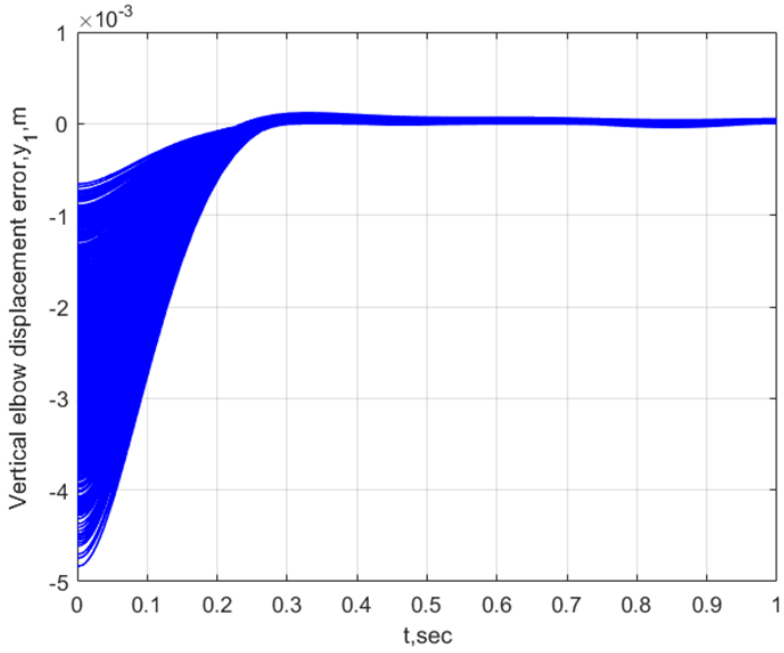

Figure (5.28): 1000 Human arm exoskeleton's histories versus time using analytical controller for vertical elbow displacement error versus time

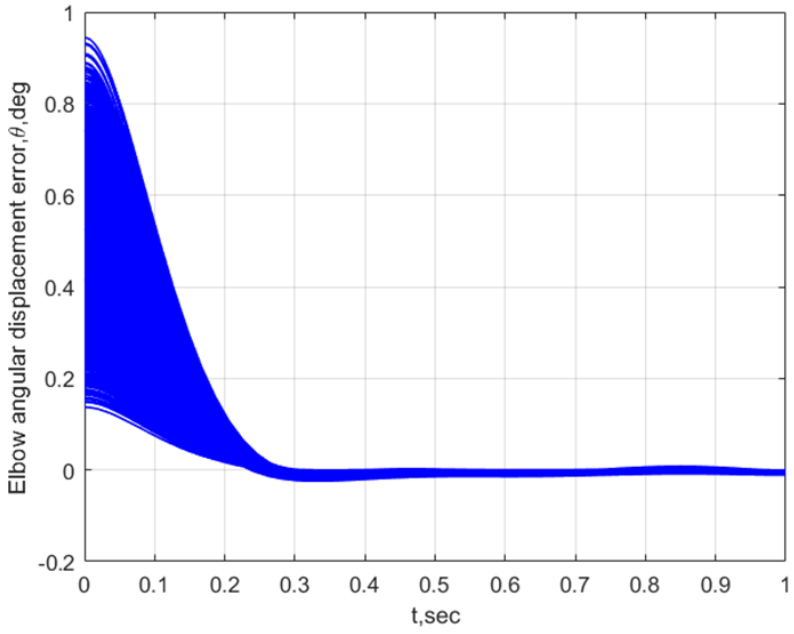

Figure (5.29): 1000 Human arm exoskeleton's histories versus time using analytical controller for elbow angular displacement error versus time

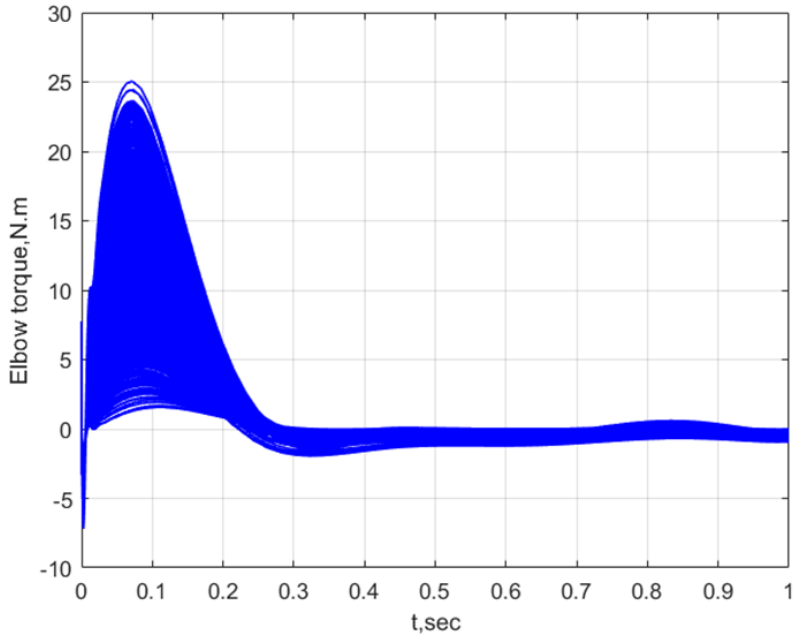

Figure (5.30): 1000 Human arm exoskeleton's histories versus time using analytical controller for elbow torque error versus time

Figures (5.31-5.36) show the statistical results of the hand displacement, forearm displacement, horizontal elbow displacement, vertical elbow displacement, and elbow angular displacement, and elbow torque errors, respectively, at the final position. It is observed from the Figures that the final errors exhibit very small values despite a broad range of dispersions in the initial conditions and system parameters.

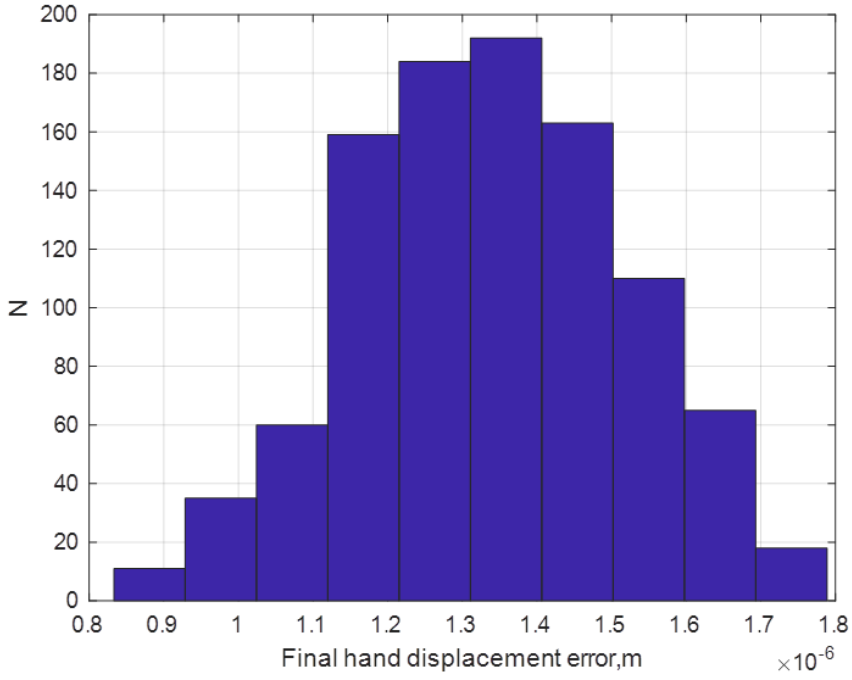

Figure (5.31): Statistics errors for the final hand displacement vs number of patients

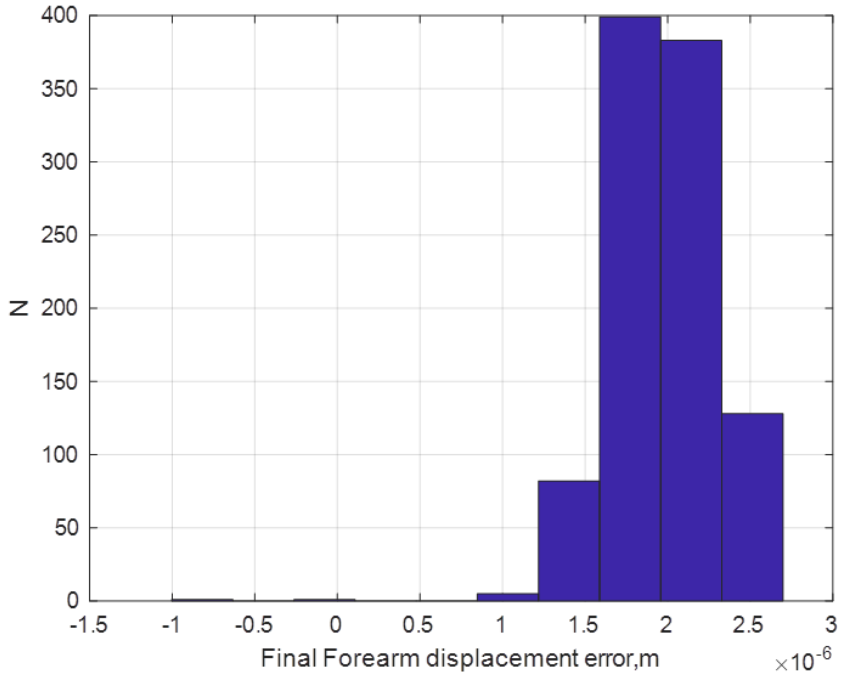

Figure (5.32): Statistical errors for the final forearm displacement vs the number of patients

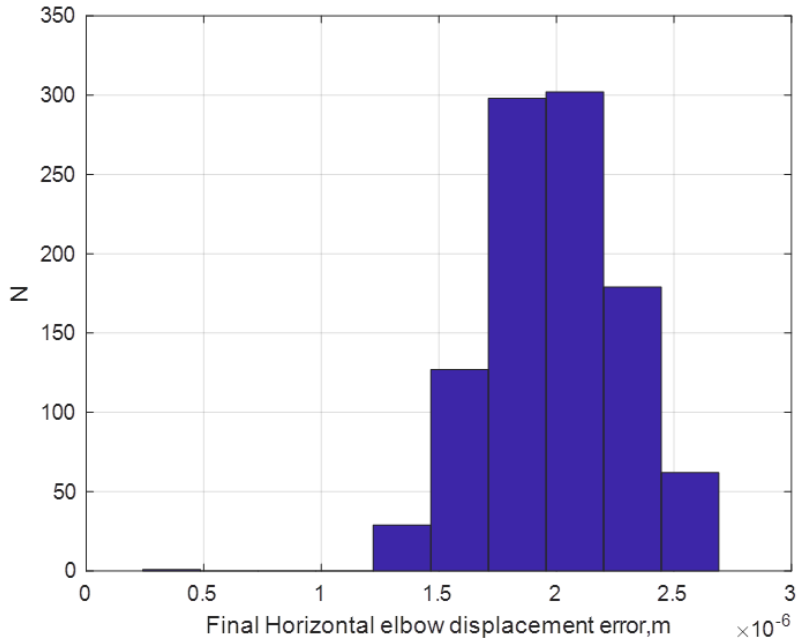

Figure (5.33): Statistical errors for the final horizontal elbow displacement vs the number of patients

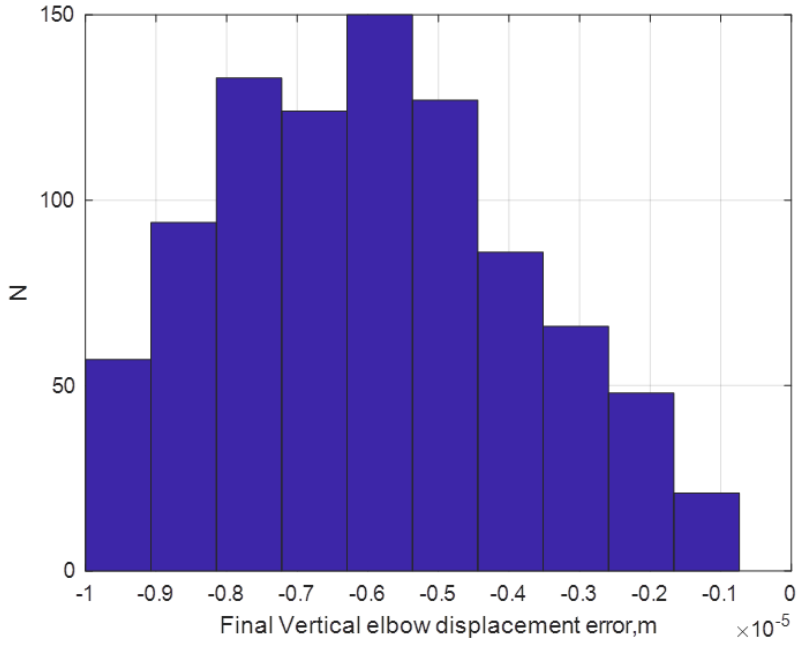

Figure (5.34): Statistical errors for the final vertical elbow displacement vs the number of patients

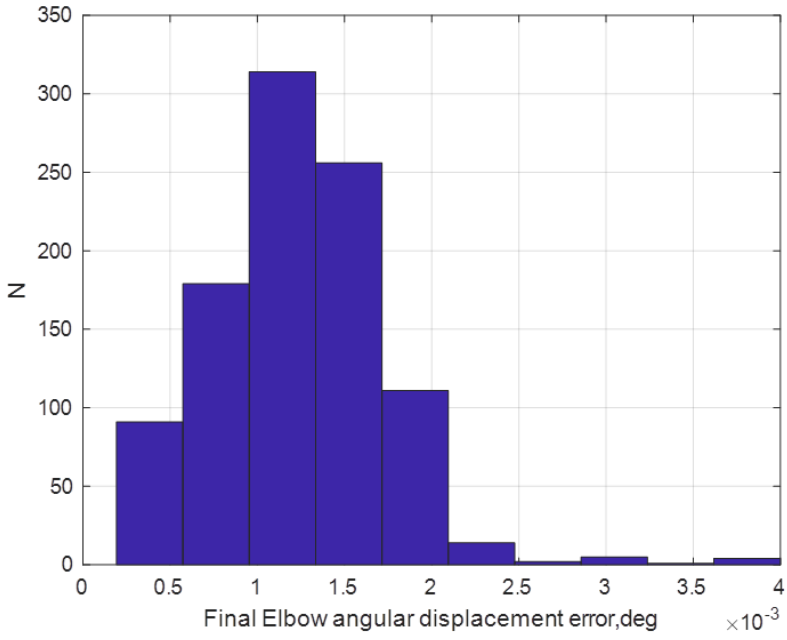

Figure (5.35): Statistical errors for the final elbow angular displacement vs the number of patients

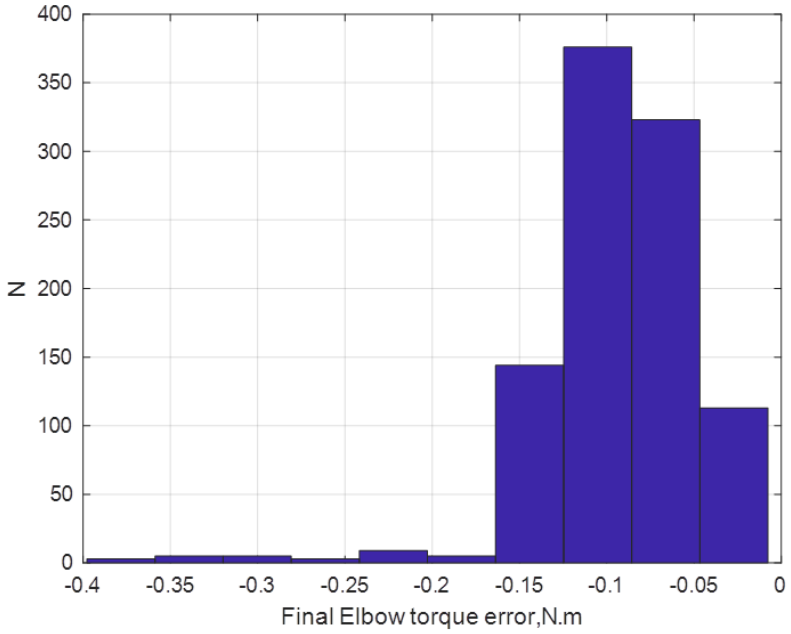

Figure (5.36): Statistical errors for the final elbow torque displacement vs the number of patients

5.6 Summary

This chapter has presented the steps for the linear and nonlinear responses. The linearization process can be applied to nonlinear state-variable equations to displacement responses of various segments of the human arm (hand, forearm, and elbow). It is also demonstrated how optimization of human arm stiffness, that is, the process of making something as effective, functional, or perfect as possible within given constraints. Monte Carlo Simulation has been proposed. It is a computational method that uses repeated random sampling to model a system's potential outcomes and analyze uncertainty, particularly useful in complex or unpredictable processes. By running a model thousands of times with randomly selected input variables, it generates a probability distribution of possible results, helping to forecast

future scenarios, histories of hand, forearm, horizontal elbow, vertical elbow, and elbow angular displacement errors, and histories of the required elbow torque vs. time. The results have shown that all the simulated displacement errors exhibit a fast decay during the first 0.25 sec, and then the errors converge seamlessly to zero with no overshoot throughout the rest of the simulation.

Chapter Six: Conclusions and Recommendations

6.1. Conclusion:

The purposed tequnch successfully identified of the optimal parameters for (5-Dof) artificial arm using Lagrangian multipliers method achieving rapid response (0.25) second with no overshoot across 1000 simulated cases. From the following conclusions can be drawn:

1. The Lagrangian multipliers optimization method demonstrated a high capability in accurately estimating the arm parameters, including masses, damping coefficients, and stiffness, while ensuring a short settling time and minimum overshoot. Even under relatively large initial displacements, the hand, forearm, and elbow responses converged rapidly to their desired values, achieving a settling time of no more than 0.0385 s and an overshoot limited to 3.345%.
2. The vertical displacement of the elbow exhibited a smooth and stable response toward its steady-state position, while preserving fast convergence. The maximum settling time did not exceed 0.0581 s, and the overshoot remained within an acceptable upper bound of 14.45%.
3. Overall, these results confirm the effectiveness of the proposed control strategy, which is based on eight-term exponential functions for generating analytical reference trajectories of the system displacements. By incorporating the excited displacement along with the initial, intermediate, and final boundary conditions, the eight-term analytical expressions were linearly solved to derive the required analytical elbow torque, enabling the arm exoskeleton to move smoothly from the initial state to the desired steady-state configuration.

4. One of the more significant findings to emerge from this study is that numerical simulations with different initial conditions and system parameters were implemented to confirm the presented algorithm. A wide range of dispersions of hand, forearm, and upper-arm masses, segment lengths, arm stiffness, and damping coefficients with ($\pm$6%) added to the nominal conditions have been conducted.

5. The results revealed rapid convergence, ensuring steady state within 0.25 sec and zero overshoot in both system displacements and elbow torque without requiring any further feedback elbow torque.

6. In addition, the statistical results illustrated that the steady-state errors remained very small with a maximum error of (4×10^{-3}) deg in the elbow angle, a minimum error of (-1×10^{-5}) m in the vertical elbow displacement, and a minimum elbow torque error as small as (-0.4) N.m even across 1000 patients.

6.2 Recommendation for future work

This thesis has developed to find the torque that must be applied to a five-degree-of-freedom artificial human arm to control the system's efficiency and motion response. Although the desired human arm functions have been achieved, further improvement could be made, and new capabilities could be developed in the future.

1. The mathematical model can be expanded to include additional degrees of freedom.

2. Other nonlinear control methods , such as adaptive, fuzzy,optimal , or sliding mode controls can be used to control the nonlinear arm system and their performance might be compared with the proposed analytical controller.

3. Future researchers are encouraged to link the numerical results to practical simulations to verify the effectiveness of the mathematical model.

4. Future studies should be directed toward using the model in medical rehabilitation for patients after stroke and linking it to real patient data.

Reference

[1] E. Rocon, A. F. Ruiz, J. L. Pons, J. M. Belda-Lois, and J. J. Sanchez-Lacuesta, "Rehabilitation Robotics: A Wearable Exoskeleton for Tremor Assessment and Suppression," in Proc. Int. Conf. on Robotics and Automat., Barcelona, Spain, 2005, pp. 241-246.

[2] "Mechanical_designs_of_active_upper_limb"

[3] J. C. Perry, J. Rosen, and S. Burns "Upper-Limb Powered Exoskeleton Design," IEEE/ASME Trans. on Mechatronics, vol. 12, no. 4, pp. 408-417, 2007.

[4] P. K. Artemiadis, P. T. Katsiaris, M. V Liarokapis, and K. J. Kyriakopoulos, "Human arm impedance: Characterization and modeling in 3D space," in *2010 IEEE/RSJ International Conference on Intelligent Robots and Systems*, IEEE, Oct. 2010, pp. 3103–3108. doi: 10.1109/IROS.2010.5652025.

[5] S. I. . Ao, *International MultiConference of Engineers and Computer Scientists : IMECS 2009 : 18-20 March, 2009, Regal Kowloon Hotel, Kowloon, Hong Kong*. Newswood Ltd. : International Association of Engineers, 2009.

[6] G. Schmeisser and W. Seamone, "An Upper Limb Prosthesis-Orthosis Power and Control System with Multi-Level Potential," J. Bone Joint Surg. Am., vol. 55, pp. 1493–1501, 1973.

[7] I. Kawabuchi, "A Designing of Humanoid Robot Hands in Endo skeleton and Exoskeleton Styles," Humanoid Robots, New Developments, Book edited by Armando Carlos de Pina Filho, pp. 401-426, 2007.

[8] M. Mailah, H. Jahanabadi, M. Z. M. Zain, and G. Priyandoko, "Modelling and control of a human-like arm incorporating muscle models," *Proc Inst Mech Eng C J Mech Eng Sci*, vol. 223, no. 7, pp. 1569–1577, Jul. 2009, doi: 10.1243/09544062JMES1289.

[9] W. G. Hao, Y. Y. Leck, and L. C. Hun, "6-DOF PC-Based Robotic Arm (PC-ROBOARM) with efficient trajectory planning and speed control," in *2011 4th International Conference on Mechatronics (ICOM)*, IEEE, May 2011, pp. 1–7. doi: 10.1109/ICOM.2011.5937171.

[10] B. C. N. Jolly Shah, S.S.Rattan and Abstract—Automatic, "Kinematic Analysis of 2-DOF Planer Robot Using Artificial Neural Network," *International Journal of Mechanical and Mechatronics Engineering*, vol. 5, no. 9, pp. 1720–1723, 2011, doi: https://doi.org/10.5281/zenodo.1058563.

[11] L. A. Al-zu, A. A. Al-tamimi, T. D. Al-momani, A. J. Alkarala, and M. A. Alzawahreh, "Modeling and simulating human arm movement using a 2 dimensional 3 segments coupled pendulum System," 2012.

[12] T. Fadhil Abbas, "Forward Kinematics Modeling of 5 DOF Stationary Articulated Robots," 2013. doi: 10.30684/etj.31.3a.8.

[13] K. Serbest, M. Cilli, M. Z. Yildiz, and O. Eldogan, "Development of a human hand model for estimating joint torque using MATLAB tools," in *2016 6th IEEE International Conference on Biomedical Robotics and Biomechatronics (BioRob)*, IEEE, Jun. 2016, pp. 793–797. doi: 10.1109/BIOROB.2016.7523724.

[14] B. Sheng, W. Meng, C. Deng, and S. Xie, "Model based kinematic & dynamic simulation of 6-DOF upper-limb rehabilitation robot," 2016. doi: 10.1109/ACIRS.2016.7556181.

[15] A. N. Barakat, K. A. Gouda, and K. A. Bozed, “Kinematics analysis and simulation of a robotic arm using MATLAB,” in *4th International Conference on Control Engineering and Information Technology, CEIT 2016*, IEEE, Dec. 2017, pp. 1–5. doi: 10.1109/CEIT.2016.7929032.

[16] M. C. Agarana and E. T. Akinlabi, “Lagrangian analysis of total mechanical energy of human arm as an inverted triple pendulum robot in motion,” *International Journal of Mechanical Engineering and Technology*, vol. 9, no. 8, pp. 1313–1320, 2018.

[17] M. C. Agarana and E. T. Akinlabi, “Mathematical Modelling and Analysis of Human Arm as a Triple Pendulum System using Euler - Lagragian Model,” in *IOP Conference Series: Materials Science and Engineering*, Sep. 2018, p. 012010. doi: 10.1088/1757-899X/413/1/012010.

[18] Y. Li *et al.*, “Optimization of dynamic load distribution of a serial-parallel hybrid humanoid arm,” *Mech Mach Theory*, vol. 149, p. 103792, Jul. 2020, doi: 10.1016/j.mechmachtheory.2020.103792.

[19] H. Khan, H. H. Kim, S. J. Abbasi, and M. C. Lee, “Real-Time Inverse Kinematics Using Dual Particle Swarm Optimization DPSO of 6-DOF Robot for Nuclear Plant Dismantling,” *IFAC-PapersOnLine*, vol. 53, no. 2, pp. 9885–9890, 2020, doi: 10.1016/j.ifacol.2020.12.2695.

[20] T. Mohanto, A. Talukde, and Z. Tasneem, “Development of a 3DOF Color Sorting based Robotic Arm using MATLAB GUI,” in *2020 23rd International Conference on Computer and Information Technology (ICCIT)*, IEEE, Dec. 2020, pp. 1–6. doi: 10.1109/ICCIT51783.2020.9392750.

[21] H. Dawood Salman, M. Noori Hamzah, and S. Hussein Bakhy, “KINEMATICS ANALYSIS AND IMPLEMENTATION OF THREE

DEGREES OF FREEDOM ROBOTIC ARM BY USING MATLAB," *THE IRAQI JOURNAL FOR MECHANICAL AND MATERIALS ENGINEERING*, vol. 21, no. 2, pp. 118–129, Jun. 2021, doi: 10.32852/iqjfmme.v21i2.547.

[22] S. O. Moses, E. I. Olalekan, E. T. Aniemeka, and A. Lukman, "Development of a programmable robotics arm using MATLAB," 2022. doi: 10.33545/27076571.2022.v3.i1a.41.

[23] 2 1Rohit Kumar, 2Sachin Kalsi, 3Ishbir Singh 1, "Effect of vibration while a human subject comes in contact with vibration conditions," *Emerging Technologies and Innovative Research*, vol. 8, no. 9, pp. e416–e419, 2021.

[24] R. G. Dong, J. Z. Wu, X. S. Xu, D. E. Welcome, and K. Krajnak, "A Review of Hand–Arm Vibration Studies Conducted by US NIOSH since 2000," 2021. doi: 10.3390/vibration4020030.

[25] S. Liu, Y. Wang, and Q. Zhu, "Development of a new EDRNN procedure in control of human arm trajectories," *Neurocomputing*, vol. 72, no. 1–3, pp. 490–499, Dec. 2008, doi: 10.1016/j.neucom.2007.12.012.

[26] A. H. M. Mohammed Z. Al-Faiz, MIEEE, Abduladhem A .Ali, "Simulation of Digital Control of Human Arm Based PSO Algorithm in Virtual Reality," *Journal of Engineering and Development*, vol. 16, no. 3, pp. 126–138, 2012.

[27] M. A. Rashidifar, A. A. Rashidifar, and D. Ahmadi, "Modeling and Control of 5DOF Robot Arm Using Fuzzy Logic Supervisory Control," 2013. doi: 10.11591/ijra.v2i2.2974.

[28] R. Mourya, A. Shelke, S. Satpute, S. Kakade, and M. Botre, "Design and Implementation of Pick and Place Robotic Arm," 2015. [Online]. Available: www.paperpublications.org

[29] Mohit Dhaka, Dr. Vikram Sharma, and Kaushal Khetan, "Control of Mechanisms and Robots using LabVIEW and SolidWorks and Arduino," *International Journal of Engineering Research and*, vol. V5, no. 02, Feb. 2016, doi: 10.17577/IJERTV5IS020312.

[30] A. Nasr, A. E. Gaber, and H. A. El Gamal, "Design and Position Control of Arm Manipulator; Experimentally and in MATLAB SimMechanics." [Online]. Available: www.ijert.org

[31] A. Okubanjo, O. Oluwadamilola, O. Martins, and O. Olaluwoye, "Modeling of 2-DOF robot arm and control," *Futo Journal Series (FUTOJNLS)*, vol. 3, no. 2, pp. 80–92, 2017, [Online]. Available: www.futojnls.org

[32] N. M. Ghaleb and A. A. Aly, "Modeling and Control of 2-DOF Robot Arm," 2018.

[33] M. Bi, "Control of robot arm motion using trapezoid fuzzy two-degree-of-freedom PID algorithm," 2020. doi: 10.3390/SYM12040665.

[34] H. T. Nguyen, V. C. Trinh, and T. D. Le, "An adaptive fast terminal sliding mode controller of exercise-assisted robotic arm for elbow joint rehabilitation featuring pneumatic artificial muscle actuator," 2020. doi: 10.3390/act9040118.

[35] M. Salman, H. Khan, S. J. Abbasi, and M. C. Lee, "Dynamics Analysis and Control of 5 DOF Robot Manipulator," in *International Conference on Control, Automation and Systems*, IEEE, Oct. 2021, pp. 1705–1709. doi: 10.23919/ICCAS52745.2021.9649858.

[36] H. Majeed, S. Kadhim, and A. Jaber, “Design of a Sliding Mode Controller for a Prosthetic Human Hand’s Finger,” *Engineering and Technology Journal*, vol. 40, no. 1, pp. 257–266, Jan. 2022, doi: 10.30684/etj.v40i1.1943.

[37] F. Grimm, J. Kraugmann, G. Naros, and A. Gharabaghi, “Clinical validation of kinematic assessments of post-stroke upper limb movements with a multi-joint arm exoskeleton,” *J Neuroeng Rehabil*, vol. 18, no. 1, Dec. 2021, doi: 10.1186/s12984-021-00875-7.

[38] S. Kansal, M. Zubair, B. Suthar, and S. Mukherjee, “Tele-operation of an industrial robot by an arm exoskeleton for peg-in-hole operation using immersive environments,” *Robotica*, vol. 40, no. 2, pp. 234–249, Feb. 2022, doi: 10.1017/S0263574721000485.

[39] A. W. de Vries, S. J. Baltrusch, and M. P. de Looze, “Field study on the use and acceptance of an arm support exoskeleton in plastering,” *Ergonomics*, vol. 66, no. 10, pp. 1622–1632, 2023, doi: 10.1080/00140139.2022.2159067.

[40] B. Chen *et al.*, “Volitional control of upper-limb exoskeleton empowered by EMG sensors and machine learning computing,” *Array*, vol. 17, Mar. 2023, doi: 10.1016/j.array.2023.100277.

[41] G. Ramella, L. Grazi, F. Giovacchini, E. Trigili, N. Vitiello, and S. Crea, “Evaluation of antigravitational support levels provided by a passive upper-limb occupational exoskeleton in repetitive arm movements,” *Appl Ergon*, vol. 117, May 2024, doi: 10.1016/j.apergo.2024.104226.

[42] L. Grazi *et al.*, “Passive shoulder occupational exoskeleton reduces shoulder muscle coactivation in repetitive arm movements,” *Sci Rep*, vol. 14, no. 1, Dec. 2024, doi: 10.1038/s41598-024-78090-2.

[43] Thomas, C., Rakheja, S., Bhat, R.B., Stiharu, I.: A study of the modal behavior of the human hand arm system. J. Sound Vibr. 191(1), 171–176 (1996).

[44] Cherian, T., Rakheja, S. and Bhat, R.B., 1996. An analytical investigation of an energy flow divider to attenuate hand-transmitted vibration. International Journal of Industrial Ergonomics, 17(6), pp.455-467.

[45] Ali, H.H., Khafaji, S.O.W. and Al-Bakri, F.F., 2021. H∞ loop shaping control design of the rotational velocity of a hydraulic motor. Internation

[46] Laheeb, M., Salwan, K., Fawaz, A.B. and Sarah, L., 2018, January. Online algorithm for controlling a cruise system under uncertainty in design parameters and environmental conditions using Monte-Carlo simulation. In 2018 IEEE 8th Annual Computing and Communication Workshop and Conference (CCWC) (pp. 424-430). IEEE.

الخلاصة

تلعب الأطراف الاصطناعية الذكية للذراع دورًا هامًا في تعزيز الحركة والاستقلالية للأشخاص ذوي الإعاقة. تُستخدم هذه الأجهزة الميكانيكية لتوفير حركات وظيفية للذراع البشرية في تطبيقات متنوعة، مثل إعادة التأهيل والرياضة والابتكار التكنولوجي، ومنها الهيكل الخارجي للذراع البشرية. لذا، يصبح من الضروري تقييم الاستجابة الديناميكية للأطراف الاصطناعية البشرية. تركز هذه الدراسة على دراسة الاستجابة الديناميكية لذراع اصطناعية بشرية بخمس درجات حرية.

تم نمذجة نظام الذراع البشري باستخدام طريقة لاغرانج-أويلر، مما أسفر عن خمس معادلات تفاضلية عادية من الرتبة الثانية. ولتسهيل عملية التحسين المطلوبة والحصول على معلمات النظام المثلى محليًا، تم تبسيط النموذج غير الخطي حول نقطة تشغيل محددة. أُجري تحليل مقارن بين استجابات النظام الخطي وغير الخطي للتأكد من قدرة النموذج المبسط على تمثيل ديناميكيات النظام غير الخطي الحقيقي والتعويض عنها بشكل كافٍ.

تم تحديد معلمات الذراع، بما في ذلك الكتل ومعاملات التخميد وقيم الصلابة، باستخدام طريقة تحسين مضاعفات لاغرانج بهدف تحقيق زمن استقرار قصير وتجاوز ضئيل. علاوة على ذلك، استُخدمت دوال أسية ثمانية الحدود لتوليد منحنيات الإزاحة المطلوبة لليد والساعد والمرفق الأفقي والمرفق الرأسي وحركات المرفق الزاوية، مع مراعاة شروط الحدود الأولية والمتوسطة والنهائية، بالإضافة إلى قيود عزم دوران المرفق.

تم حساب عزم دوران الكوع المرجعي تحليليًا بناءً على مسارات الإزاحة المحددة مسبقًا. وللتحقق من صحة المنهجية المقترحة، أُجريت محاكاة عددية باستخدام تقنية محاكاة مونت كارلو ضمن نطاق واسع من الشروط الابتدائية وتغيرات في معلمات النظام بنسبة $\pm 6\%$ عن القيم الاسمية. أظهرت النتائج المُحَصَّلة تقاربًا سريعًا لجميع أجزاء الذراع، حيث تحققت استجابات الحالة المستقرة في غضون 0.25 ثانية دون أي تجاوز في كل من إزاحات النظام وعزم دوران الكوع. علاوة على ذلك، ظلت أخطاء الحالة المستقرة صغيرة للغاية، حيث بلغ الحد الأقصى للخطأ الزاوي للكوع (4×10^{-3}) درجة، والحد الأدنى لخطأ الإزاحة الرأسية للكوع (-1×10^{-5}) متر في الاتجاه الرأسي، وخطأ عزم دوران الكوع منخفضًا جدًا يصل إلى (0.4-) نيوتن متر عبر ١٠٠٠ تجربة محاكاة.

جمهورية العراق

وزارة التعليم العالي و البحث العلمي

جامعة كربلاء

كلية الهندسة

قسم الهندسة الميكانيكيه

التصميم الأمثل والتحكم في الهيكل الخارجي للطرف العلوي

رسالة مقدمة الى مجلس كلية الهندسة / جامعة كربلاء وهي جزء من متطلبات نيل درجة الماجستير في علوم الهندسة الميكانيكيه

المؤلف:

زهراء عبد الاله خليل

باشراف :

الدكتور مسلم محسن علي

الدكتور فواز فريد برتو

رجب - ١٤٤٧ كانون الثاني - ٢٠٢٦